Summer school on cosmological numerical simulations
3rd week – WEDNESDAY

Helmholtz School of Astrophysics
Potsdam, July/August 2006

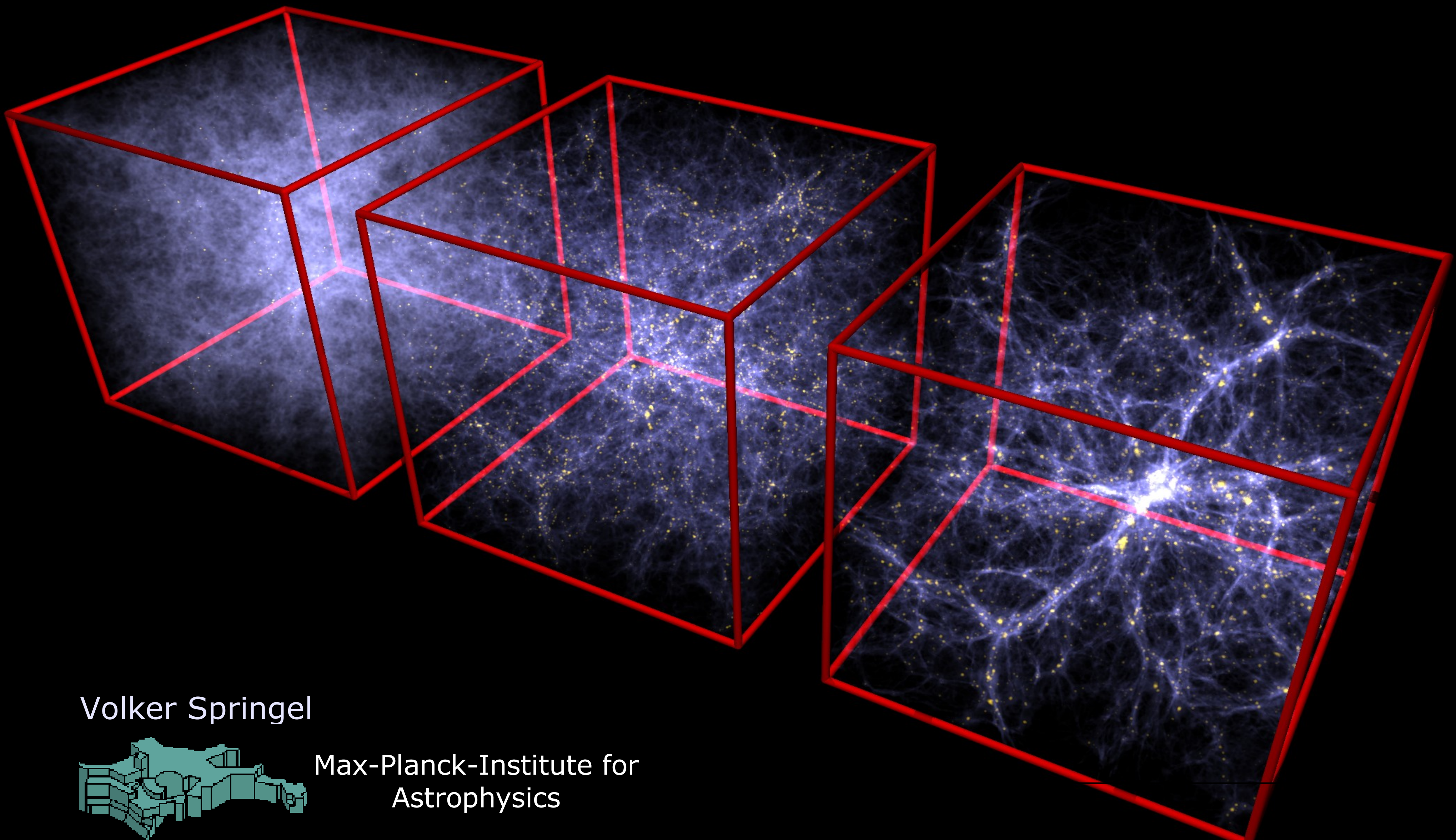

Volker Springel

Max-Planck-Institute for
Astrophysics

Time integration and dark matter substructures

WEDNESDAY-Lecture of 3rd week

Volker Springel

- **Time integration issues**
- **Issues of floating point arithmetic**
- **Dark matter substructures**
- **Merger trees and semi-analytic models**

Time integration issues

Time integration methods

Want to numerically integrate an **ordinary differential equation** (ODE)

$$\dot{\mathbf{y}} = f(\mathbf{y})$$

Note: $\mathbf{y}$ can be a vector

Example: Simple pendulum

$$\boxed{\ddot{\alpha} = -\frac{g}{l}\,\sin\alpha}$$

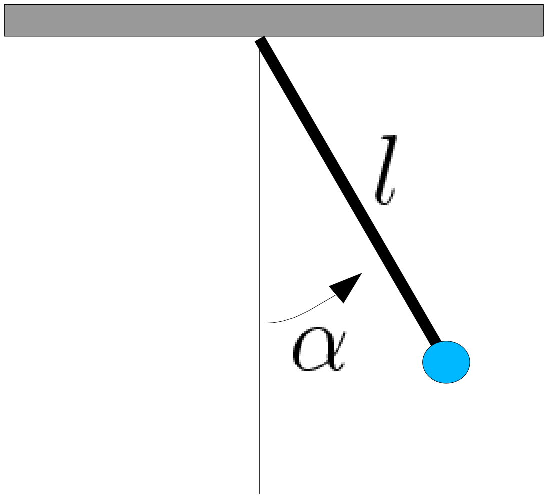

$$y_0 \equiv \alpha \qquad y_1 \equiv \dot{\alpha}$$

$$\dot{\mathbf{y}} = f(y) = \begin{pmatrix} y_1 \\ -\frac{g}{l}\,\sin y_0 \end{pmatrix}$$

A numerical approximation to the ODE is a set of values $\{\mathbf{y}_0, \mathbf{y}_1, \mathbf{y}_2, \ldots\}$ at times $\{t_0, t_1, t_2, \ldots\}$

There are many different ways for obtaining this.

Explicit Euler method

$$y_{n+1} = y_n + f(y_n)\Delta t$$

- Simplest of all
- Right hand-side depends only on things already non, **explicit method**
- The error in a single step is O(Δt^2), but for the N steps needed for a finite time interval, the total error scales as O(Δt) !
- Never use this method, it's only **first order accurate**.

Implicit Euler method

$$y_{n+1} = y_n + f(y_{n+1})\Delta t$$

- **Excellent** stability properties
- Suitable for very stiff ODE
- Requires implicit solver for y_{n+1}

Implicit mid-point rule

$$y_{n+1} = y_n + f\left(\frac{y_n + y_{n+1}}{2}\right)\Delta t$$

- **2nd order accurate**
- Time-symmetric, in fact **symplectic**
- But still implicit...

Runge-Kutta methods

whole class of integration methods

2nd order accurate

$$\begin{aligned} k_1 &= f(y_n) \\ k_2 &= f(y_n + k_1 \Delta t) \\ y_{n+1} &= y_n + \left(\frac{k_1 + k_2}{2}\right)\Delta t \end{aligned}$$

4th order accurate.

$$\begin{aligned} k_1 &= f(y_n, t_n) \\ k_2 &= f(y_n + k_1 \Delta t/2, t_n + \Delta t/2) \\ k_3 &= f(y_n + k_2 \Delta t/2, t_n + \Delta t/2) \\ k_4 &= f(y_n + k_3 \Delta t/2, t_n + \Delta t) \\ y_{n+1} &= y_n + \left(\frac{k_1}{6} + \frac{k_2}{3} + \frac{k_3}{3} + \frac{k_4}{6}\right)\Delta t \end{aligned}$$

The Leapfrog

For a second order ODE: $\ddot{\mathbf{x}} = f(\mathbf{x})$

"Drift-Kick-Drift" version

$$
\begin{aligned}
x_{n+\frac{1}{2}} &= x_n + v_n \frac{\Delta t}{2} \\
v_{n+1} &= v_n + f(x_{n+\frac{1}{2}})\Delta t \\
x_{n+1} &= x_{n+\frac{1}{2}} + v_{n+1} \frac{\Delta t}{2}
\end{aligned}
$$

"Kick-Drift-Kick" version

$$
\begin{aligned}
v_{n+\frac{1}{2}} &= v_n + f(x_n) \frac{\Delta t}{2} \\
x_{n+1} &= x_n + v_{n+\frac{1}{2}} \frac{\Delta t}{2} \\
v_{n+1} &= v_{n+\frac{1}{2}} + f(x_{n+1}) \frac{\Delta t}{2}
\end{aligned}
$$

- **2nd order accurate**
- **symplectic**
- can be rewritten into time-centred formulation

The leapfrog is behaving much better than one might expect...

INTEGRATING THE KEPLER PROBLEM

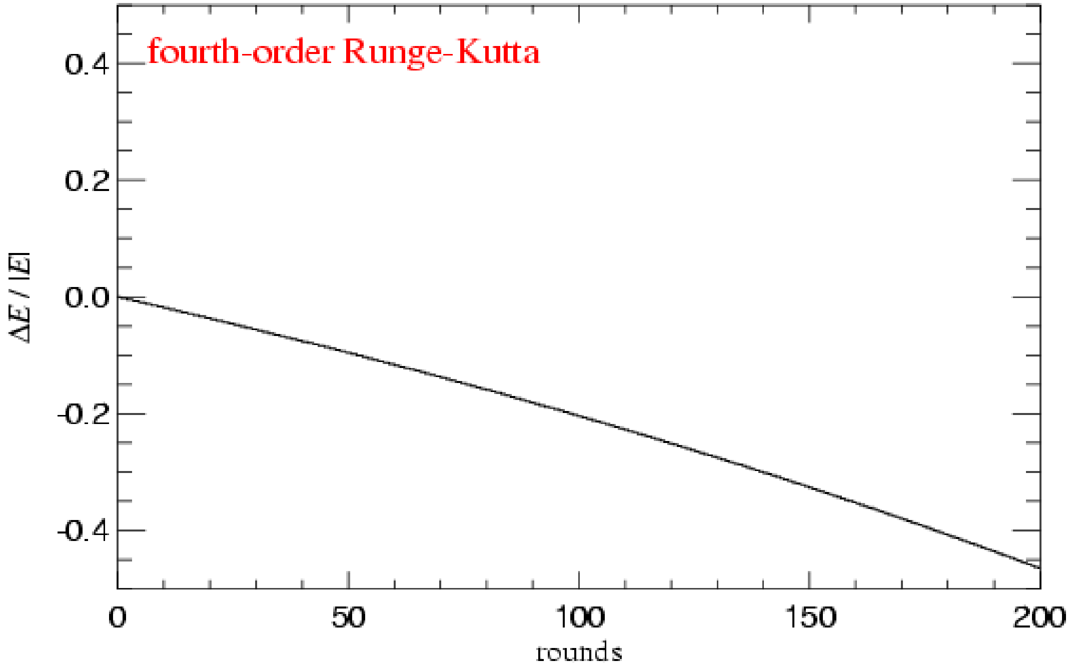

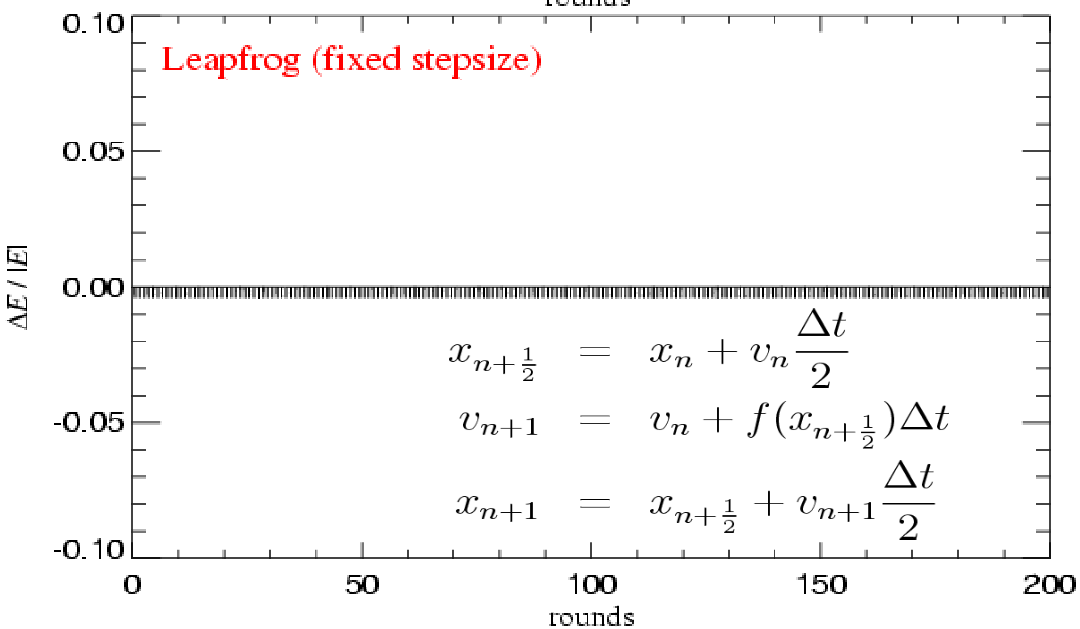

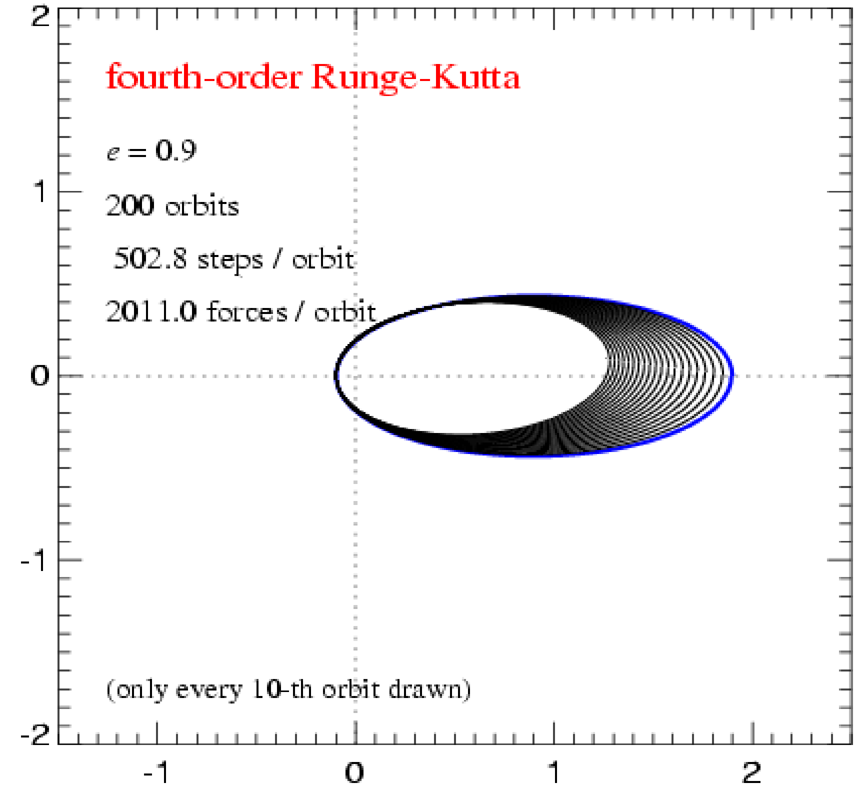

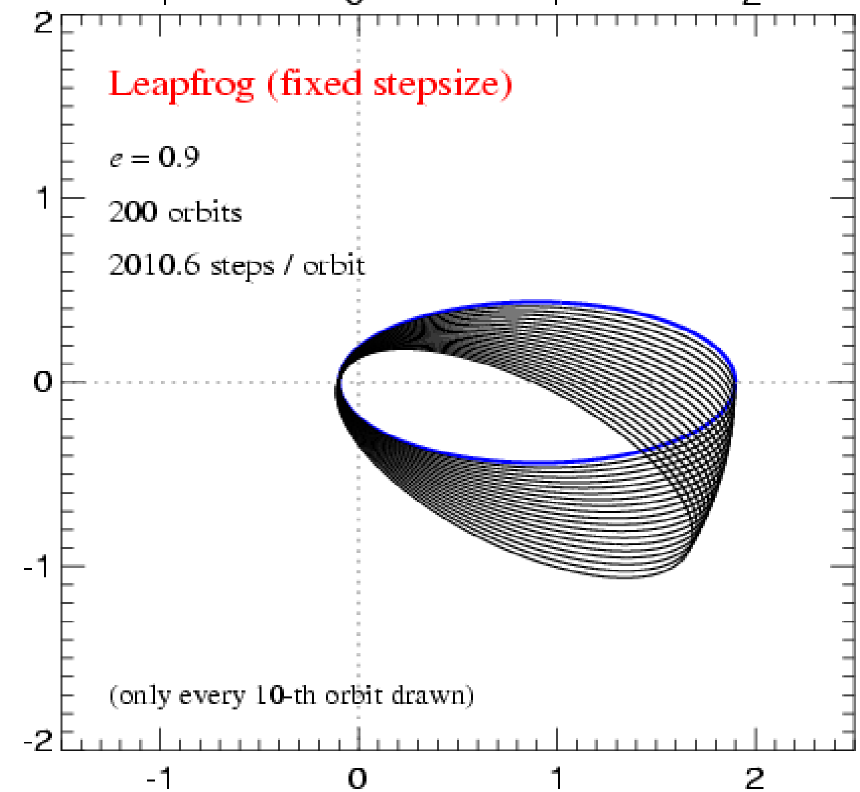

When compared with an integrator of the same order, the leapfrog is highly superior

INTEGRATING THE KEPLER PROBLEM

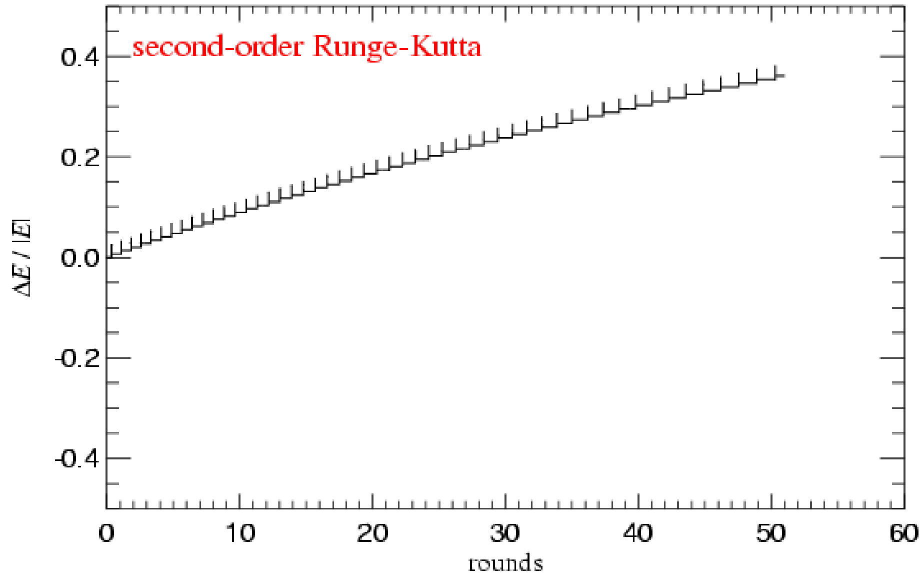

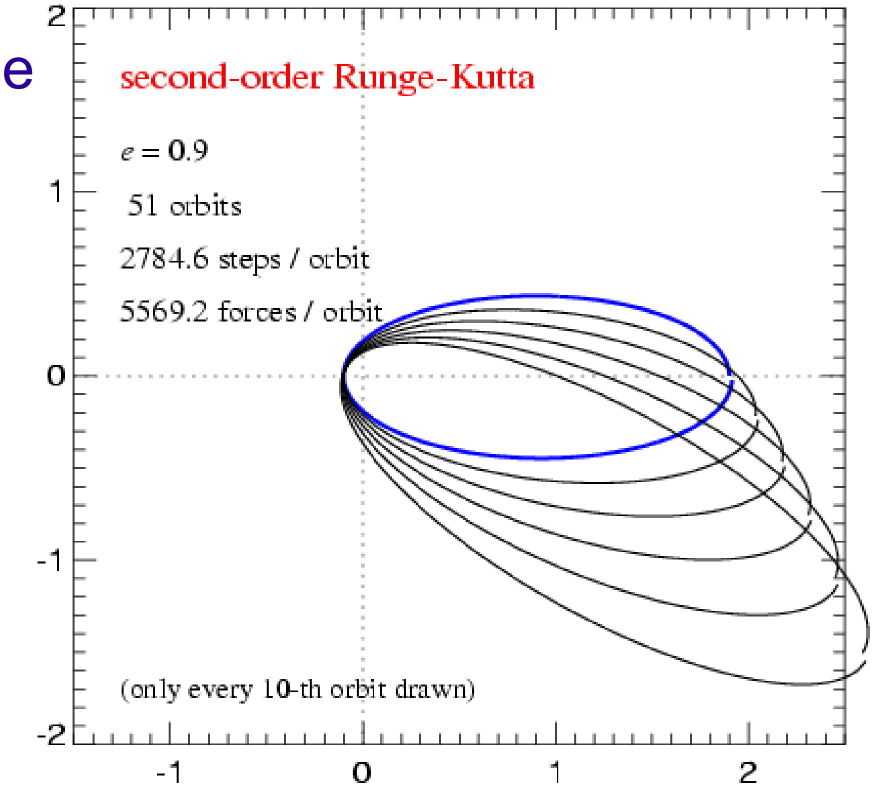

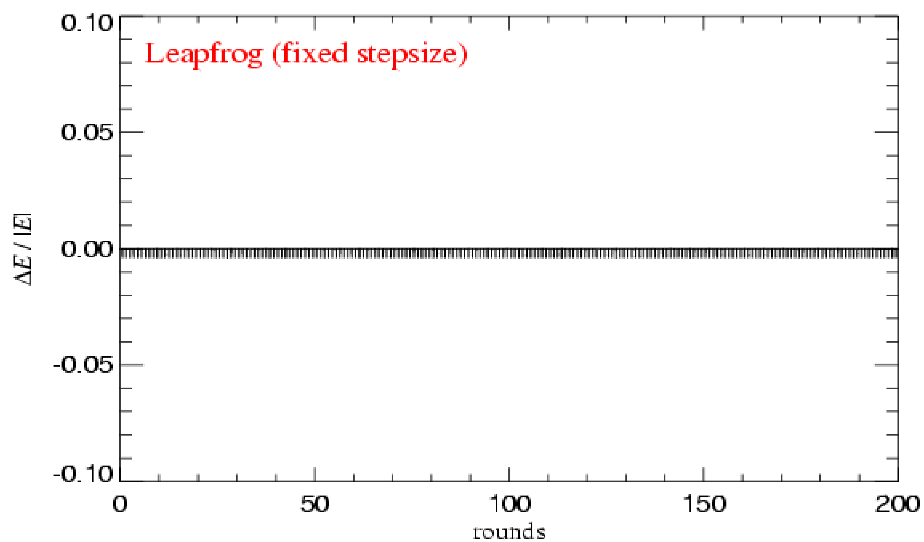

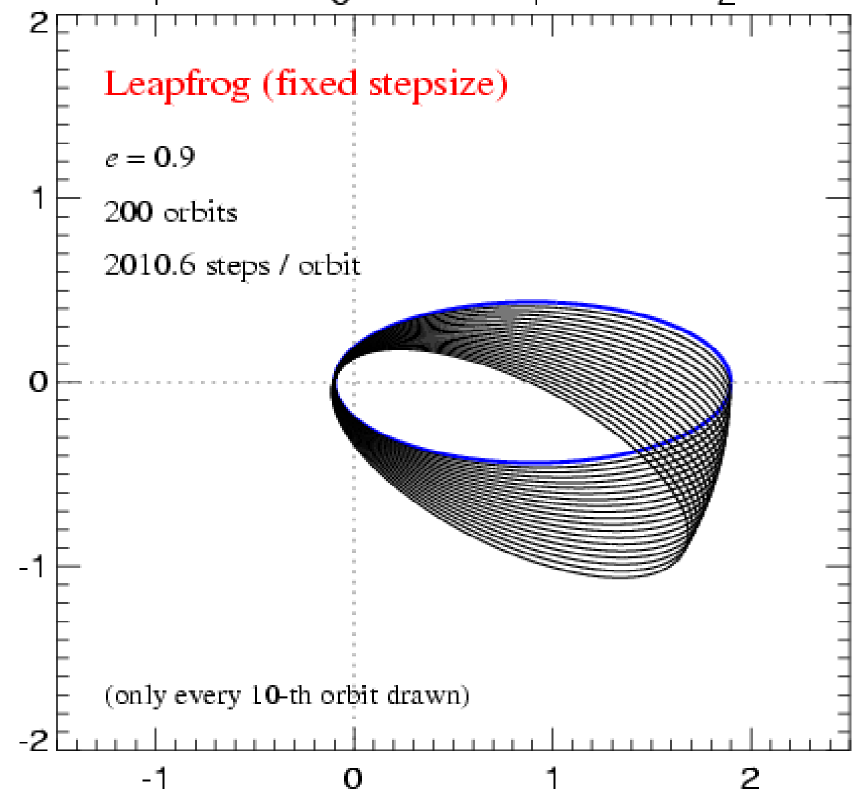

Even for rather large timesteps, the leapfrog maintains qualitatively correct behaviour without long-term secular trends

INTEGRATING THE KEPLER PROBLEM

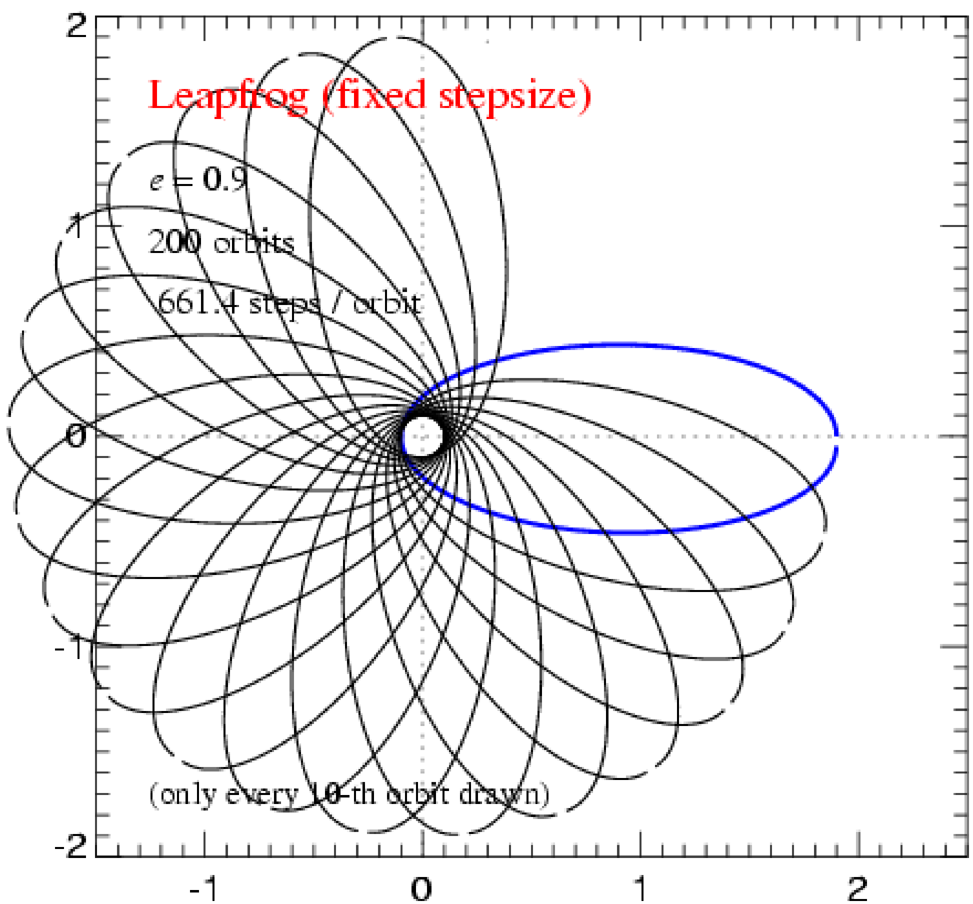

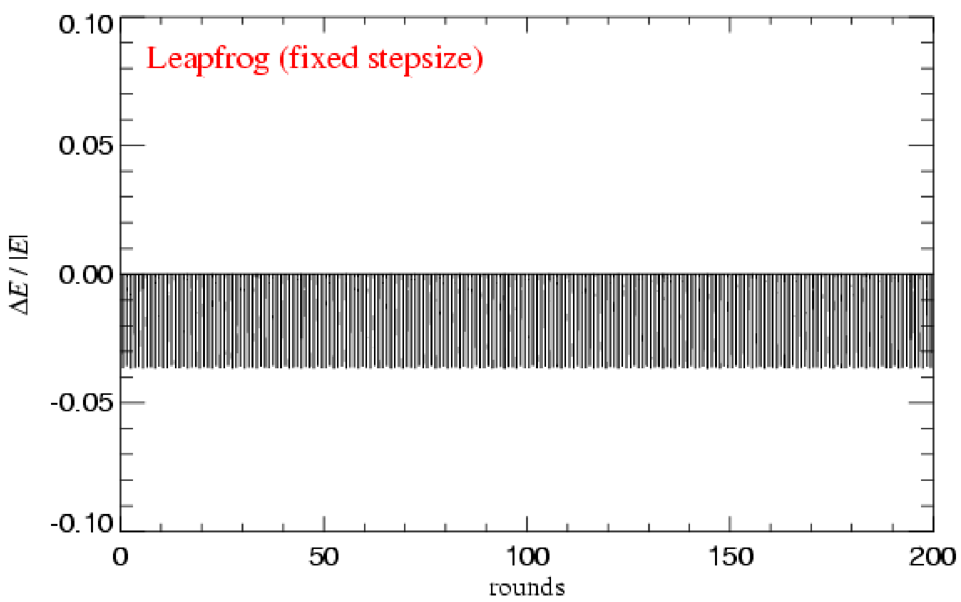

What is the underlying mathematical reason for the very good long-term behaviour of the leapfrog ?

HAMILTONIAN SYSTEMS AND SYMPLECTIC INTEGRATION

$$H(\mathbf{p}_1, \ldots, \mathbf{p}_n, \mathbf{x}_1, \ldots, \mathbf{x}_n) = \sum_i \frac{\mathbf{p}_i^2}{2m_i} + \frac{1}{2}\sum_{ij} m_i m_j \phi(\mathbf{x}_i - \mathbf{x}_j)$$

If the integration scheme introduces non-Hamiltonian perturbations, a completely different long-term behaviour results.

The Hamiltonian structure of the system can be preserved in the integration if each step is formulated as a *canoncial transformation*. Such integration schemes are called *symplectic*.

Poisson bracket:

$$\{A, B\} \equiv \sum_i \left(\frac{\partial A}{\partial \mathbf{x}_i}\frac{\partial B}{\partial \mathbf{p}_i} - \frac{\partial A}{\partial \mathbf{p}_i}\frac{\partial B}{\partial \mathbf{x}_i} \right)$$

Hamilton's equations

$$\frac{\mathrm{d}\mathbf{x}_i}{\mathrm{d}t} = \{\mathbf{x}_i, H\}$$

$$\frac{\mathrm{d}\mathbf{p}_i}{\mathrm{d}t} = \{\mathbf{p}_i, H\}$$

Hamilton operator

$$\mathbf{H} f \equiv \{f, H\}$$

System state vector

$$|t\rangle \equiv |\mathbf{x}_1(t), \ldots, \mathbf{x}_n(t), \mathbf{p}_1(t), \ldots, \mathbf{p}_n(t), t\rangle$$

Time evolution operator

$$|t_1\rangle = \mathbf{U}(t_1, t_0)\ |t_0\rangle$$

$$\mathbf{U}(t + \Delta t, t) = \exp\left(\int_t^{t+\Delta t} \mathbf{H}\,\mathrm{d}t \right)$$

The time evolution of the system is a continuous canonical transformation generated by the Hamiltonian.

Symplectic integration schemes can be generated by applying the idea of operating splitting to the Hamiltonian

THE LEAPFROG AS A SYMPLECTIC INTEGRATOR

Separable Hamiltonian

$$H = H_{\rm kin} + H_{\rm pot}$$

Drift- and Kick-Operators

$$\mathbf{D}(\Delta t) \equiv \exp\left(\int_t^{t+\Delta t} \mathrm{d}t\, \mathbf{H}_{\rm kin}\right) = \begin{cases} \mathbf{p}_i & \mapsto \quad \mathbf{p}_i \\ \mathbf{x}_i & \mapsto \quad \mathbf{x}_i + \frac{\mathbf{p}_i}{m_i}\Delta t \end{cases}$$

$$\mathbf{K}(\Delta t) = \exp\left(\int_t^{t+\Delta t} \mathrm{d}t\, \mathbf{H}_{\rm pot}\right) = \begin{cases} \mathbf{x}_i & \mapsto \quad \mathbf{x}_i \\ \mathbf{p}_i & \mapsto \quad \mathbf{p}_i - \sum_j m_i m_j \frac{\partial \phi(\mathbf{x}_{ij})}{\partial \mathbf{x}_i}\Delta t \end{cases}$$

The drift and kick operators are symplectic transformations of phase-space !

The Leapfrog

Drift-Kick-Drift: $$\tilde{\mathbf{U}}(\Delta t) = \mathbf{D}\left(\frac{\Delta t}{2}\right)\mathbf{K}(\Delta t)\,\mathbf{D}\left(\frac{\Delta t}{2}\right)$$

Kick-Drift-Kick: $$\tilde{\mathbf{U}}(\Delta t) = \mathbf{K}\left(\frac{\Delta t}{2}\right)\mathbf{D}(\Delta t)\,\mathbf{K}\left(\frac{\Delta t}{2}\right)$$

Hamiltonian of the numerical system: $$\tilde{H} = H + H_{\rm err} \qquad H_{\rm err} = \frac{\Delta t^2}{12}\left\{\{H_{\rm kin}, H_{\rm pot}\}, H_{\rm kin} + \frac{1}{2}H_{\rm pot}\right\} + \mathcal{O}(\Delta t^3)$$

When an adaptive timestep is used, much of the symplectic advantage is lost

INTEGRATING THE KEPLER PROBLEM

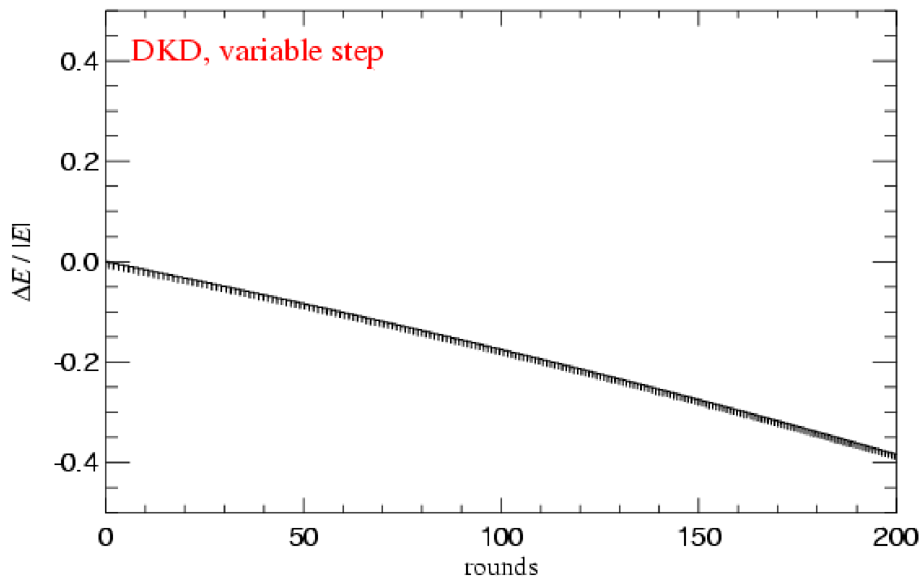

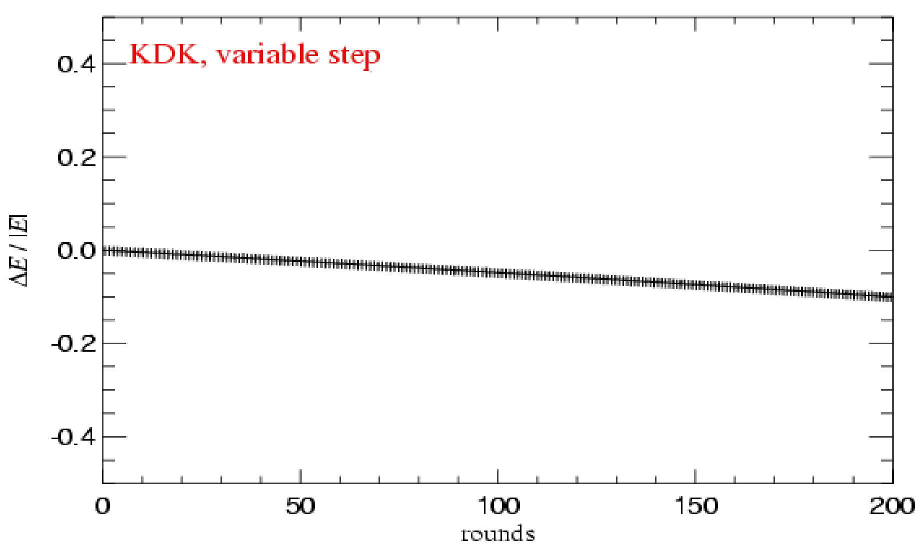

→ Going to KDK reduces the error by a factor 4, at the same cost !

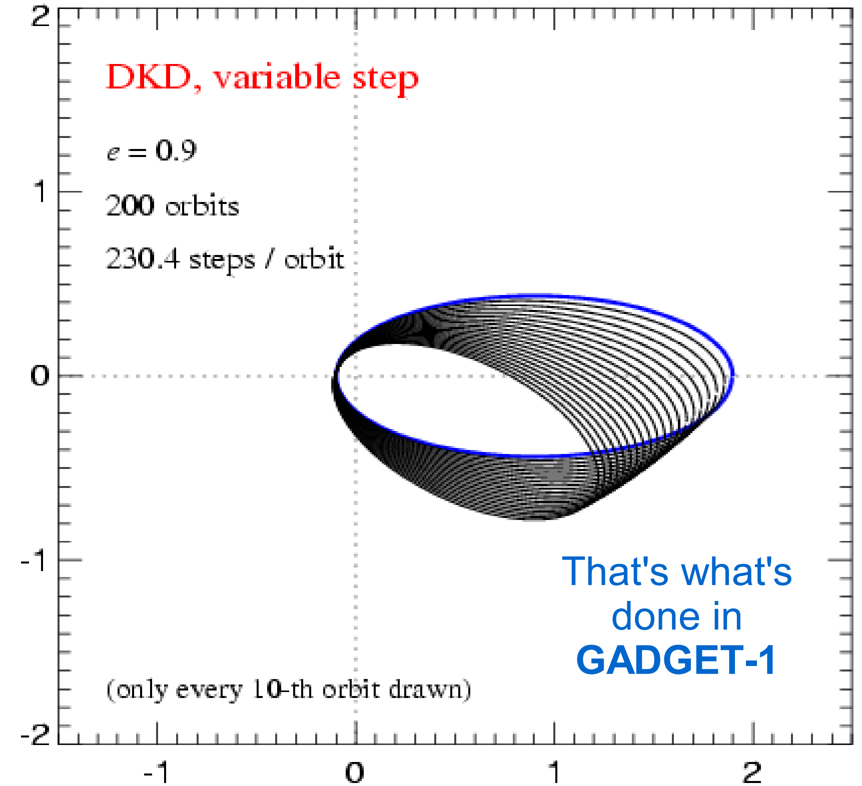

That's what's done in **GADGET-1**

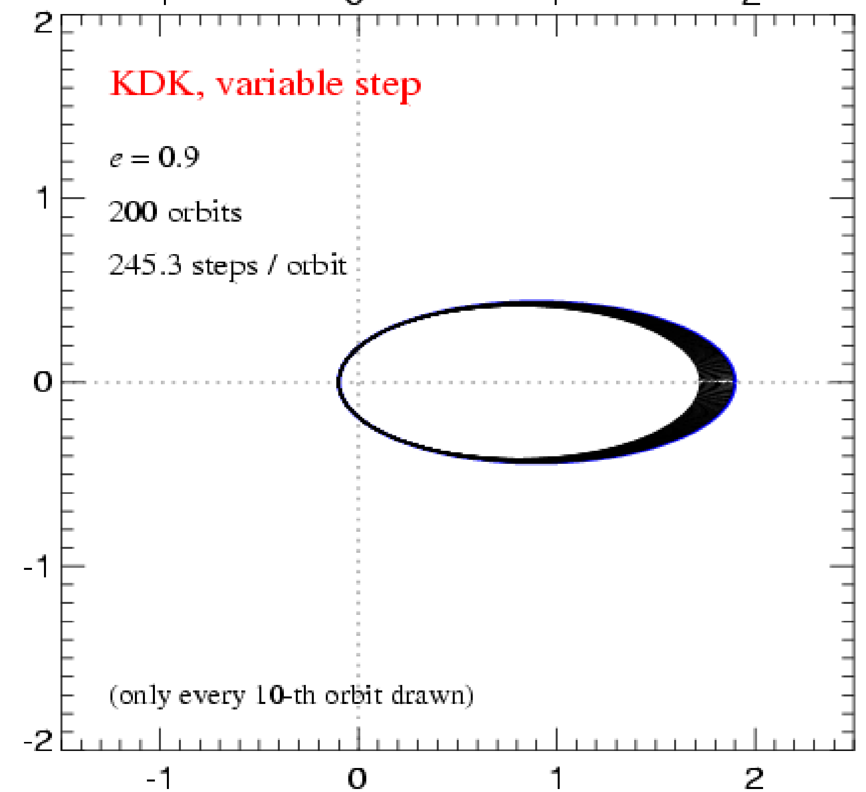

For periodic motion with adaptive timesteps, the DKD leapfrog shows more time-asymmetry than the KDK variant

LEAPFROG WITH ADAPTIVE TIMESTEP

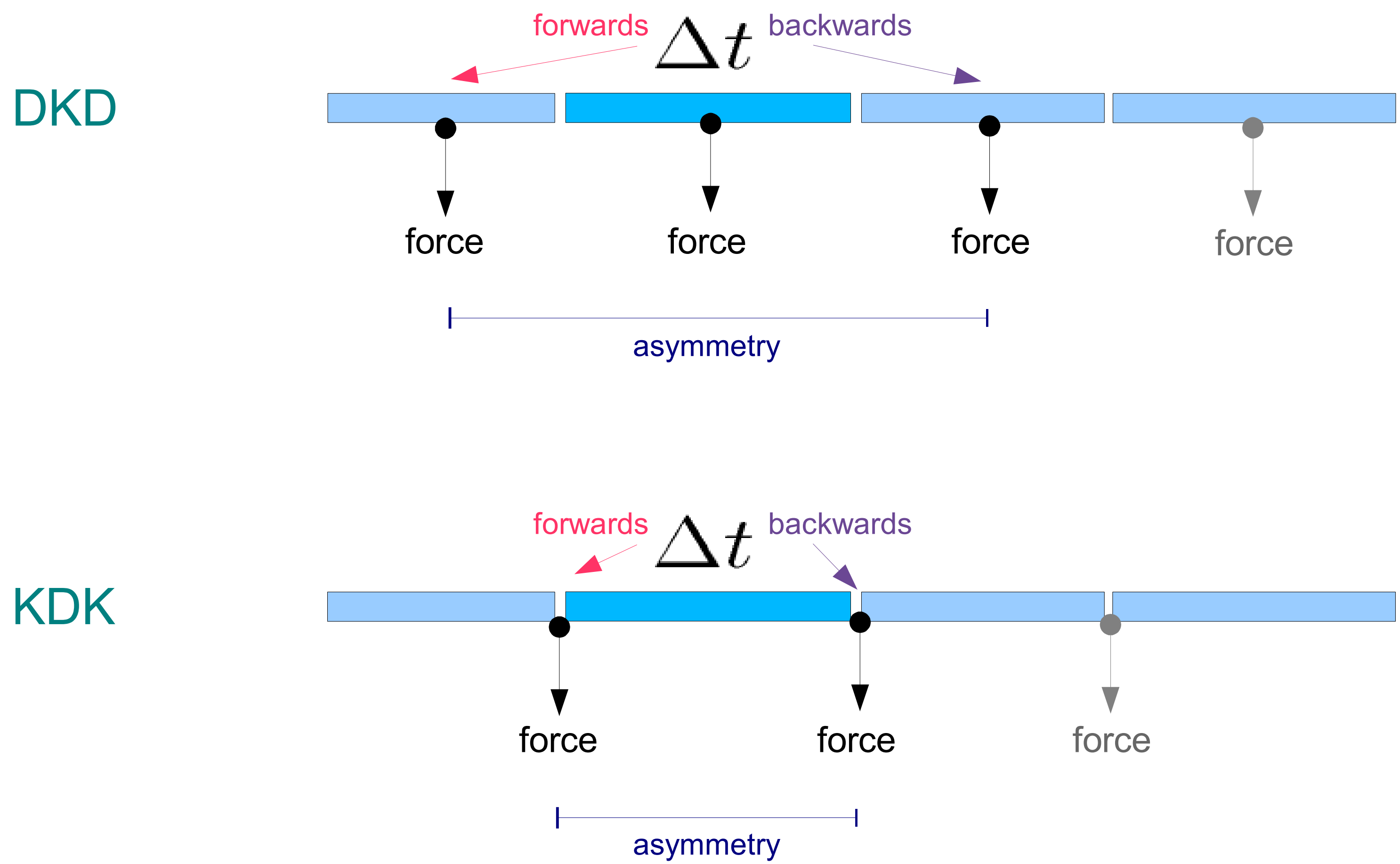

The key for obtaining better long-term behaviour is to make the choice of timestep time-reversible

INTEGRATING THE KEPLER PROBLEM

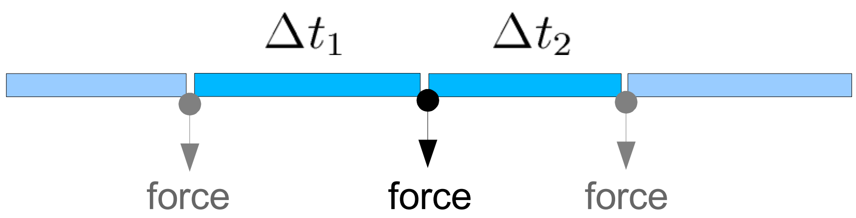

$$\frac{\Delta t_1 + \Delta t_2}{2} = f(\mathbf{a}, \mathbf{v})$$

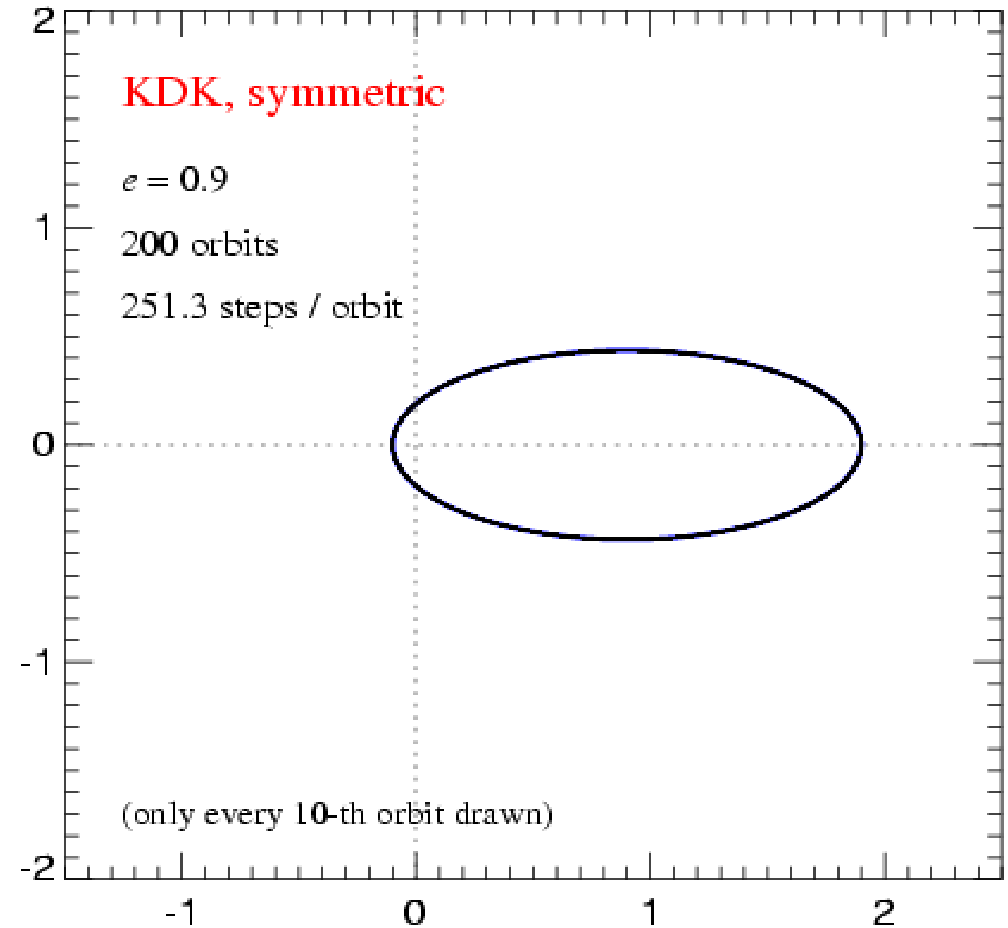

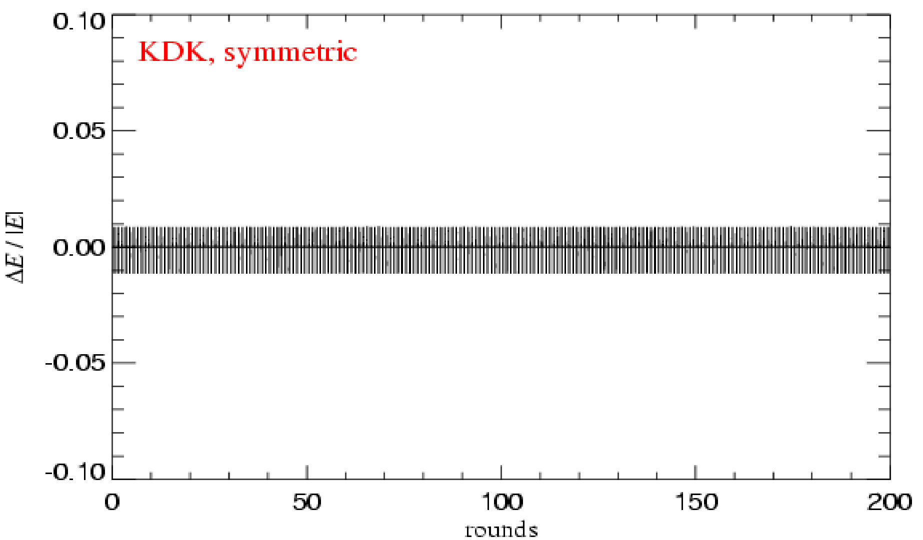

Symmetric behaviour can be obtained by using an implicit timestep criterion that depends on the end of the timestep

INTEGRATING THE KEPLER PROBLEM

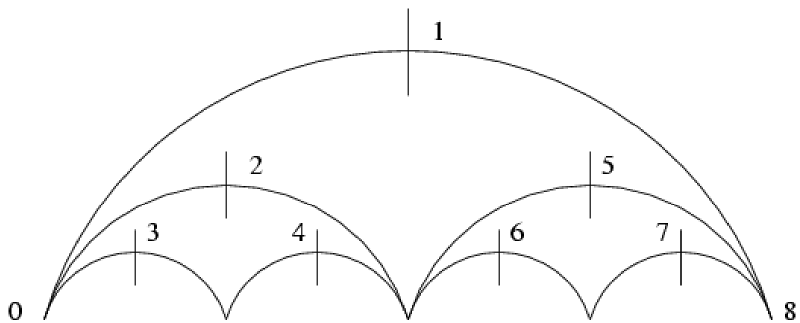

Quinn et al. (1997)

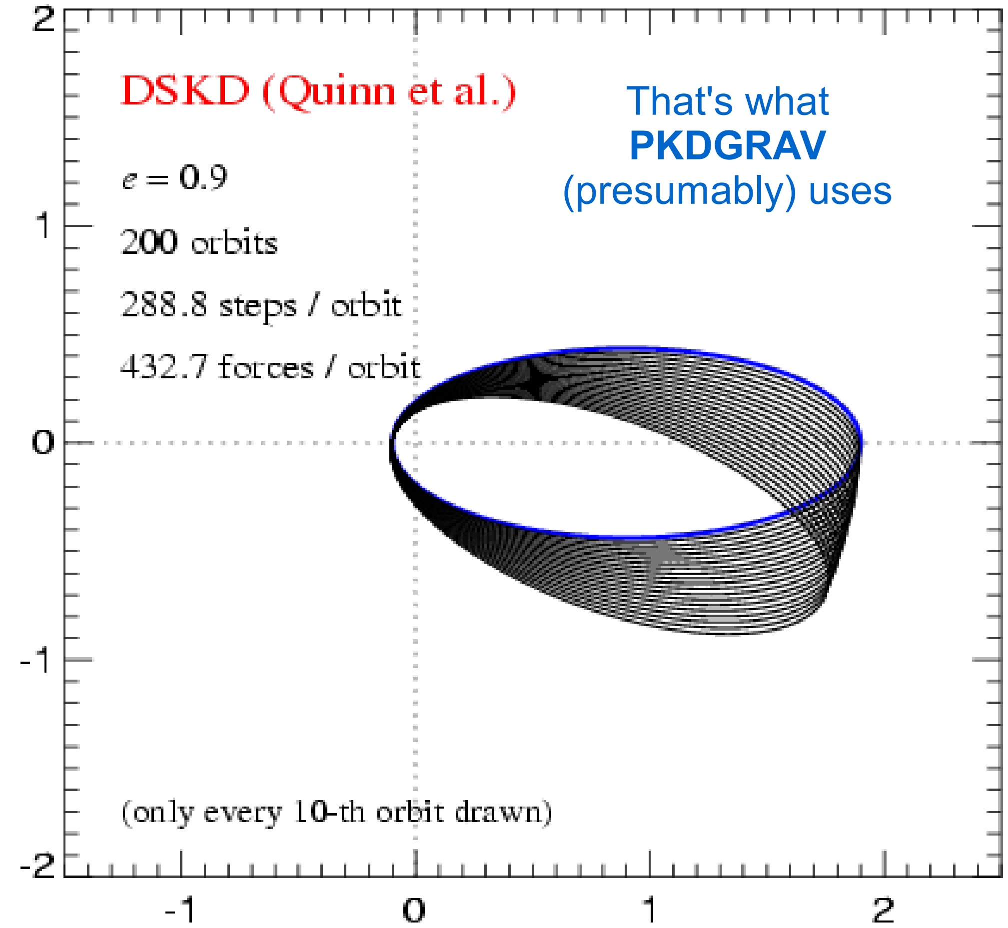

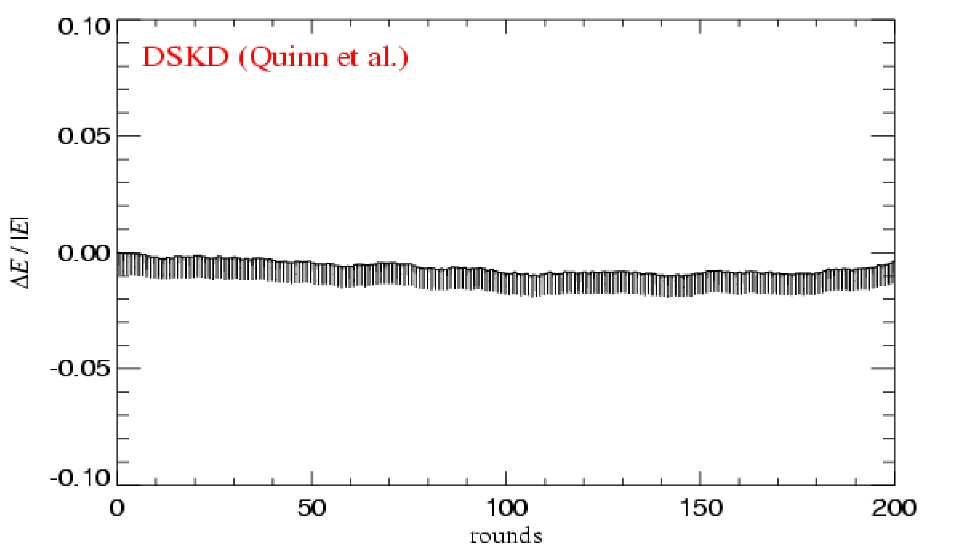

- Force evaluations have to be thrown away in this scheme
- reversibility is only approximatively given
- Requires back-wards drift of system - difficult to combine with SPH

Pseudo-symmetric behaviour can be obtained by making the evolution of the expectation value of the numerical Hamiltonian time reversible

INTEGRATING THE KEPLER PROBLEM

KDK scheme

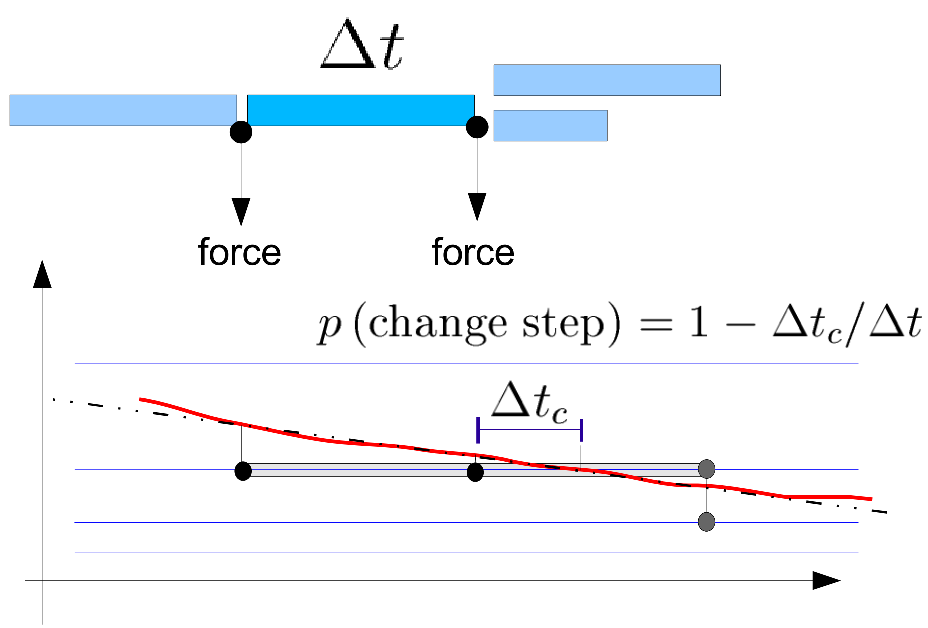

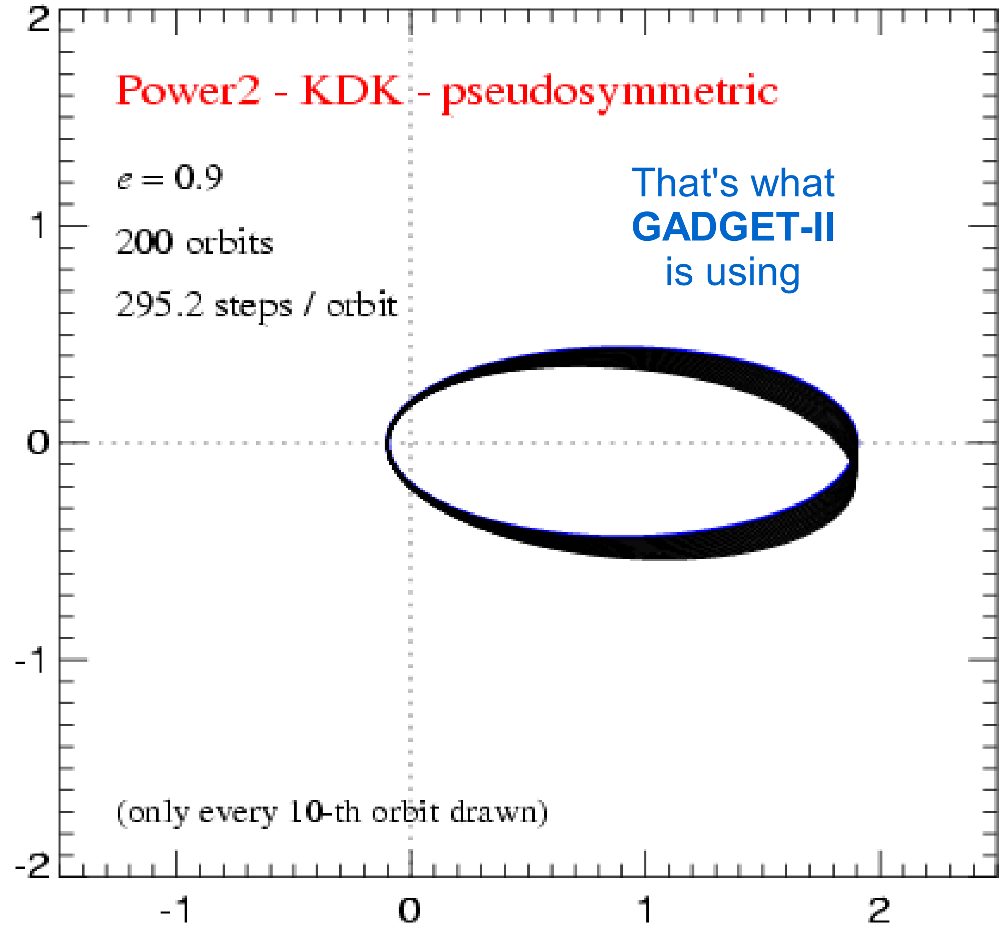

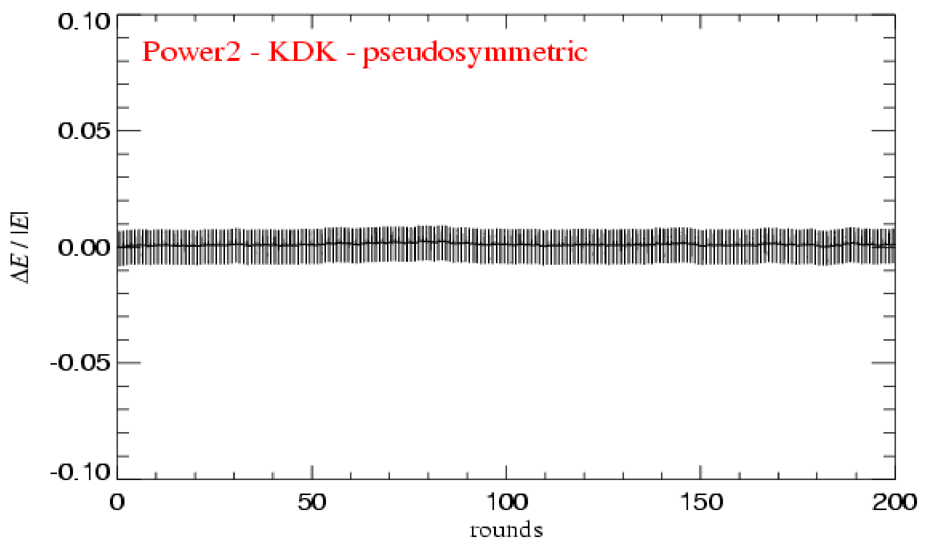

Gives the best result at a given number of force evaluations.

Collisionless dynamics in an expanding universe is described by a Hamiltonian system

THE HAMILTONIAN IN COMOVING COORDINATES

Conjugate momentum $\mathbf{p} = a^2 \dot{\mathbf{x}}$

$$H(\mathbf{p}_1, \ldots, \mathbf{p}_n, \mathbf{x}_1, \ldots, \mathbf{x}_n, t) = \sum_i \frac{\mathbf{p}_i^2}{2m_i a(t)^2} + \frac{1}{2}\sum_{ij} \frac{m_i m_j \phi(\mathbf{x}_i - \mathbf{x}_j)}{a(t)}$$

Drift- and Kick operators

$$\mathbf{D}(t+\Delta t, t) = \exp\left(\int_t^{t+\Delta t} \mathrm{d}t\, \mathbf{H}_{\mathrm{kin}}\right) = \begin{cases} \mathbf{p}_i & \mapsto \quad \mathbf{p}_i \\ \mathbf{x}_i & \mapsto \quad \mathbf{x}_i + \frac{\mathbf{p}_i}{m_i} \boxed{\int_t^{t+\Delta t} \frac{\mathrm{d}t}{a^2}} \end{cases}$$

$$\mathbf{K}(t+\Delta t, t) = \exp\left(\int_t^{t+\Delta t} \mathrm{d}t\, \mathbf{H}_{\mathrm{pot}}\right) = \begin{cases} \mathbf{x}_i & \mapsto \quad \mathbf{x}_i \\ \mathbf{p}_i & \mapsto \quad \mathbf{p}_i - \sum_j m_i m_j \frac{\partial \phi(\mathbf{x}_{ij})}{\partial \mathbf{x}_i} \boxed{\int_t^{t+\Delta t} \frac{\mathrm{d}t}{a}} \end{cases}$$

Choice of timestep

For linear growth, fixed step in log(a) appears most appropriate... → timestep is then a constant fraction of the Hubble time

$$\Delta t = \frac{\Delta \log a}{H(a)}$$

The force-split can be used to construct a symplectic integrator where long- and short-range forces are treated independently

TIME INTEGRATION FOR LONG AND SHORT-RANGE FORCES

Separate the potential into a long-range and a short-range part:

$$H = \sum_i \frac{\mathbf{p}_i^2}{2m_i a(t)^2} + \frac{1}{2}\sum_{ij} \frac{m_i m_j \,\varphi_{\rm sr}(\mathbf{x}_i - \mathbf{x}_j)}{a(t)} + \frac{1}{2}\sum_{ij} \frac{m_i m_j \,\varphi_{\rm lr}(\mathbf{x}_j - \mathbf{x}_j)}{a(t)}$$

The short-range force can then be evolved in a symplectic way on a smaller timestep than the long range force:

$$\tilde{\mathbf{U}}(\Delta t) = \mathbf{K}_{\rm lr}\left(\frac{\Delta t}{2}\right)\left[\mathbf{K}_{\rm sr}\left(\frac{\Delta t}{2m}\right)\mathbf{D}\left(\frac{\Delta t}{m}\right)\mathbf{K}_{\rm sr}\left(\frac{\Delta t}{2m}\right)\right]^m \mathbf{K}_{\rm lr}\left(\frac{\Delta t}{2}\right)$$

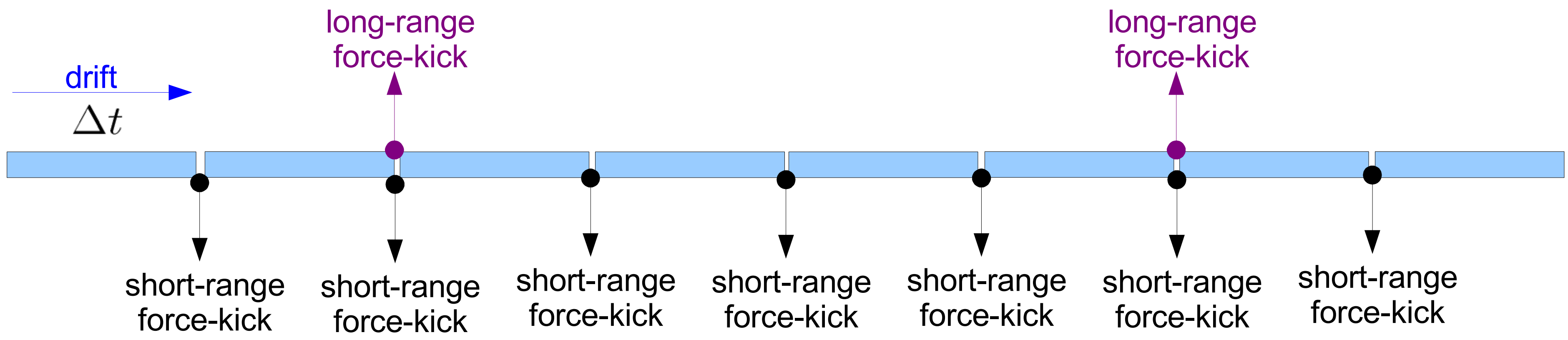

Issues of floating point accuracy

A space-filling Peano-Hilbert curve is used in GADGET-2 for a novel domain-decomposition concept

HIERARCHICAL TREE ALGORITHMS

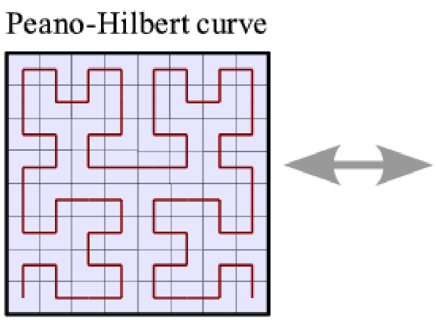

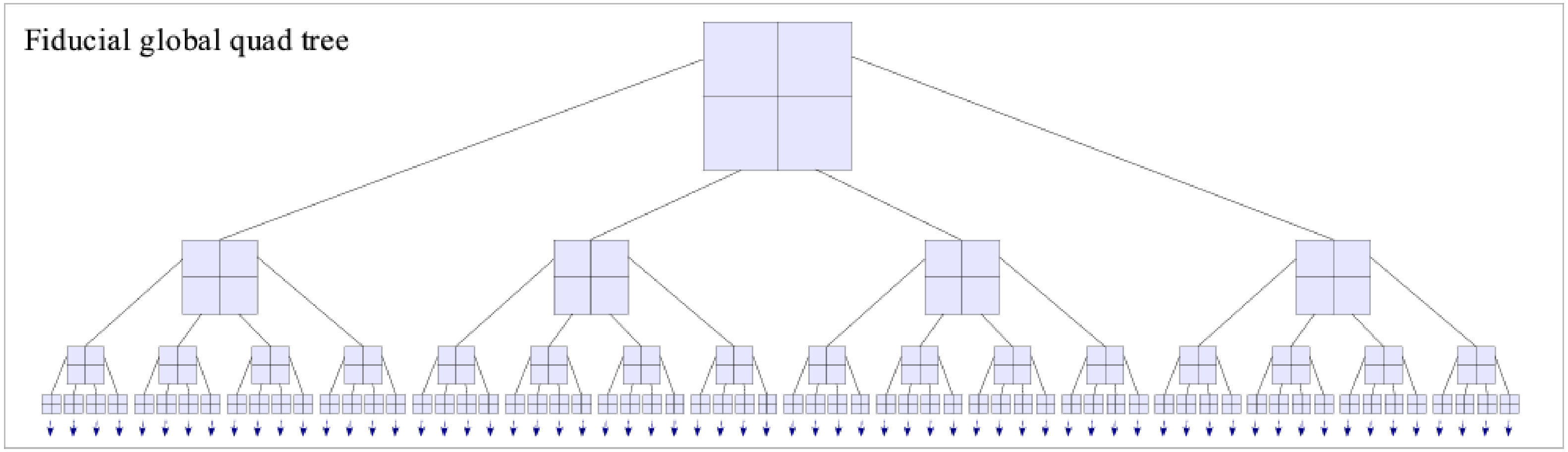

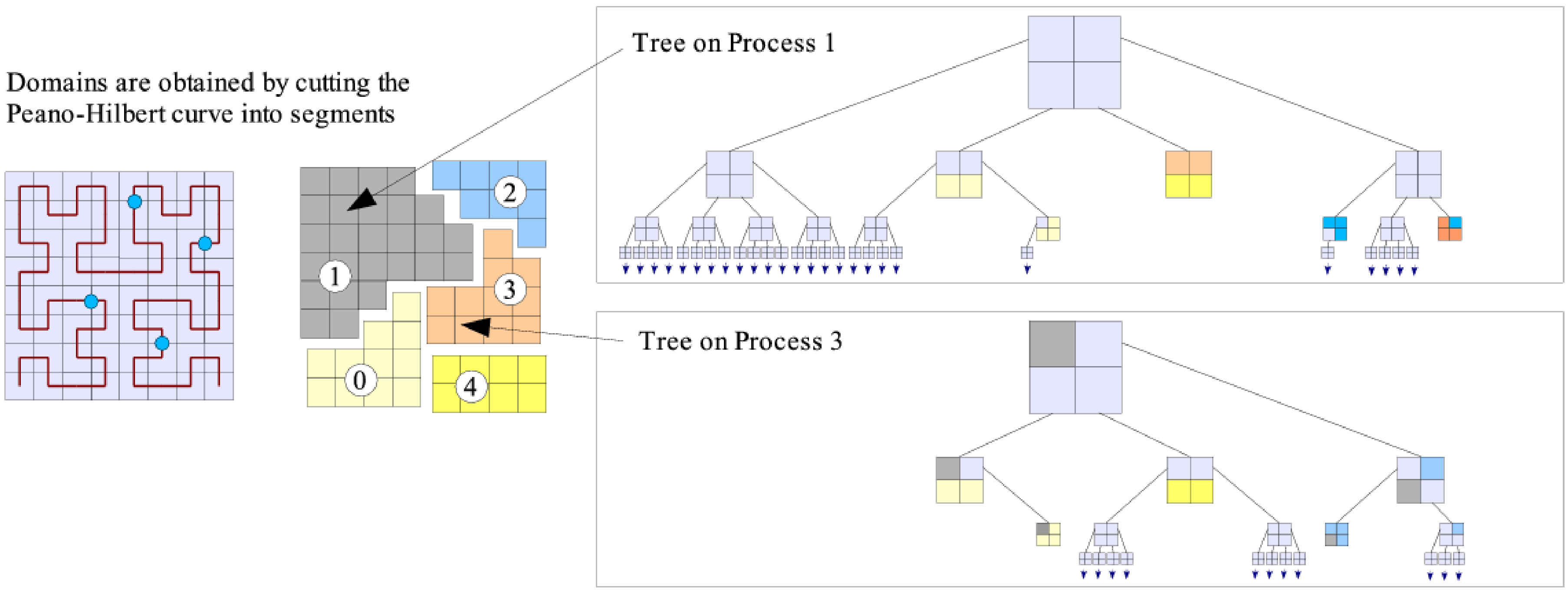

The FLTROUNDOFFREDUCTION option can make simulation results binary invariant when the number of processors is changed

INTRICACIES OF FLOATING POINT ARITHMETIC

On a computer, real numbers are approximated by floating point numbers

a 32 bit float

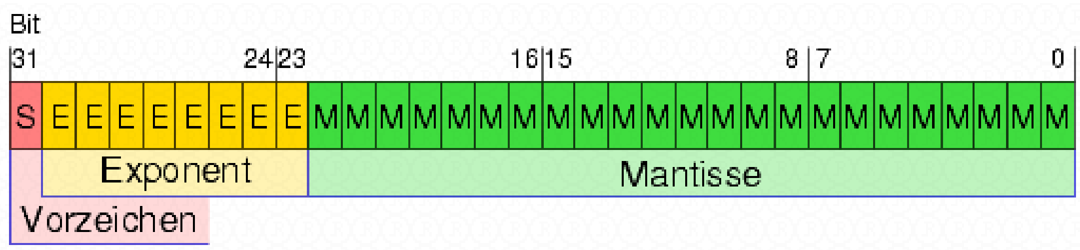

$$v = (-1)^s \cdot (1{,}m_0 m_1 m_2 \ldots) \cdot 2^{e_0 e_1 e_2 \ldots - a}$$

Mathematical operations regularly lead out of the space of these numbers.
This results in **round-off** errors.

One result of this is that the law of associativity for simple additions doesn't hold on a computer.

$$A + (B + C) \neq (A + B) + C$$

As a result of parallelization, partial forces may be computed by several processors

THE FORCE SUM IN THE TREE ALGORITHM

The tree-walk results in typically several hundred partial forces

Situation 1:

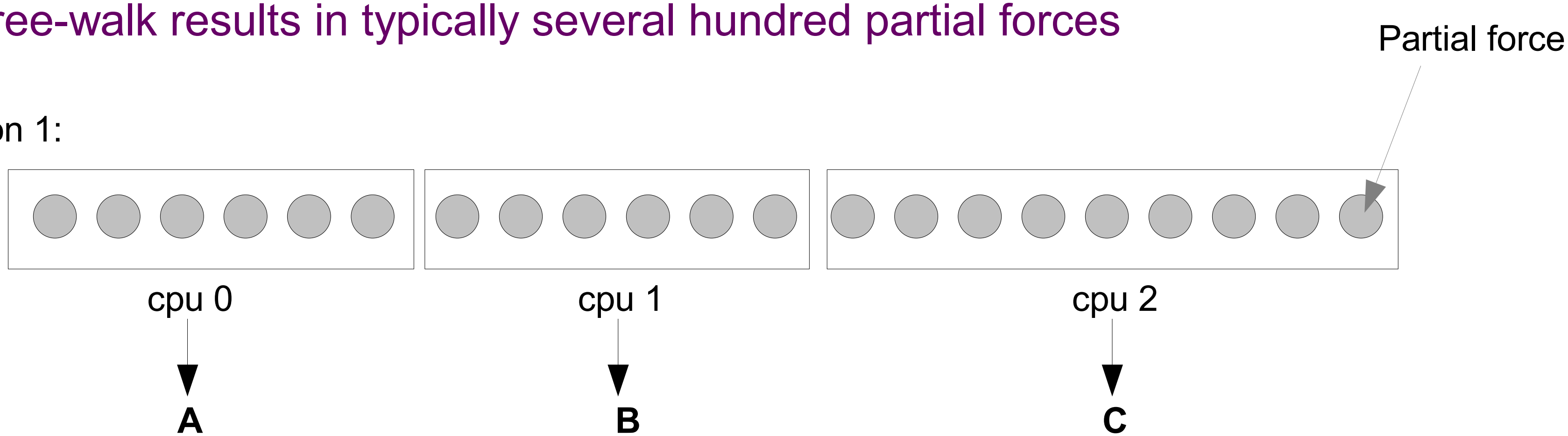

Situation 1:

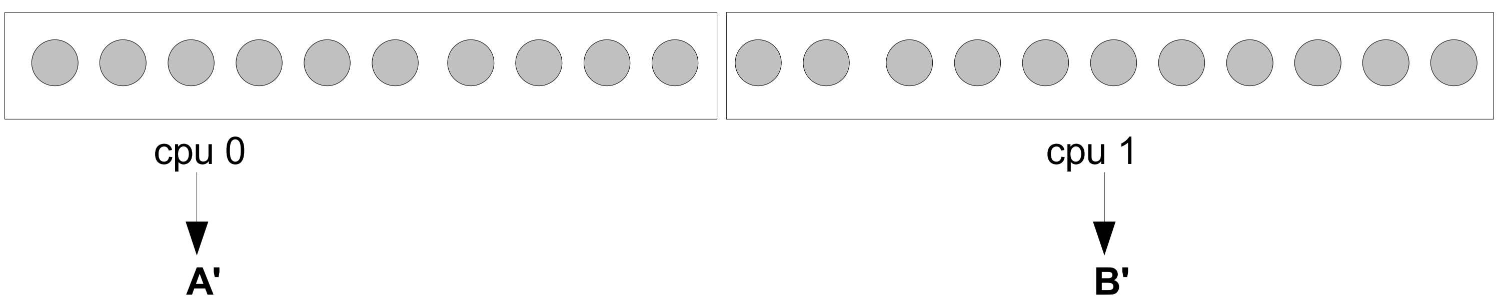

When the domain decomposition is changed, round-off differences are introduced into the results

$$A + B + C \neq A' + B'$$

Using double-double precision, the round off difference can be eliminated

THE FORCE SUM USING DOUBLE-DOUBLE PRECISION

The tree-walk computes several hundred partial forces, which are all **double precision** values. The set of numbers is identical when the domain decomposition or number of processors is changes.

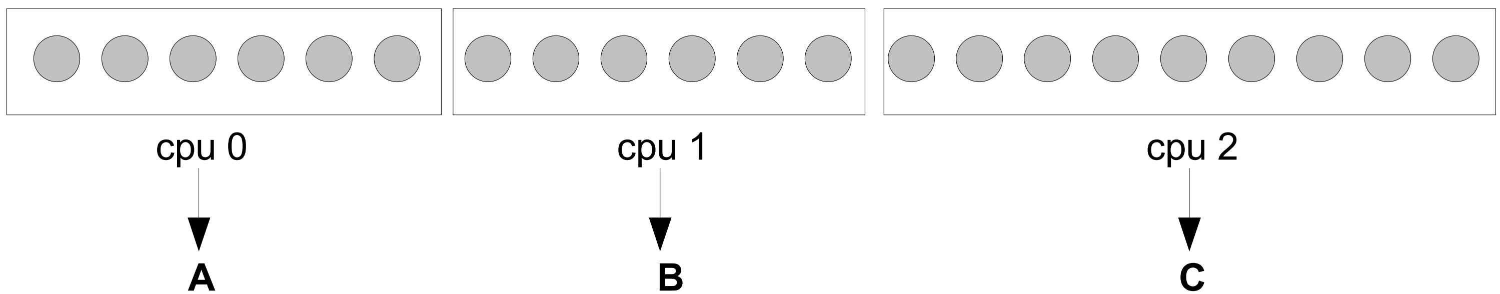

Each CPU now computes the sum in **quad** precision (128 bit, with 96 bit mantisse, “double-double”)

Then the result is added, obtaining a **quad** precision result, with a typical round-off error of a few times 10^{-34}. As before, this round-off may change when the number of CPUs is changed.

However, now we **reduce the precision** of the result to double-precision, i.e. we round to the nearest representable double-precision floating point number.

Since the mean relative spacing of such numbers is 10^{-17}, much larger than the double-double round off, we always round to the same number. (Except in one out of 10^{17} cases, which is *very* very *rare.*)

For the final result we then have

$$\mathbf{A + B + C \;\; = \;\; A' + B'}$$

Substructure in simulations

Once sufficiently high force- and mass resolution is used, the “overmerging” problem of dark matter halos can be overcome

THE APPEARENCE OF SUBHALOS IN HIGH-RESOLUTION SIMULATIONS

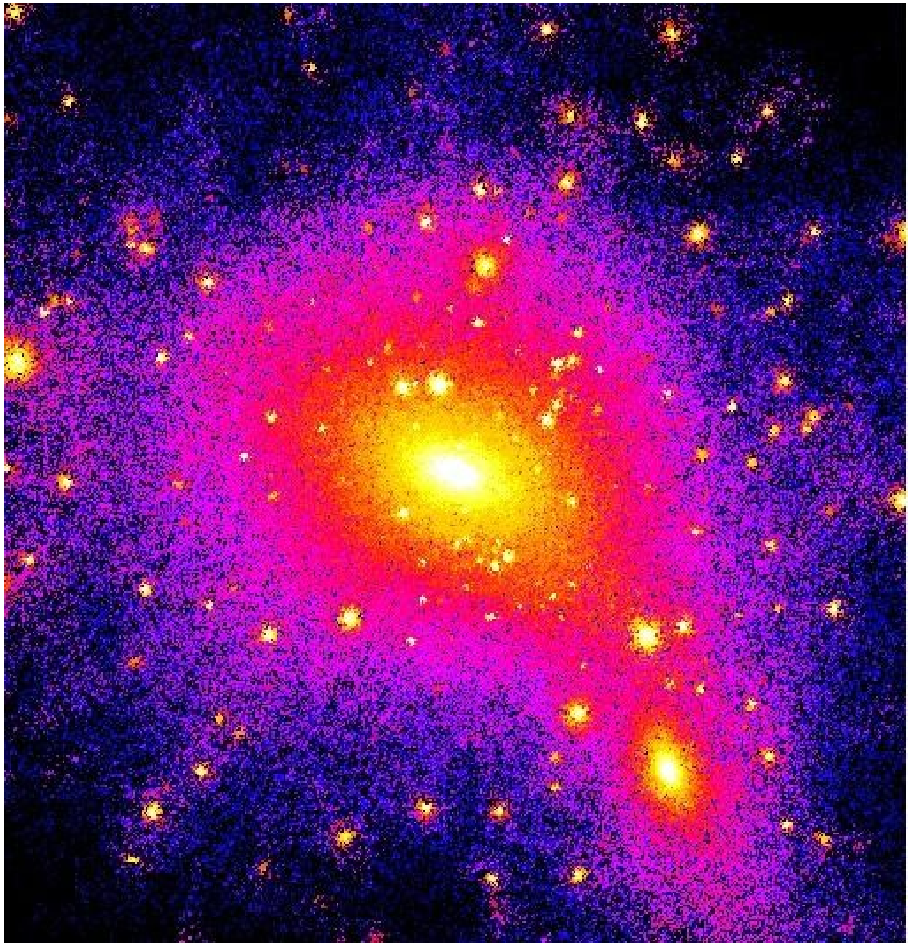

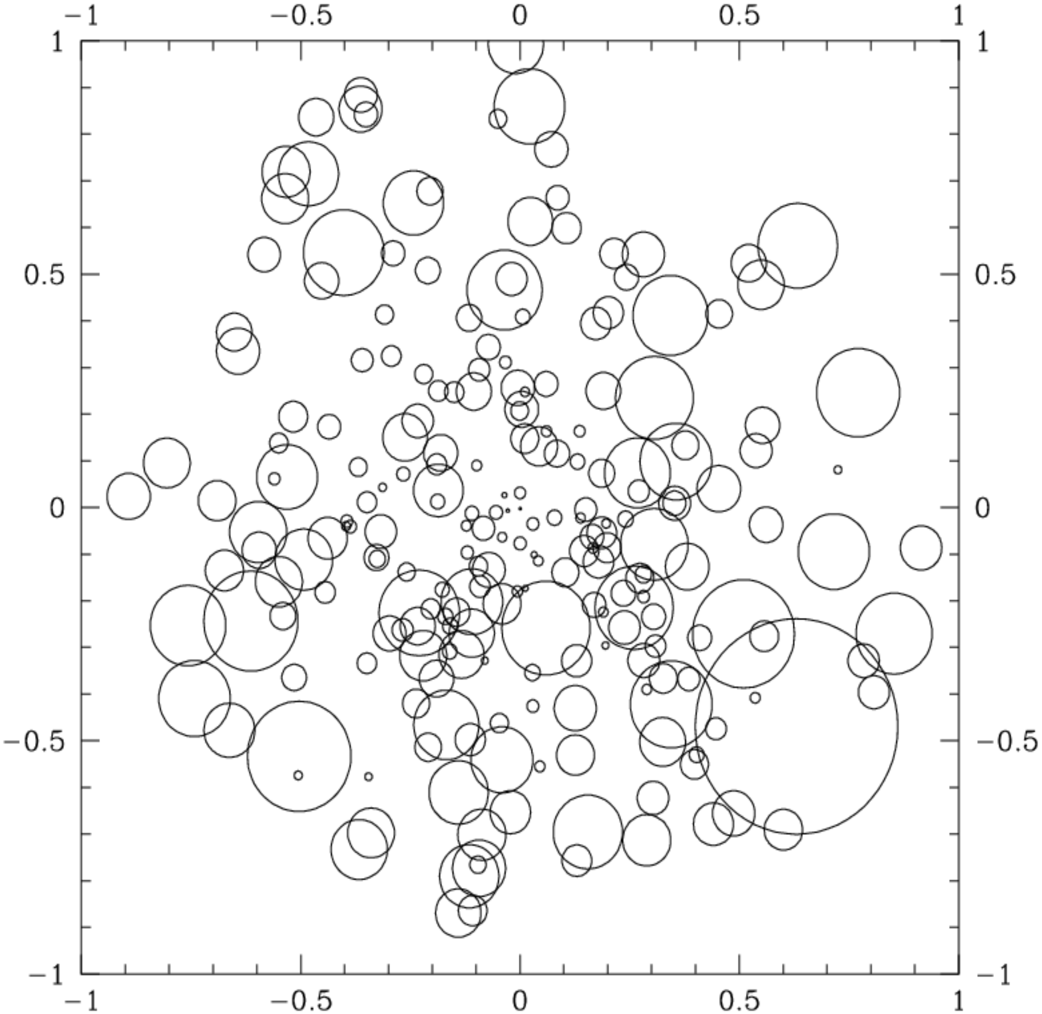

Ghigna et al. (1998)

Klypin et al. (1999), Moore et al. (1999)

Simulated dark matter halos are not spherically symmetric, nor does their structure look as simple as assumed in the analytic models models

DARK MATTER DISTRIBUTION IN A HIGH-RESOLUTION "MILKY WAY" HALO

N-body simulations find a universal profile that is not a power-law

THE NFW-PROFILE

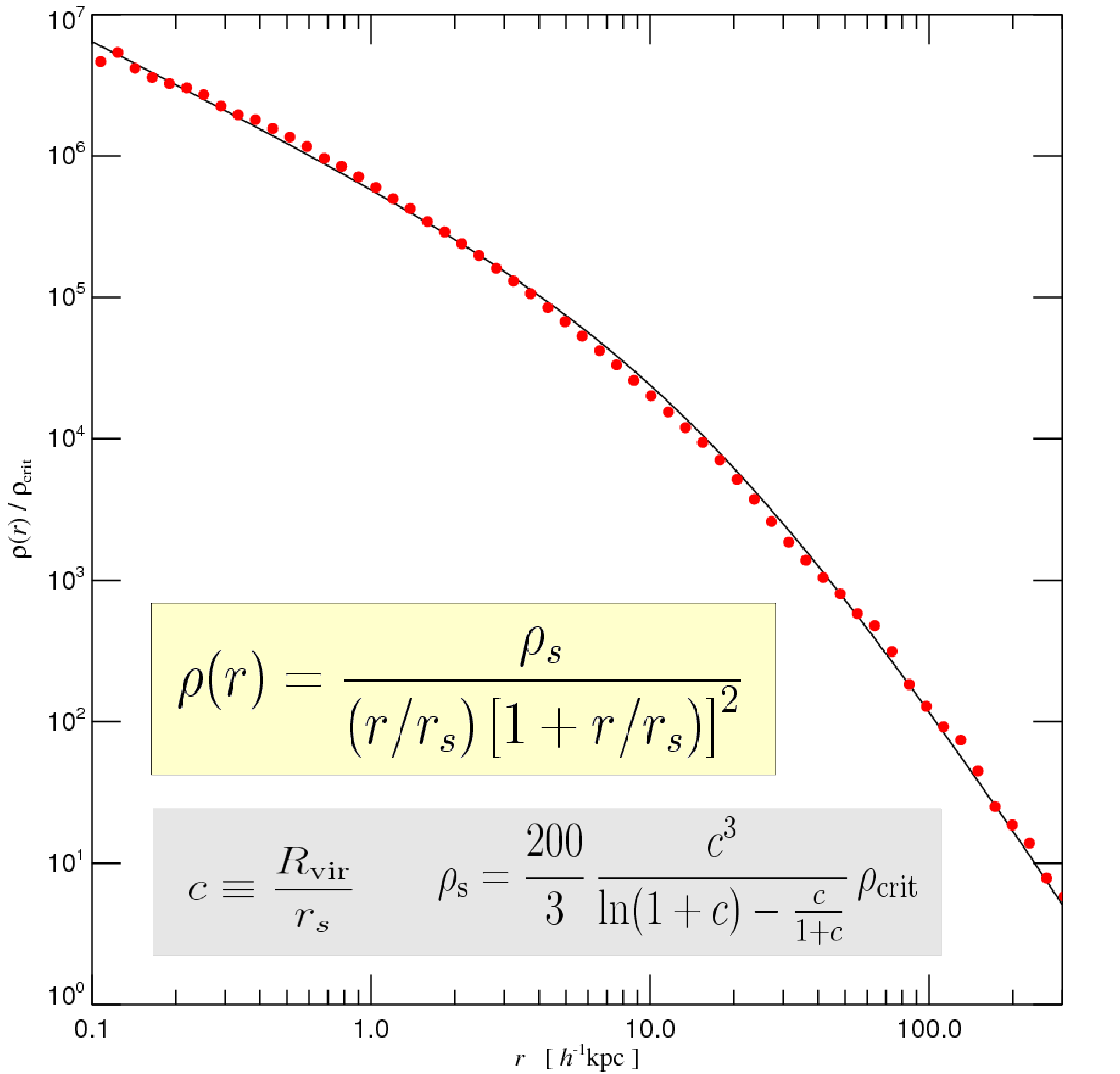

Halos formed in high-resolution simulations of cold dark matter show rich substructure

SUBHALOS IN A RICH CLUSTER

~ 20 million particles within virial radius of cluster

Springel, White, Kauffmann, Tormen (1999)

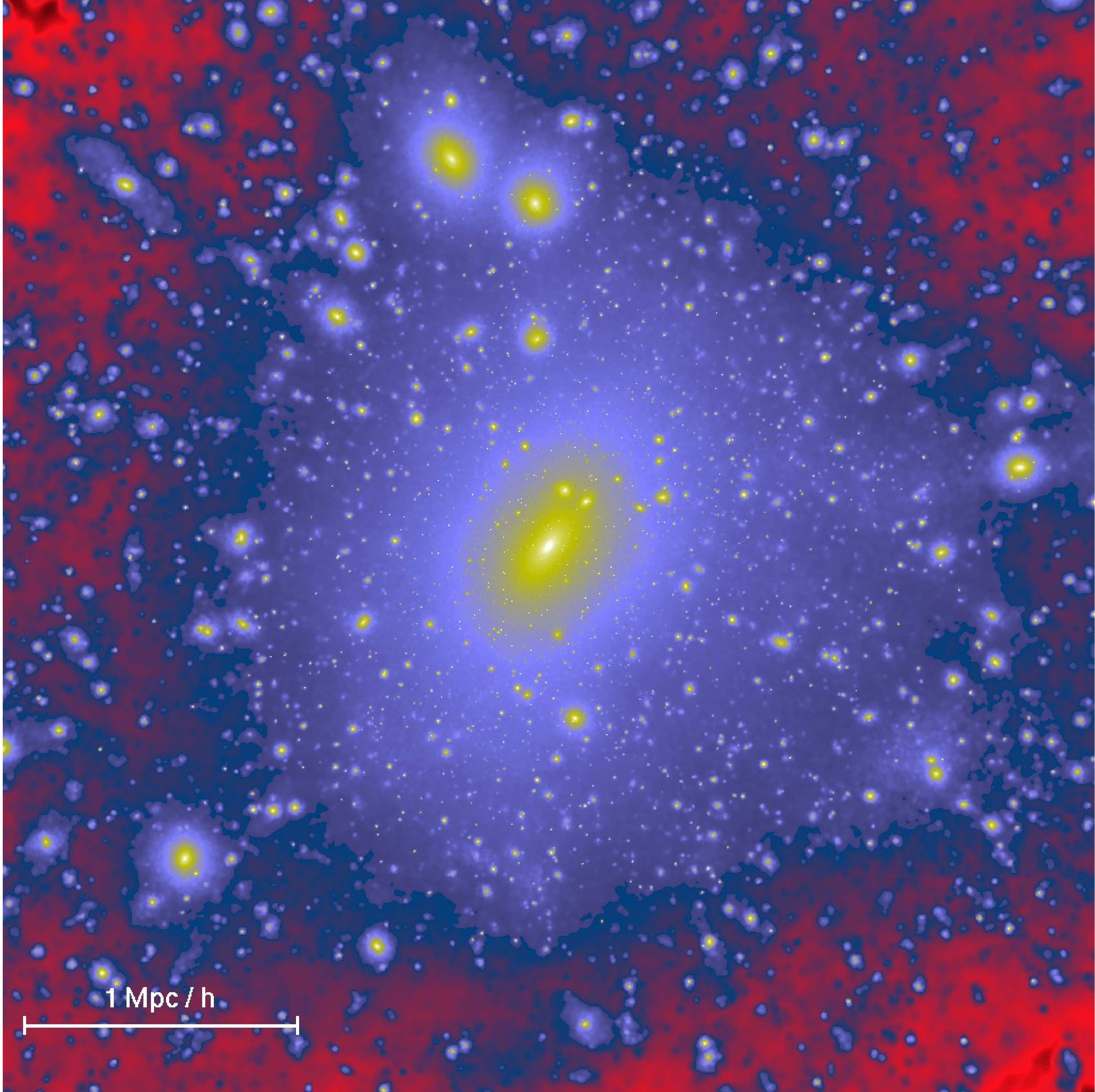

Even in the central regions, substructures can still be found

SUBHALOS AROUND A CLUSTER CENTRE

~ 20 million particles within virial radius of cluster

Springel, White, Kauffmann, Tormen (1999)

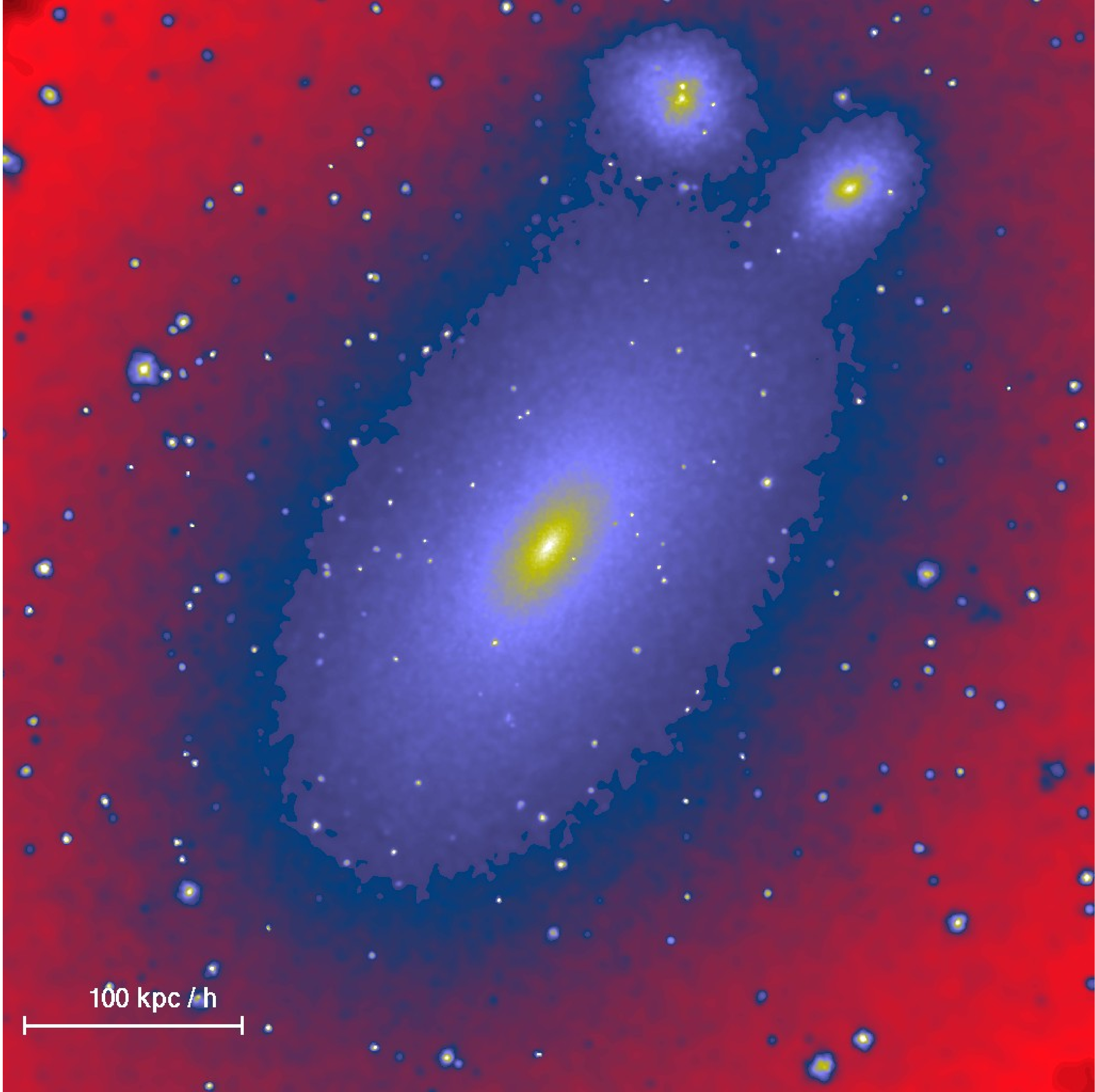

Early on, the similarity of the substructure population of halos of widely different mass has been pointed out

SUBHALOS IN A RICH CLUSTER AND A MILKY WAY-SIZED HALO

Moore et al. (1999)

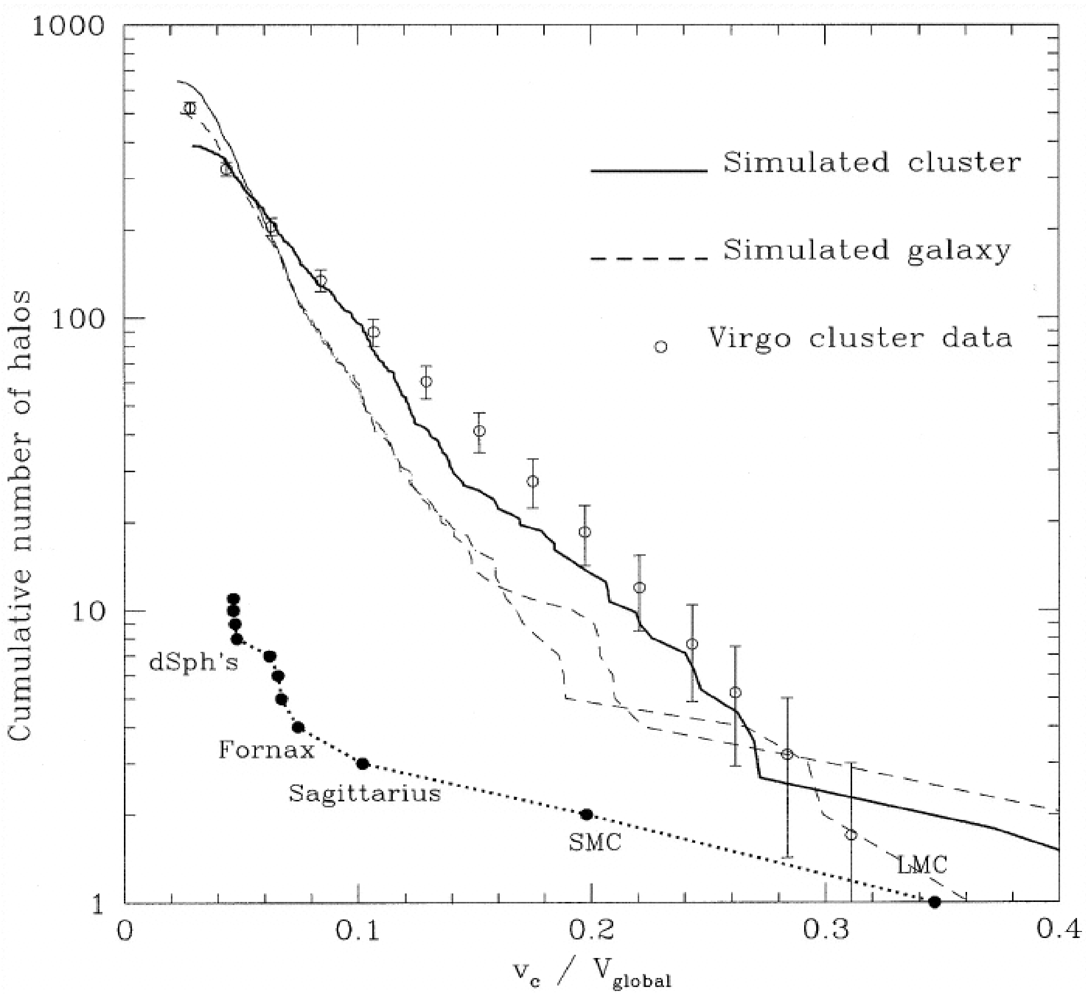

Halo with 5×10^{14} $M_\odot$

Halo with 2×10^{12} $M_\odot$

Klypin et al. (1999), Moore et al. (1999): **Where are all the missing satellites?**

Detecting Substructure: SUBFIND

Different methods are in use to find substructures, but few checks of their systematic differences have been carried out

SUBSTRUCTURE DETECTION ALGORITHMS

SKID (Stadel 1998)	Particles are moved along a local density gradient, and then grouped by FOF, followed by gravitational unbinding. (derived from DENMAX, Gelb & Bertschinger 1994)
HFOF (Gottloeber et al. 1999)	Plain FOF is applied with a hierarchy of linking lengths
BDM (Klypin et al. 1999)	Local maxima in the density are identified (there are different possibilities for this), and then the bound set of particles in spherical apertures is determined
HOP (Eisenstein & Hut 1998)	A local density estimate is computed, and then particles are attached to their nearest neighbours. A set of rules connects and prunes the isolated groups.
SUBFIND (Springel et al. 2001)	Based on local density estimates, topological criteria are used to find isolated overdense regions which are then subjected to a gravitational unbinding procedure
MHF (Gill, Knebe & Gibson 2004)	An adaptive grid is used to locate density maxima. Around each maximum, a spherical aperture is grown until an upturn in the spherical density profile is detected. This is followed by gravitational unbinding and removal of subhalo duplicates.

Finding dark matter satellites in simulations is a non-trivial task

AN ALGORITHMIC TECHNIQUE FOR SUBHALO IDENTIFICATION

SUBFIND

(1) Estimate local DM density field

(2) Find locally overdense regions with topological method

(3) Subject each substructure candidate to a gravitational unbinding procedure

Subhalo finding (SUBFIND)

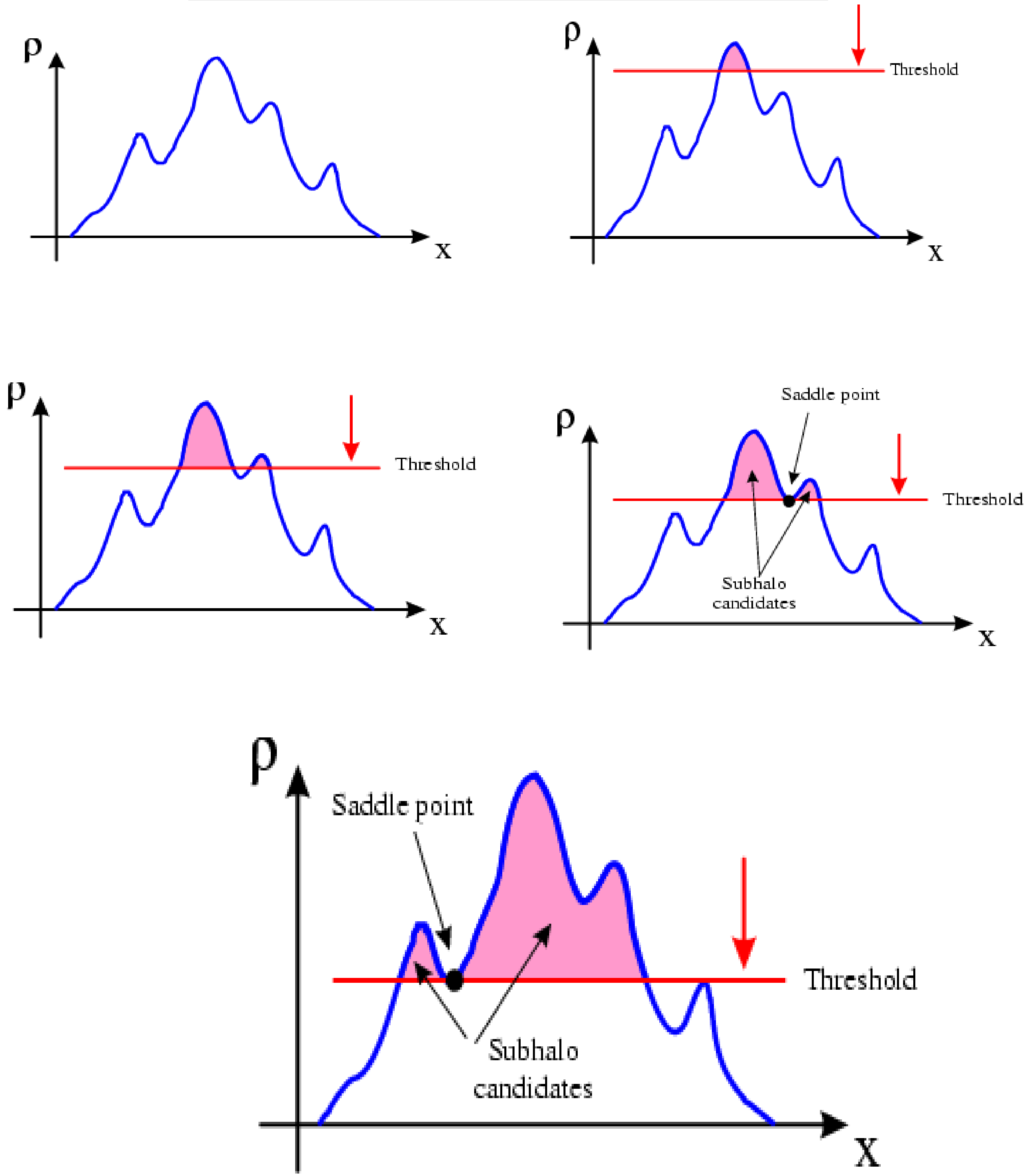

The subhalos formed in high-resolution simulations of cold dark matter can be reliably detected and extracted

SUBHALOS IN THE S2 CLUSTER IDENTIFIED WITH SUBFIND

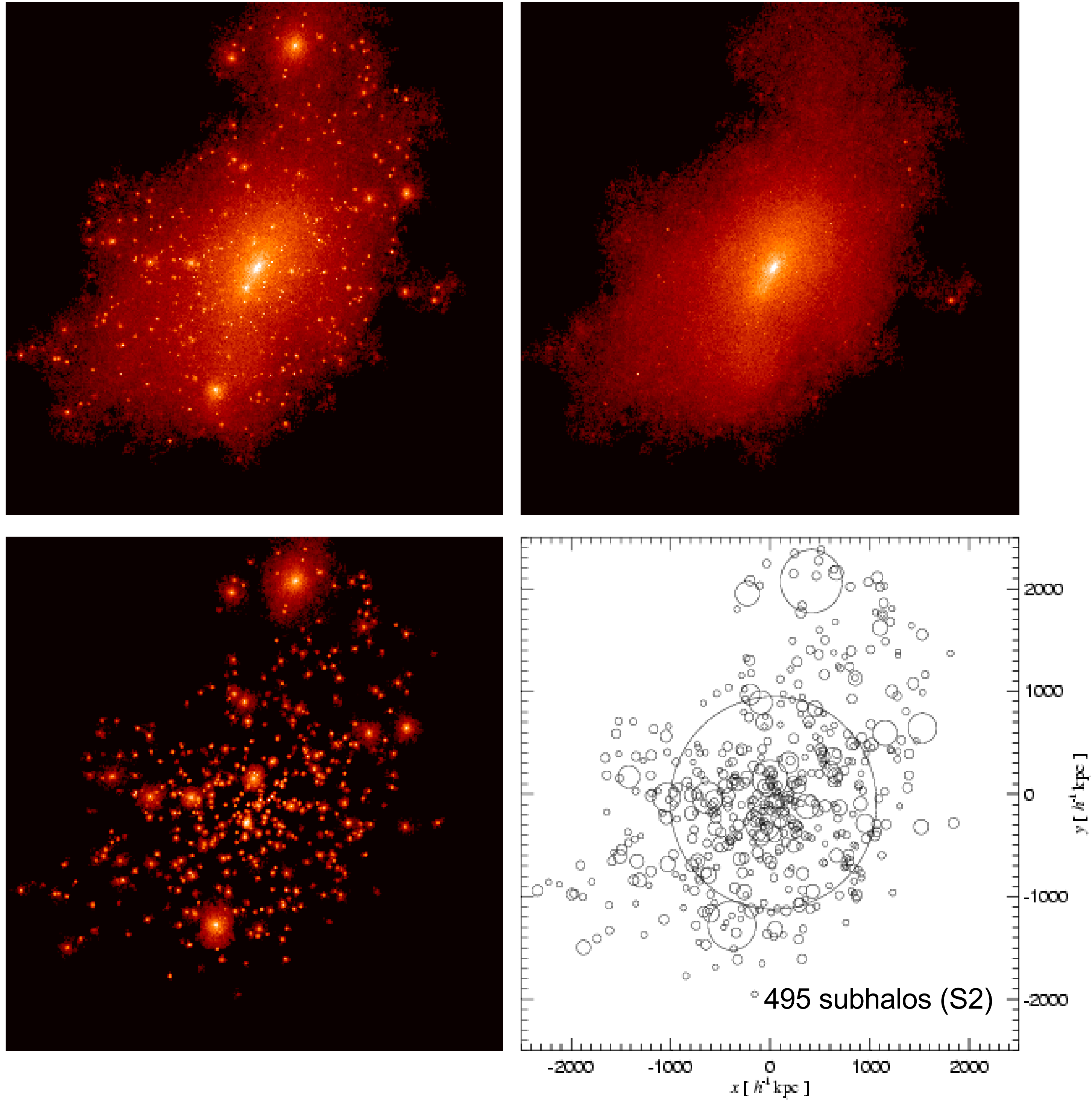

Abundance of substructure

The mass-function of subhalos contained in a halo is a power-law which is dominated by the massive end

SUBHALO ABUNDANCE

$$\frac{\mathrm{d}N}{\mathrm{d}m} \propto m^{-1.8}$$

authors appear to agree that

$$-1.7 \leq \alpha - 1.9$$

cluster	#subhalos
S1	118
S2	495
S3	1848
S4	4667

(Springel et al. 2001)

Differential mass-spectrum of subhalos

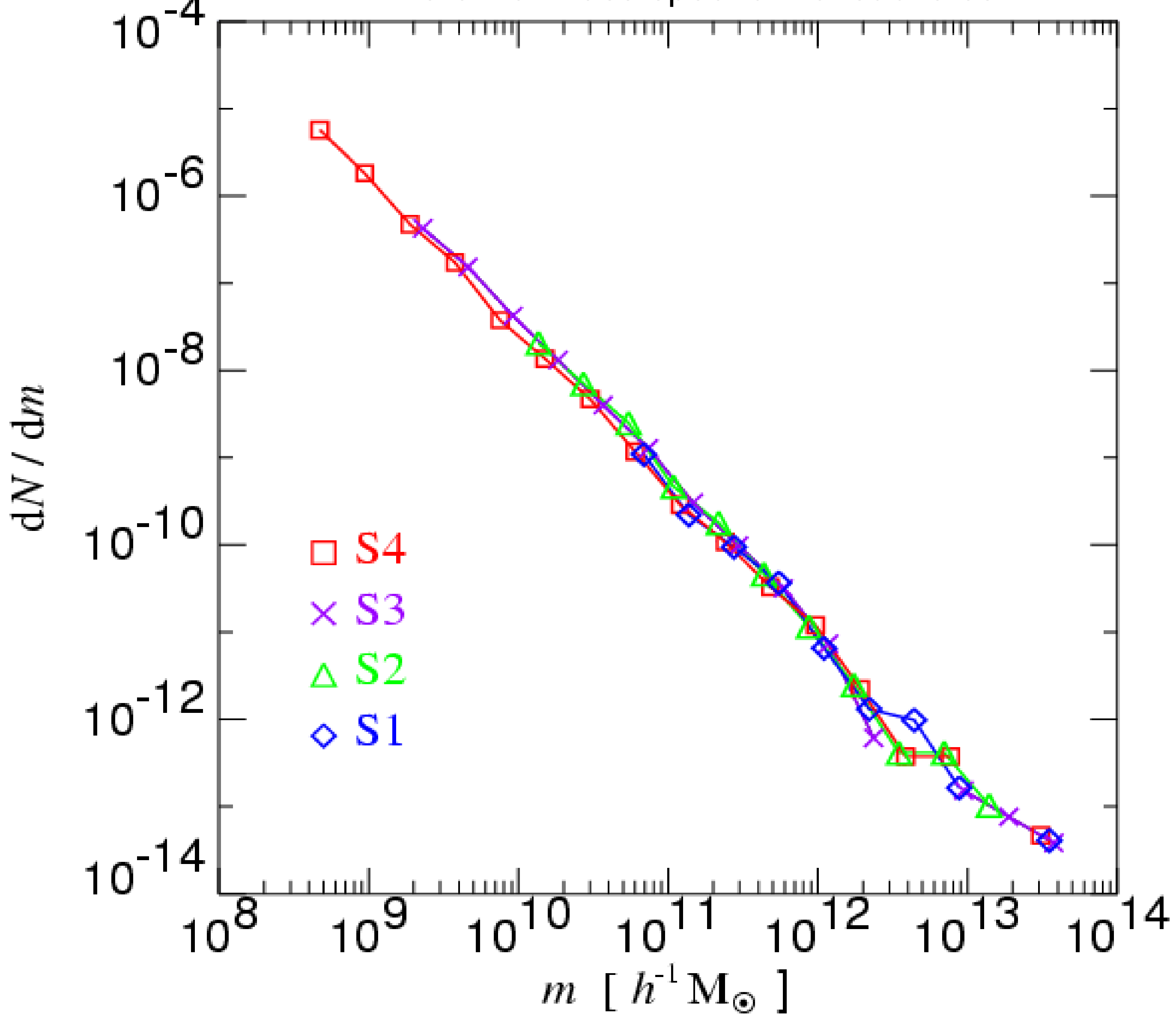

The mass-function of subhalos in halos of widely differing mass shows very similar behaviour

SUBHALO ABUNDANCE IN A RICH CLUSTER AND A MILKY WAY SIZED HALO

convergence study in rich cluster

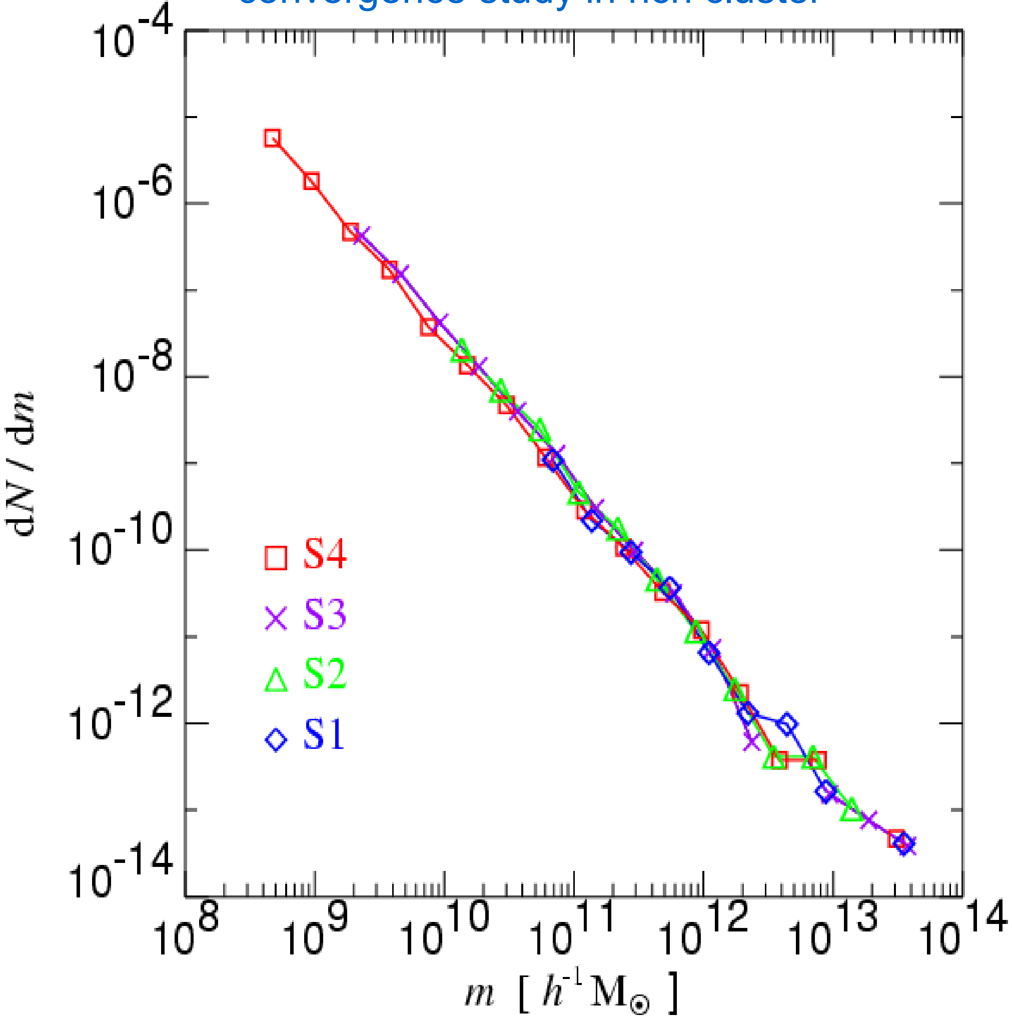

(Springel et al. 2001)

convergence study in Milky Way sized halo

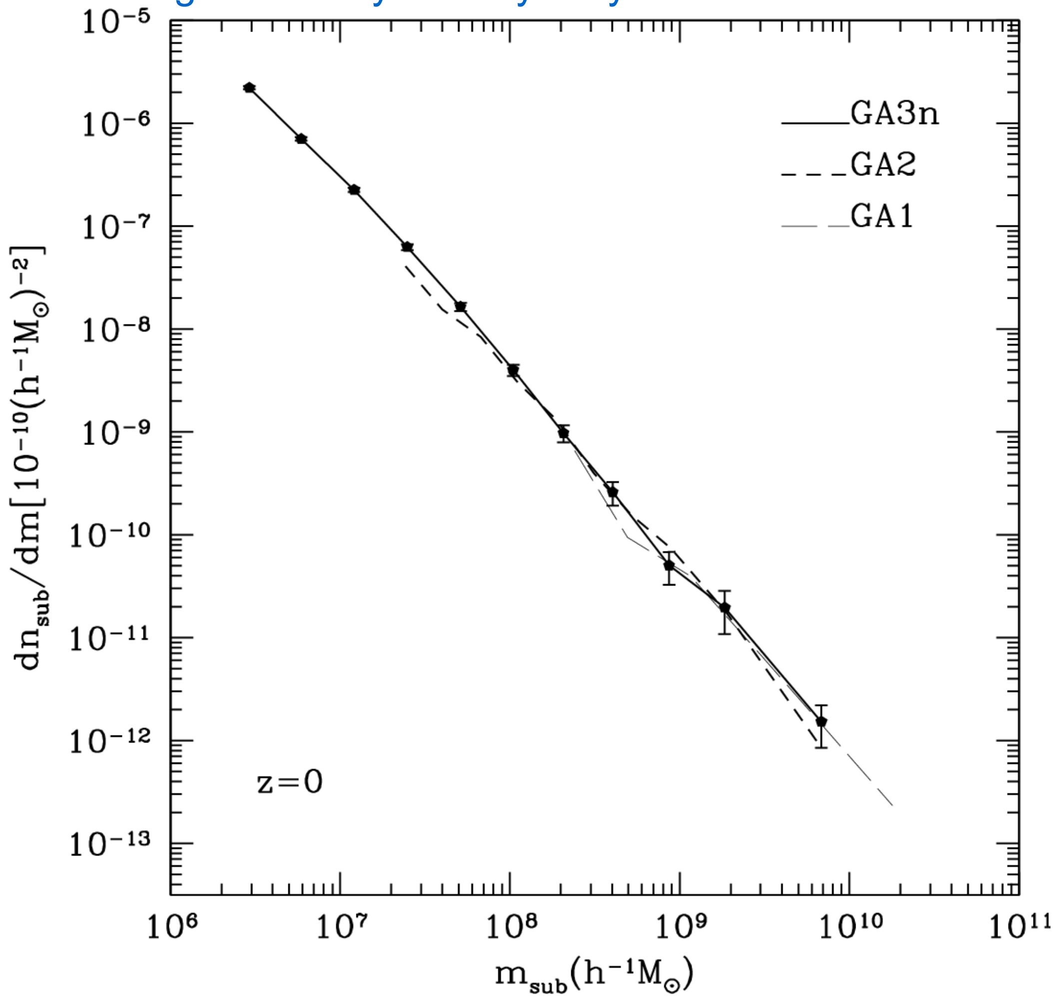

(Gao et al. 2004)

Using the “zoom” technique, a set of high-resolution halos on different mass scales has been computed

THE SIMULATION SET OF GAO ET AL. (2004)

- 8 high-res clusters, $m = 5.1 \times 10^8\,M_\odot/h$, $\epsilon = 5$ kpc/h
- A series of very high resolution simulation of a MW-sized halo (GA0-GA3)

	$GA0$	$GA1$	$GA2$	$GA3$
N_p	68323	637966	5953033	55564205
$m_p[h^{-1}\mathrm{M}_\odot]$	1.8×10^8	1.9×10^7	2.0×10^6	2.5×10^5
$\epsilon[h^{-1}\mathrm{kpc}]$	1.8	1.0	0.48	0.24

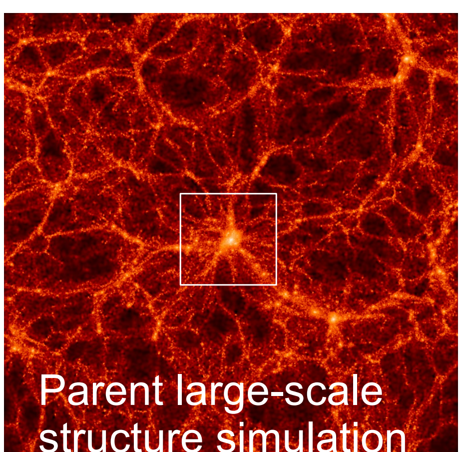
Parent large-scale structure simulation

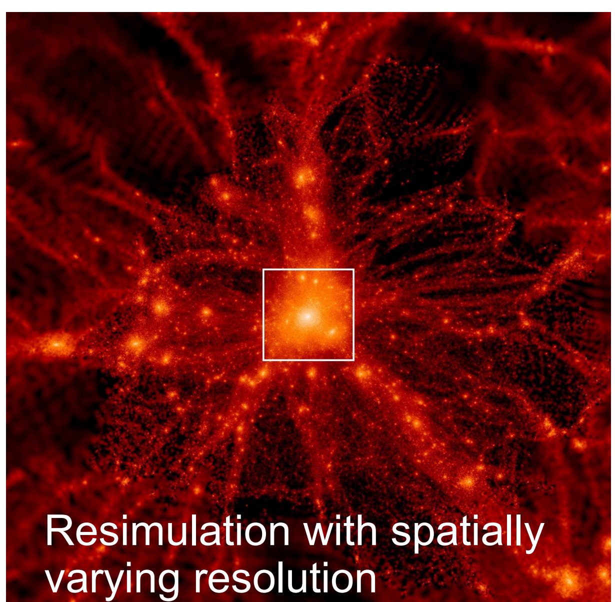
Resimulation with spatially varying resolution

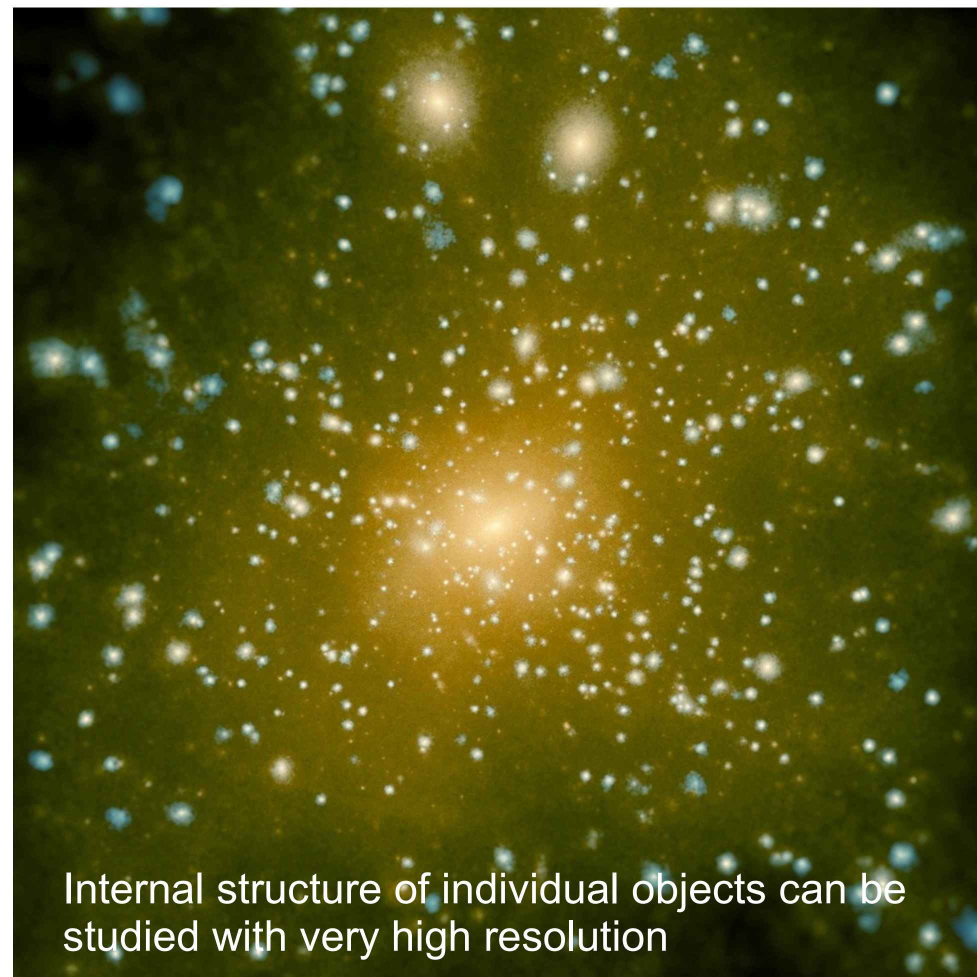
Internal structure of individual objects can be studied with very high resolution

The convergence in the velocity function suggests that we robustly measure the number of more massive subhalos

SUBHALO VELOCITY FUNCTION

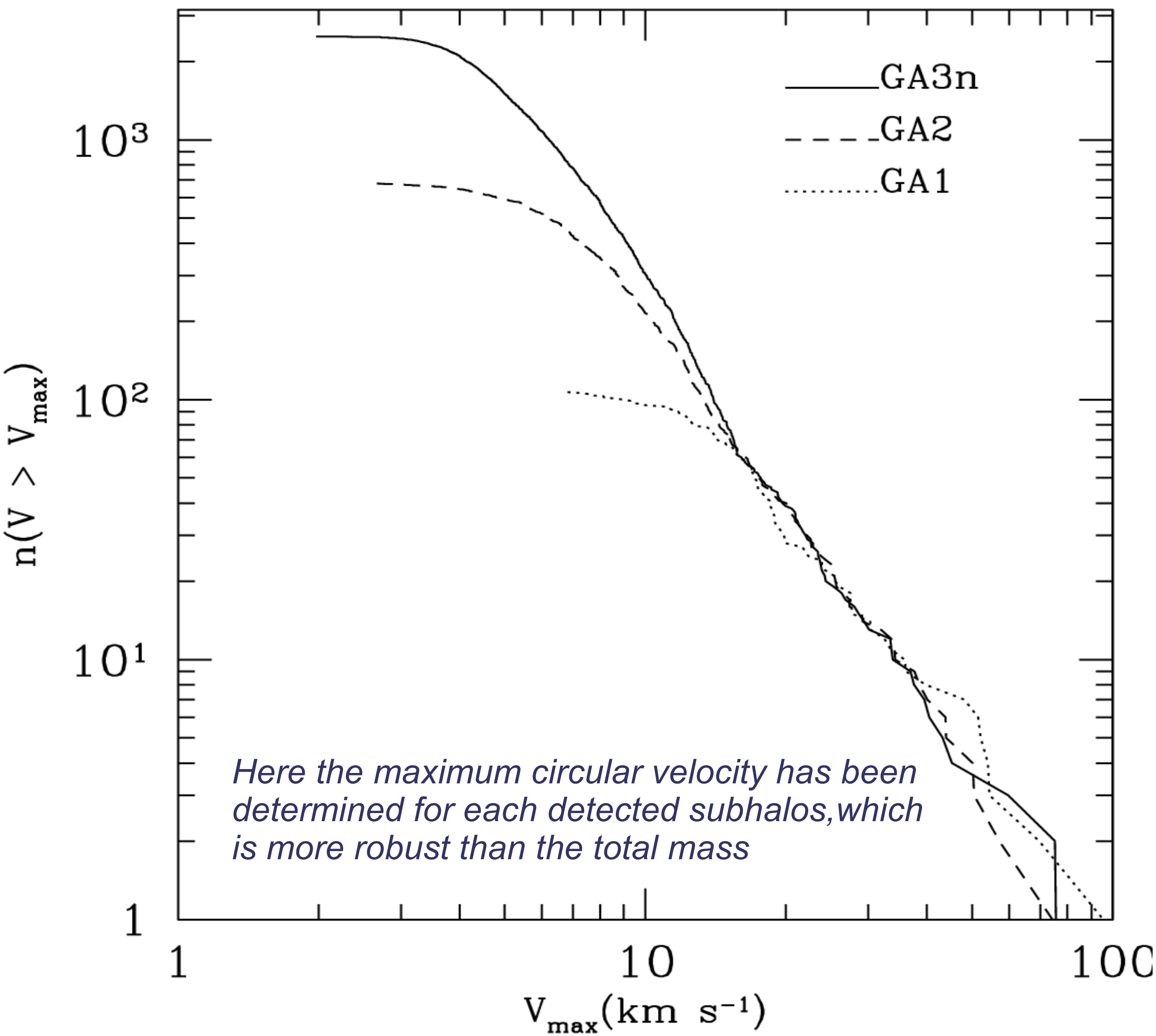

Here the maximum circular velocity has been determined for each detected subhalos,which is more robust than the total mass

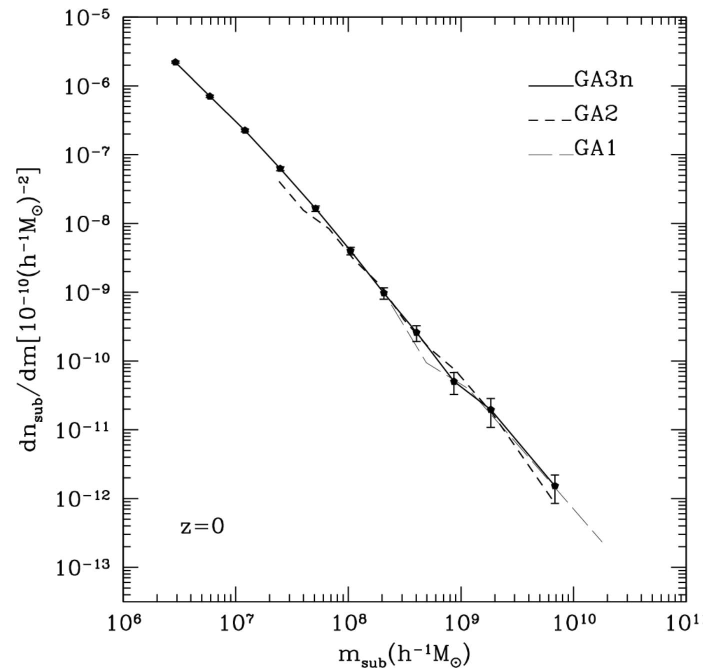

More massive halos show a slightly higher subhalo abundance

SUBHALO ABUNDANCE FOR SYSTEMS OF DIFFERENT MASS

differential

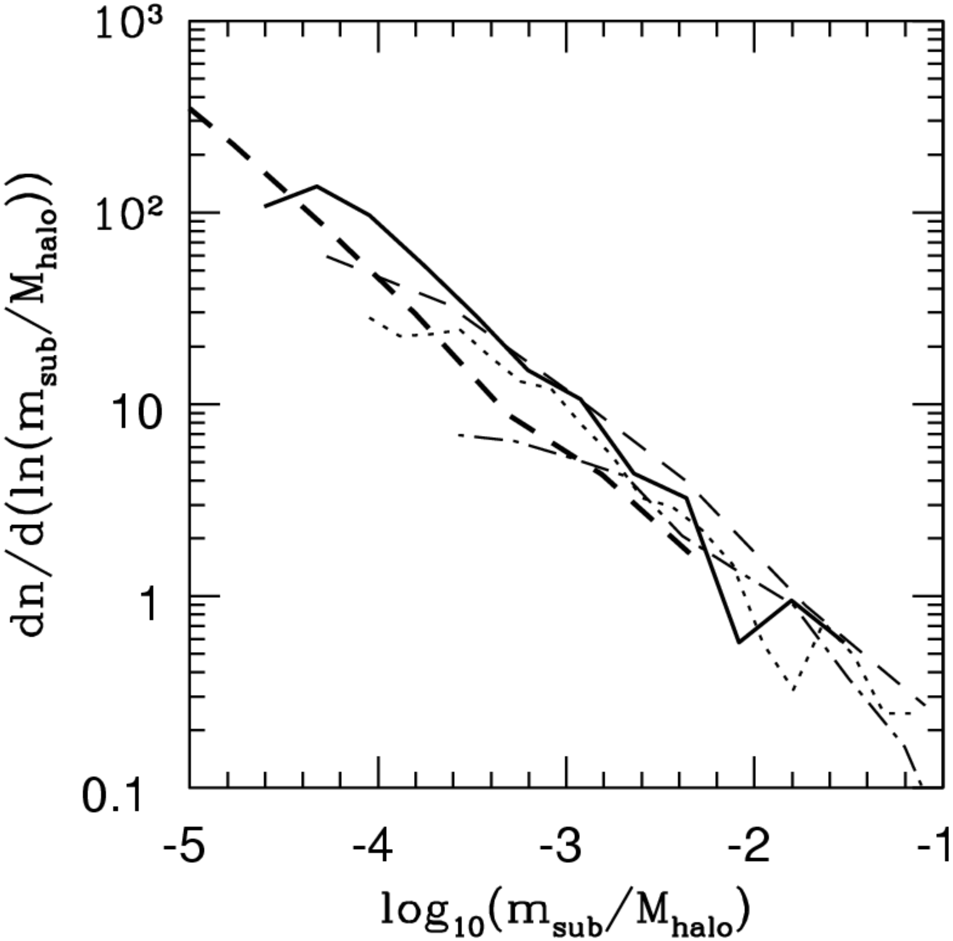

normalized subhalo mass

cumulative

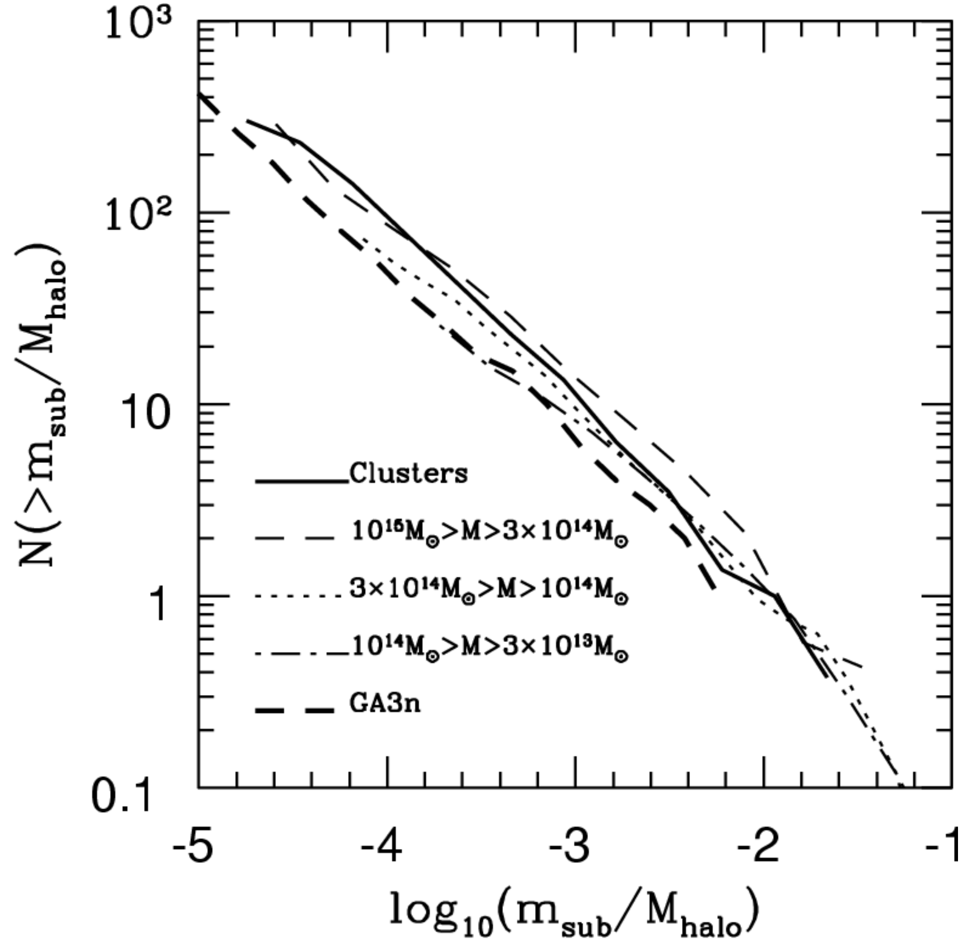

normalized subhalo mass

(Gao et al. 2004)

→ *Due to their later formation time, more massive halos retain more substructure.*

The scale-invariance of the subhalo populations of halos of different mass is broken.

The subhalo abundance per unit halo mass appears to be universal

SUBHALO ABUNDANCE FOR SYSTEMS OF DIFFERENT MASS

differential

abundance per parent halo mass

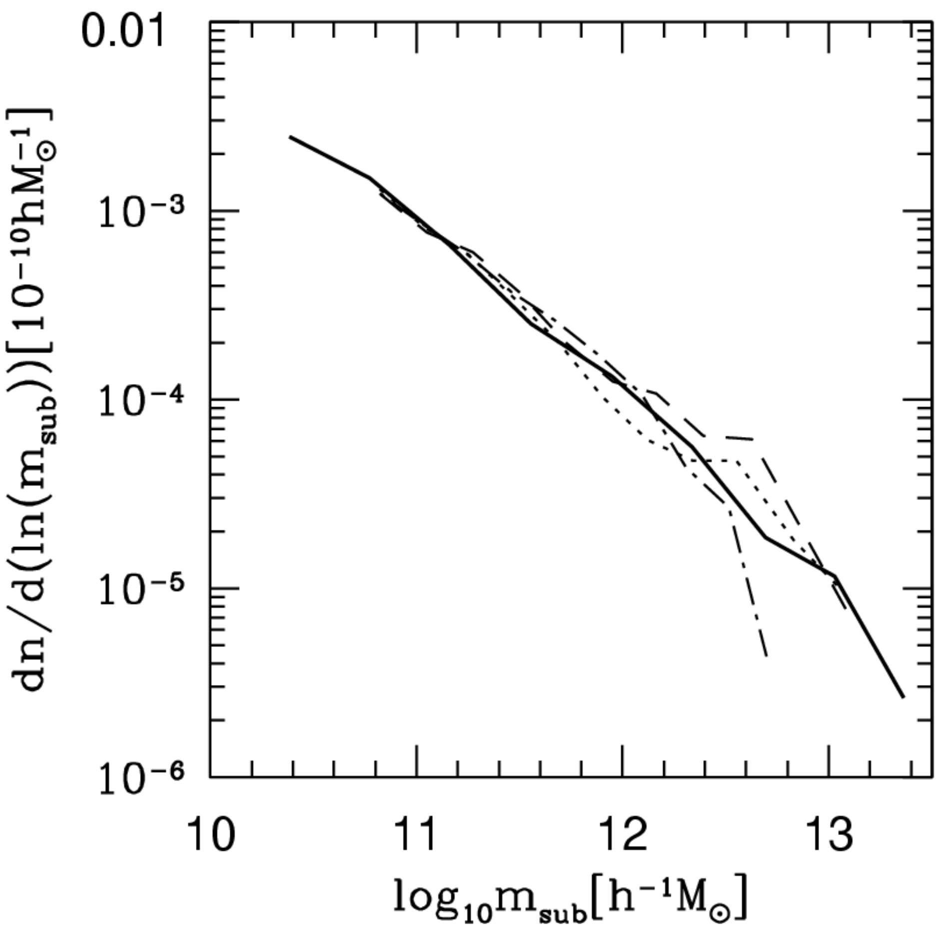

actual subhalo mass

cumulative

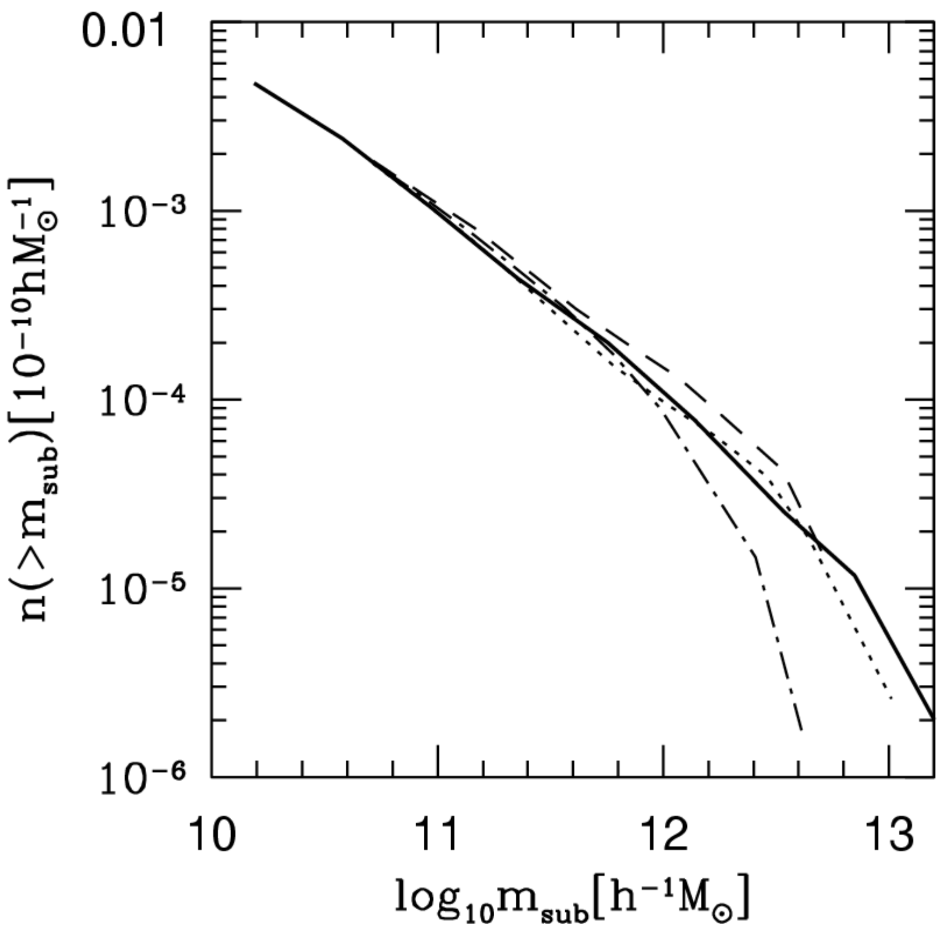

actual subhalo mass

The measurements are well described by the fitting function:

$$\frac{\mathrm{d}N}{\mathrm{d}m_{\mathrm{sub}}} \simeq 10^{-3.2}\left(\frac{m_{\mathrm{sub}}}{h^{-1}\mathrm{M}_\odot}\right)^{-1.9}\left(\frac{m_{\mathrm{parent}}}{h^{-1}\mathrm{M}_\odot}\right)$$

(a factor 2 for 3 decades in mass)

Explains trend with parent mass in: $\dfrac{\mathrm{d}N}{\mathrm{d}(m_{\mathrm{sub}}/m_{\mathrm{parent}})}$

The abundance of subhalos per unit parent mass is surprisingly close to the cosmological abundance of halos per unit mass in the Universe

SUBHALO ABUNDANCE FOR SYSTEMS OF DIFFERENT MASS

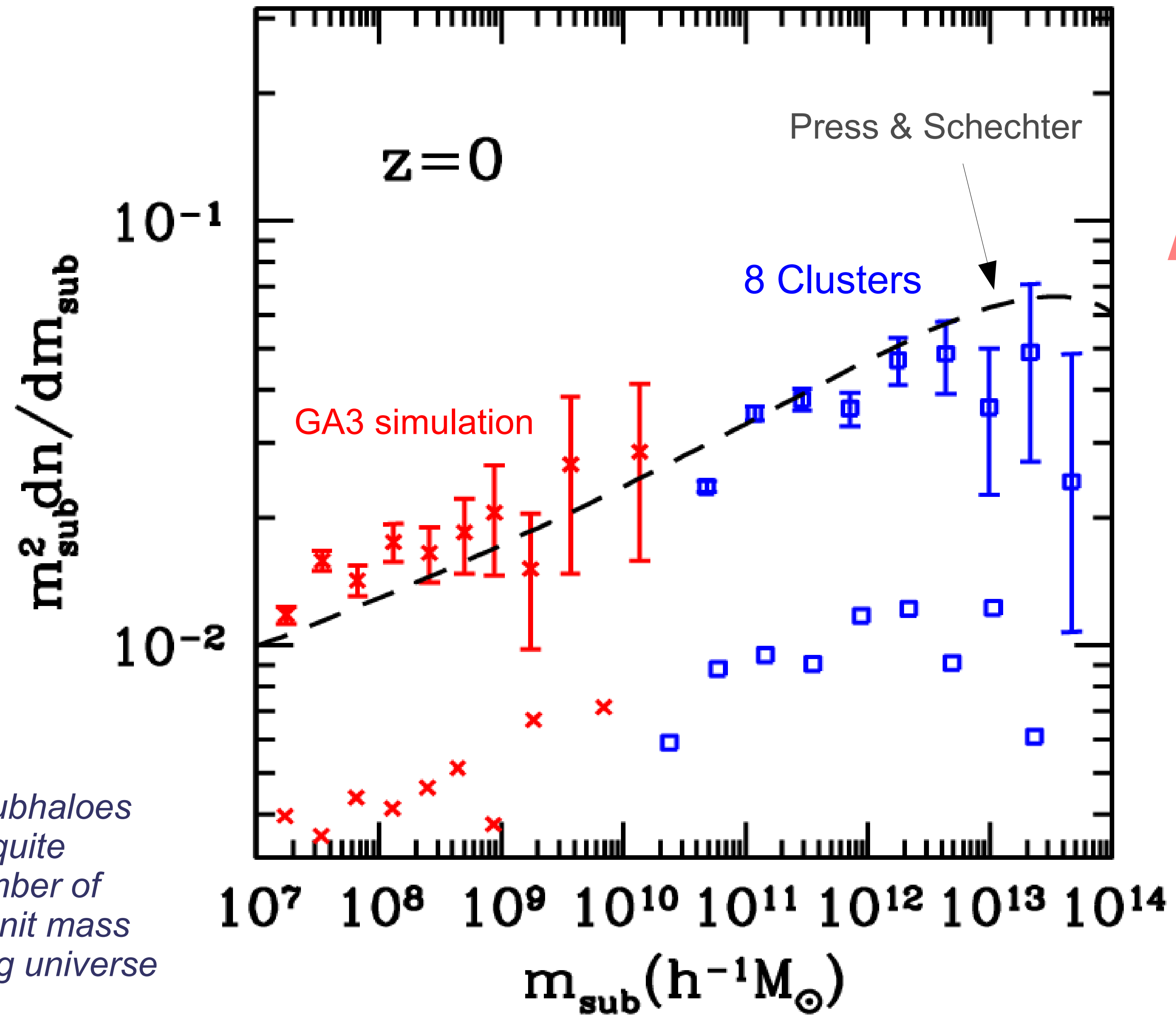

Subhalo masses boosted by factor 2

Note:
only subhalo mass above the local mean density in halo is counted by SUBFIND

The number of subhaloes per unit mass is quite similar to the number of small halos per unit mass in the surrounding universe

The close correspondence with the Press&Schechter/ Sheth&Tormen mass function is also obtained at higher redshift

SUBHALO ABUNDANCE AT DIFFERENT REDSHIFTS

Subhalo masses boosted by factor 2

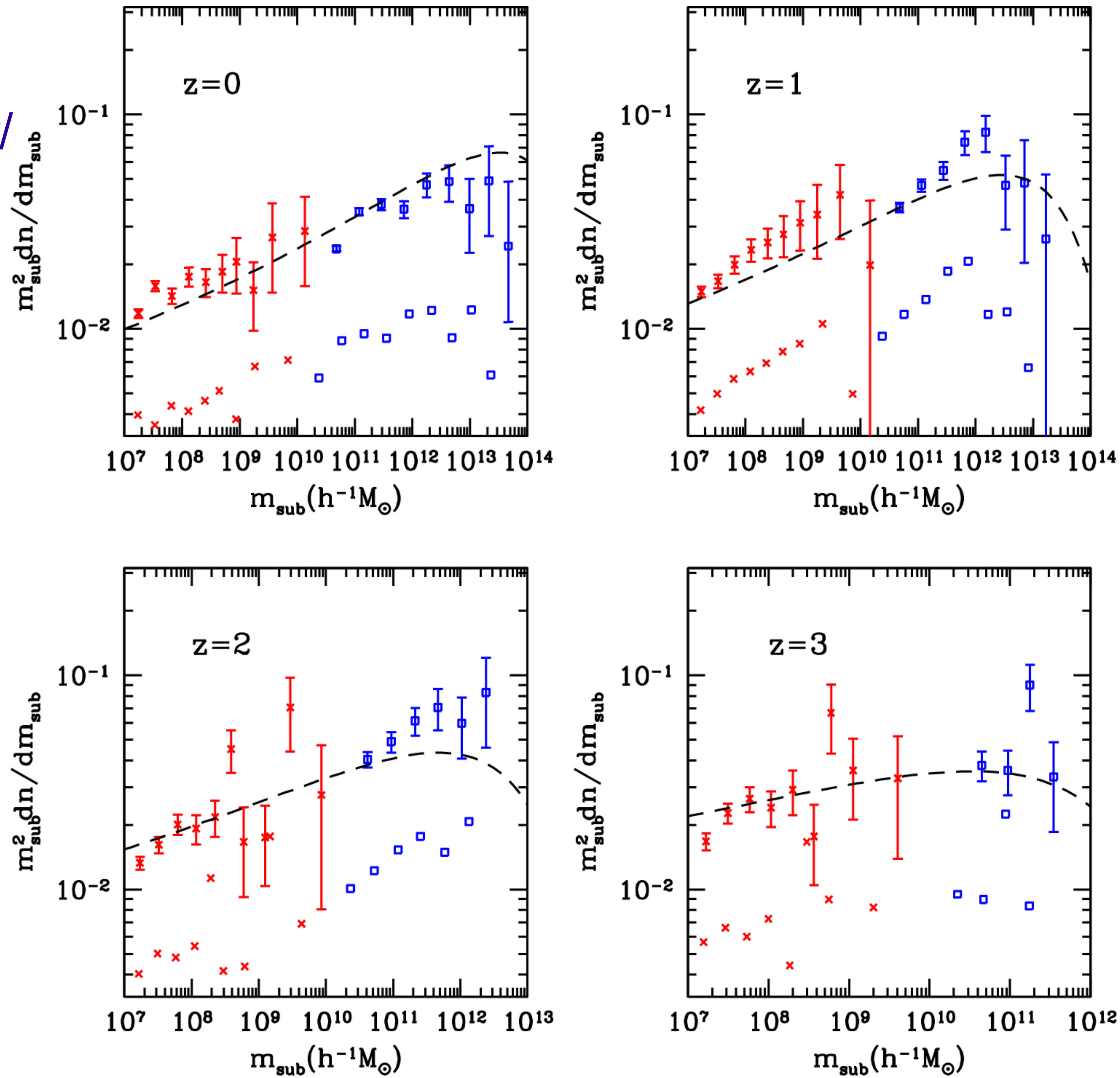

The mass fraction in substructure

Slightly conflicting results have been found for the mass fraction in subhalos

DIFFICULTIES IN DETERMINING THE SUBHALO MASS FRACTION

Ghigna et al. (1998): ~10-15 %

Moore et al. (2001): May approach unity

Springel et al. (2001): ~10 %

de Lucia et al. (2005): ~6-10 %

Obtaining precise mass fractions is problematic because:

- slope is just a bit above -2 (below it, mass fraction would diverge)
- there is large object-to-object variation because the most massive subhalos dominate the cumulative mass function
- result may be influenced by subhalo detection scheme

The mass fraction in subhalos

SUBHALO ABUNDANCE FOR SYSTEMS OF DIFFERENT MASS

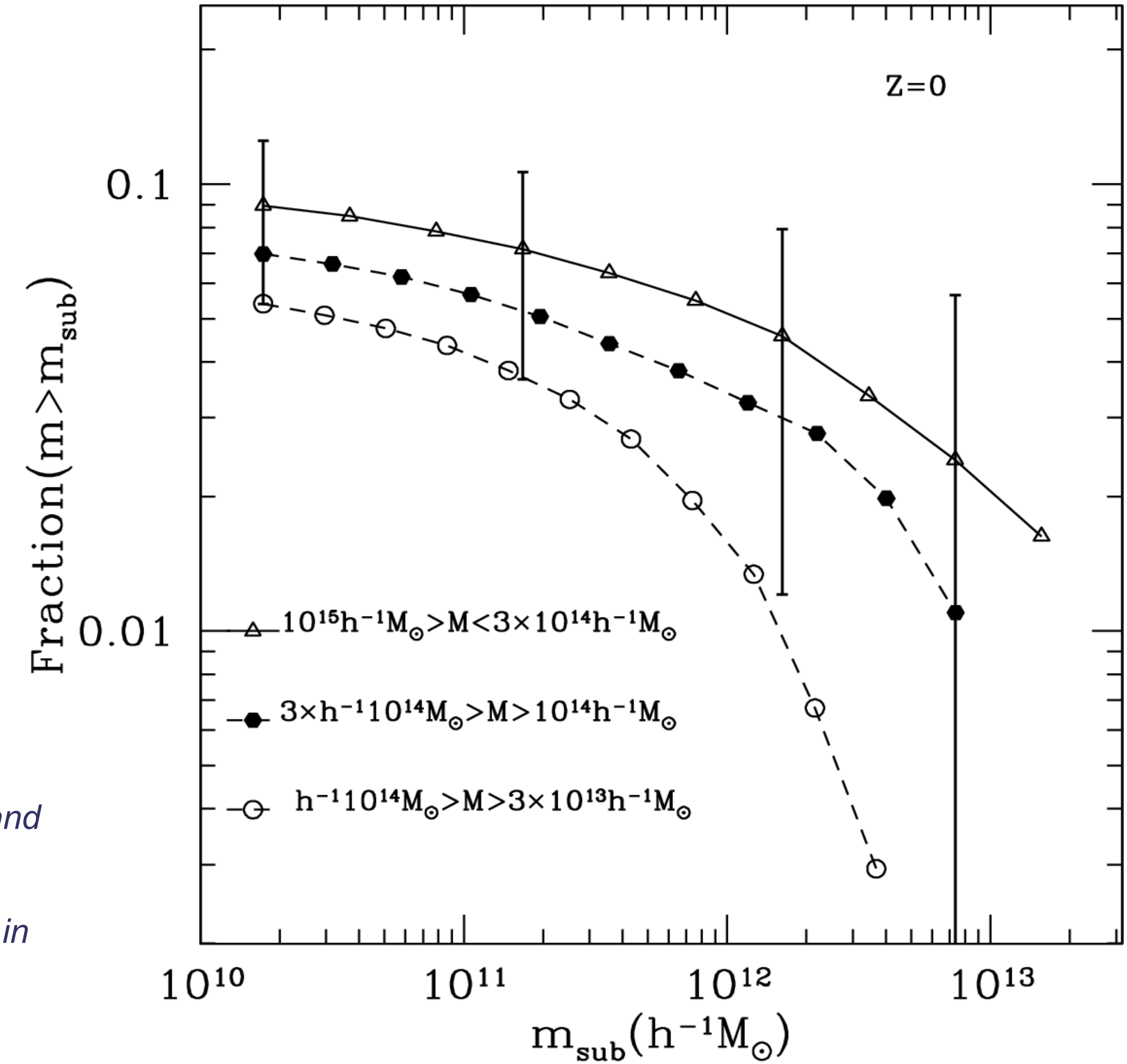

The cumulative fraction converges as smaller subhalos are included, and lower mass systems contain on average a smaller fraction of mass in subhalos.

The radial distribution of subhalos

Subhalos are substantially less concentrated than the dark matter as a whole

CUMULATIVE RADIAL DISTRIBUTION OF SUBHALOS FOR HALOS OF DIFFERENT MASS

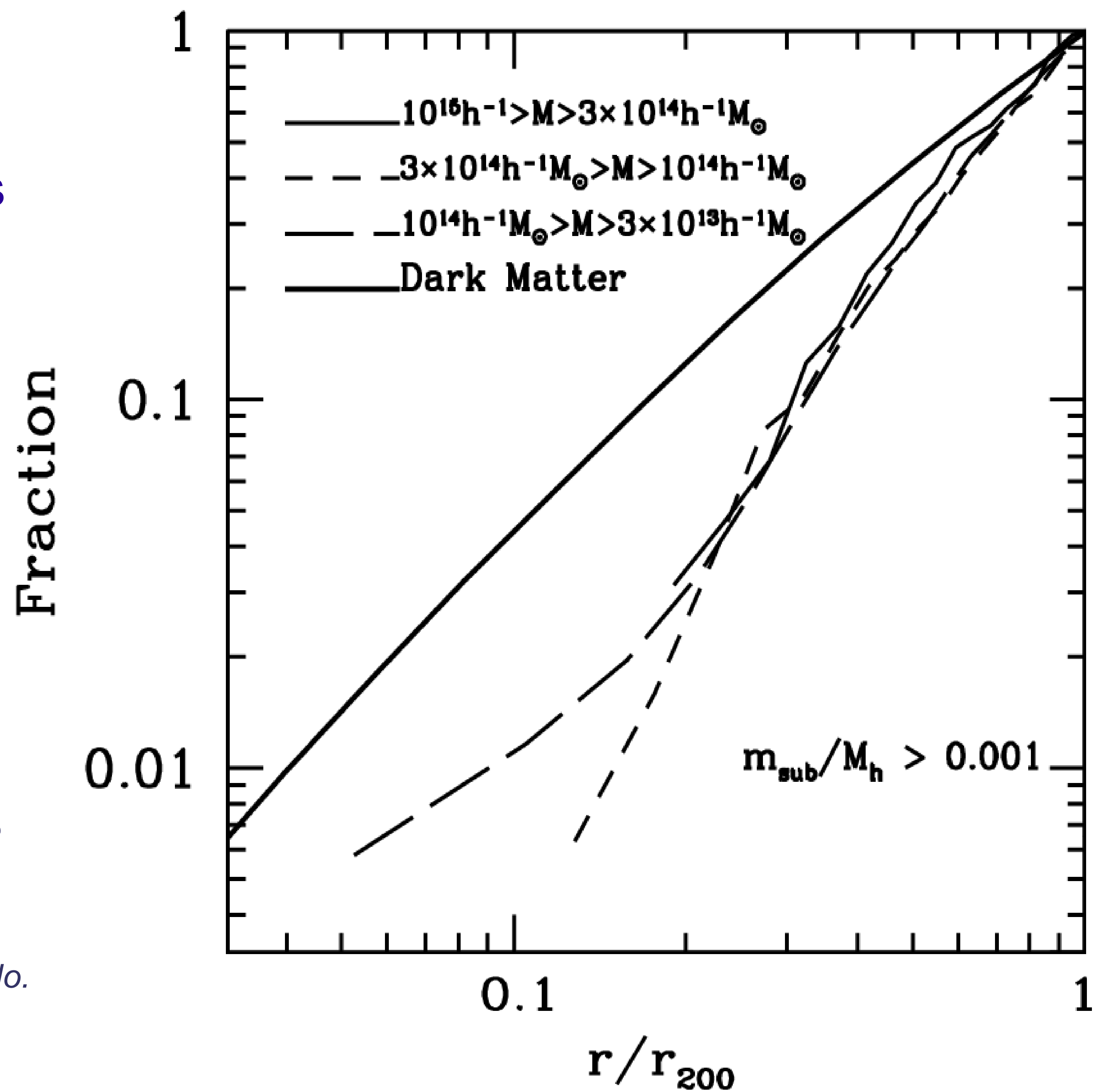

No significant dependence on the subhalo mass is found, and only very weak dependence on mass or concentration of parent halo.

Different subhalo samples show similar radial concentrations

RADIAL DISTRIBUTION OF SUBHALOS FOR SUBHALOS ABOVE DIFFERENT SIZE LIMITS

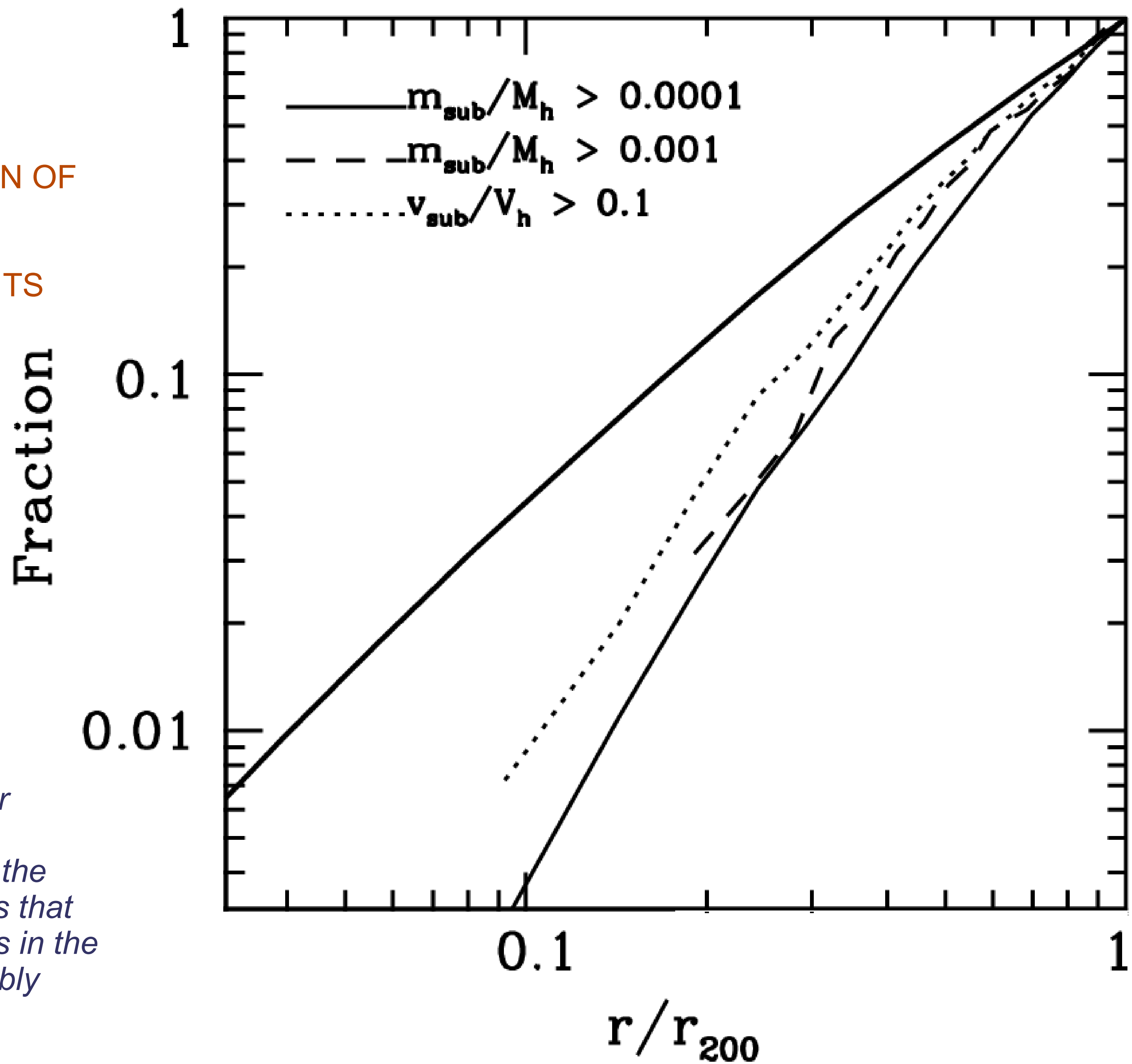

As the maximum circular velocity should be more robustly measured than the total mass, this suggests that our mass measurements in the inner parts are presumably biased low

Tracking Substructure over time

Analysis of many simulation outputs allows a measurement of the hierarchical build up of dark matter halos

FOLLOWING DARK MATTER IN TIME

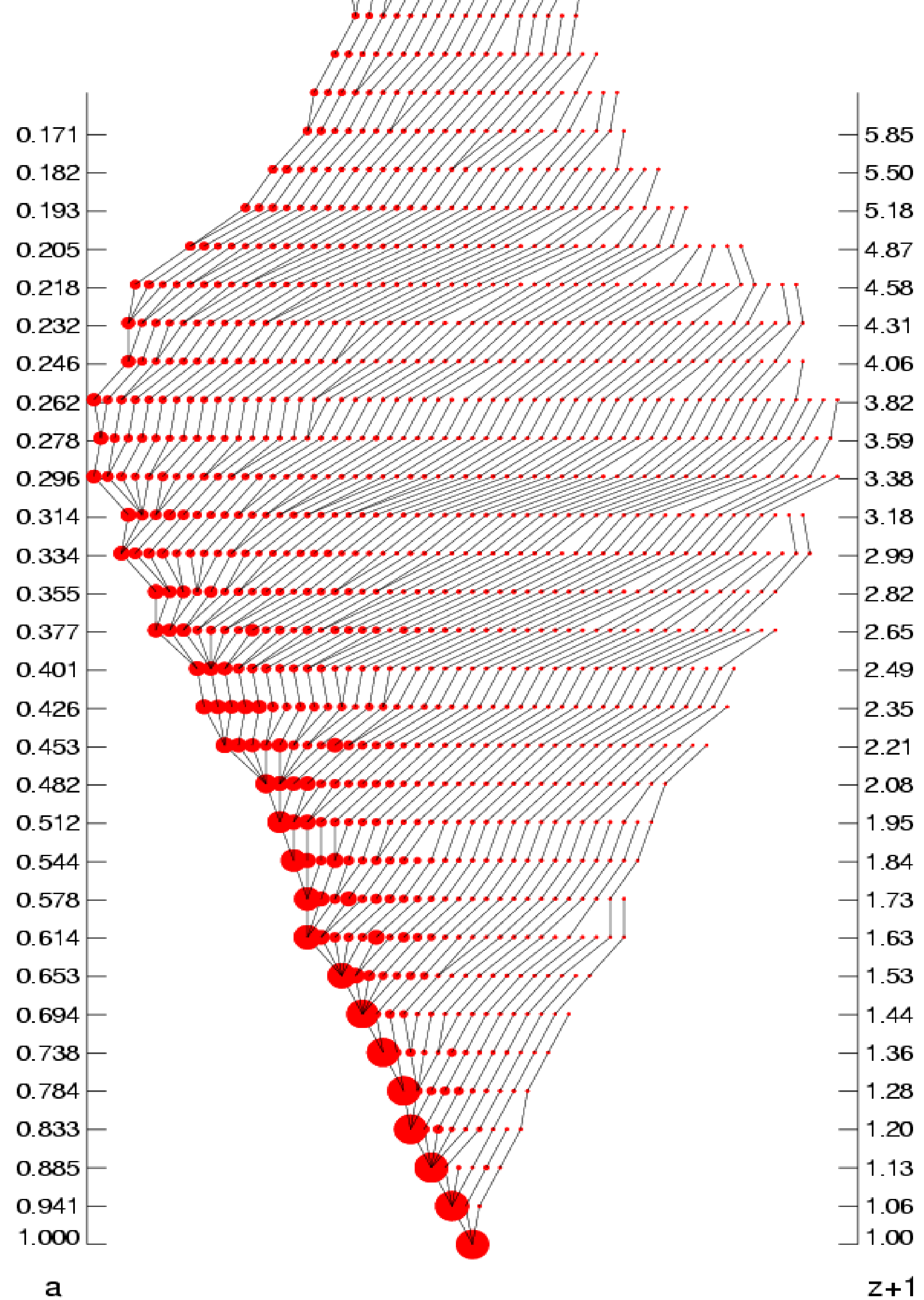

Merger tree of a cluster

(only progenitors above a minimum mass are shown)

Tracking the fate of satellite galaxies in simulations is computationally and `logistically' complicated

A SKETCH OF A SUBHALO MERGING TREE

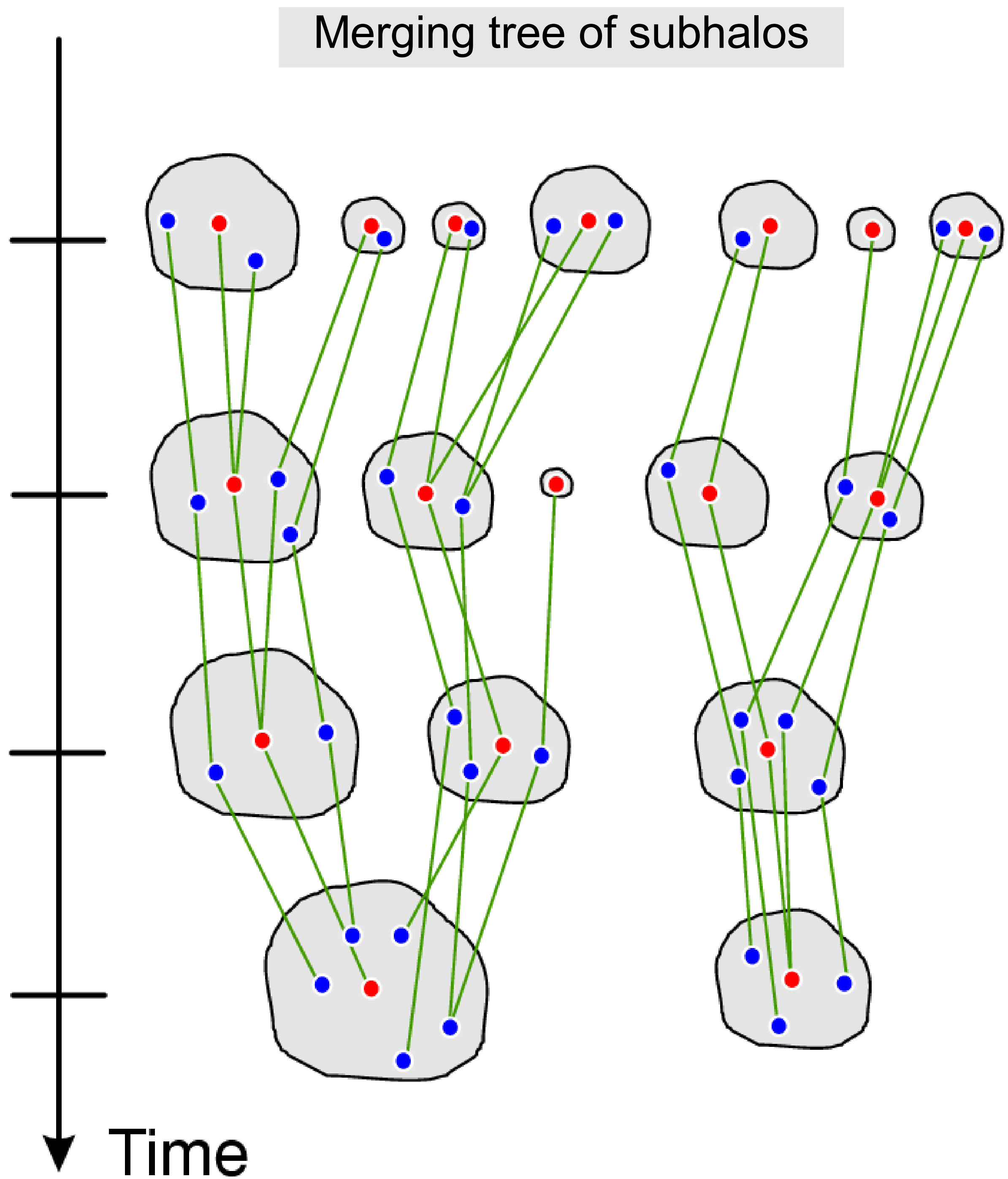

(Note: we have recently done this for a simulation with more than 10^{10} particles, and more than 20 million halos at a given output time)

Mass loss as a function of time

Accreted substructures quickly loose a substantial fraction of their mass

RETAINED SUBHALO MASS FRACTION OF **SURVIVING** SUBHALOS

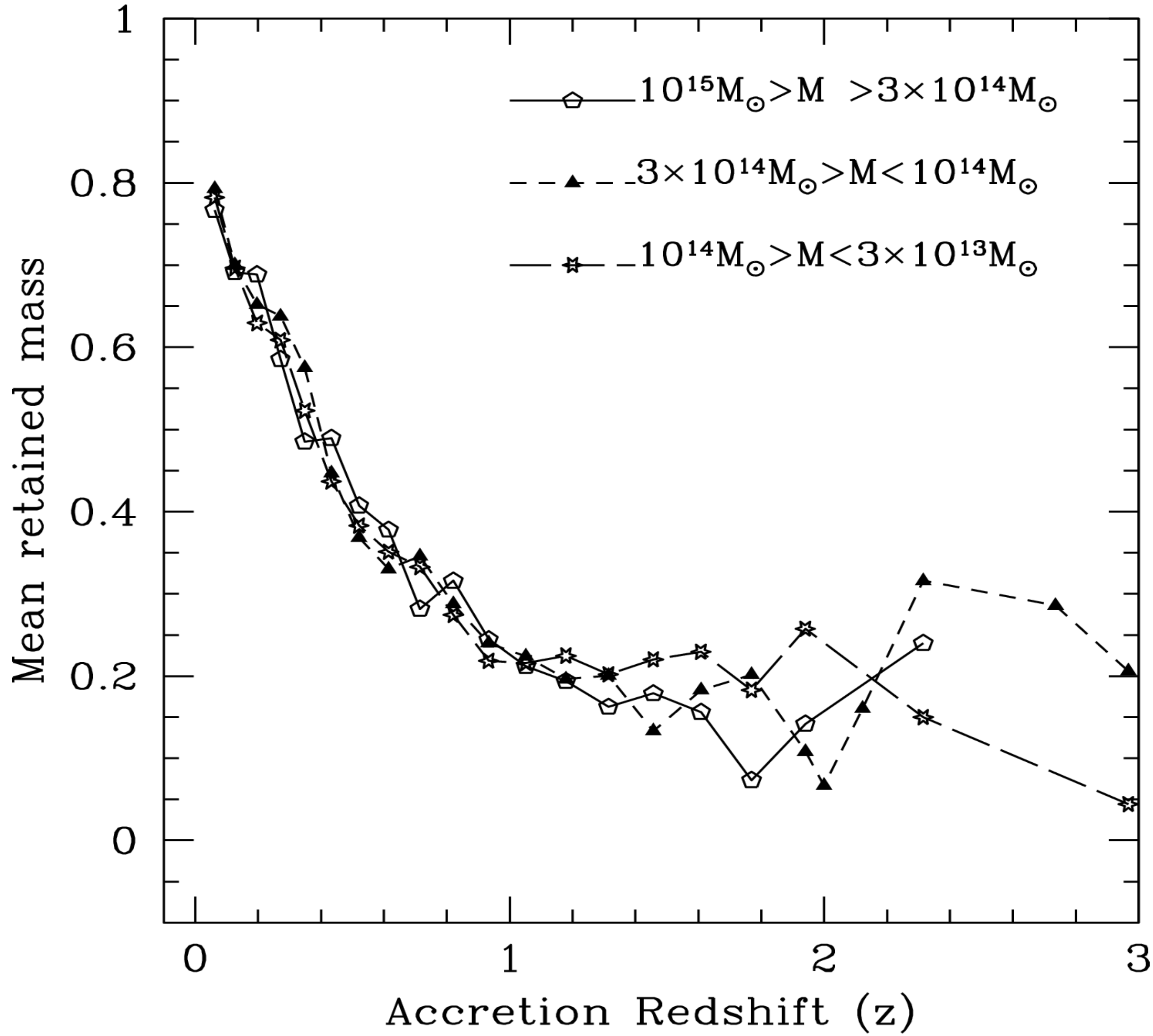

Most substructures at the present time have been accreted quite recently

FRACTION OF SUBHALOS WITH ACCRETION REDSHIFT LARGER THAN A GIVEN VALUE

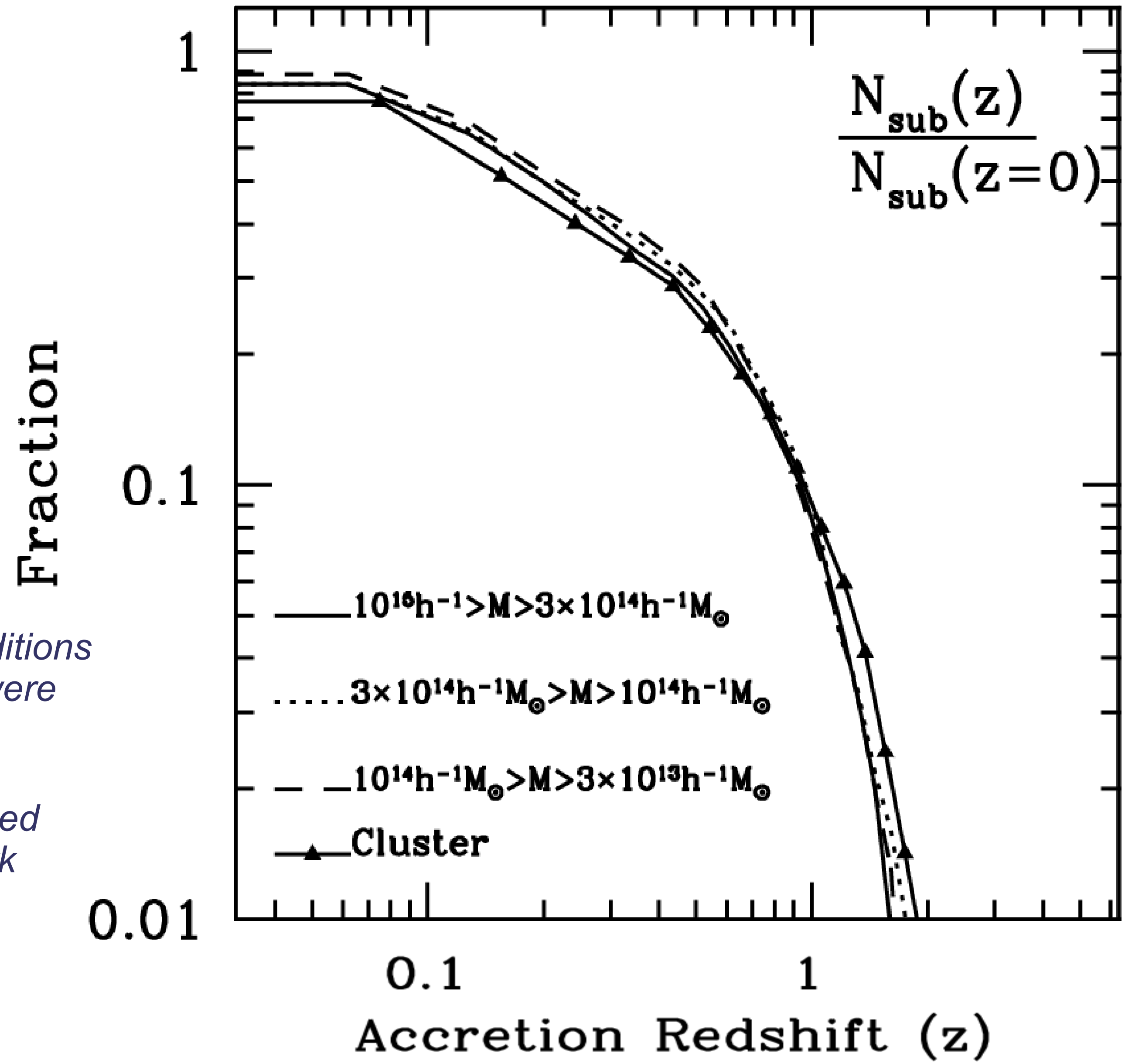

Most subhalos are recent additions to a halo: only 10% of them were accreted earlier than z=1.

Surviving subhalos are accreted more recently than typical dark matter particles.

Accreted subhalos can be tracked over long times despite their continuing mass loss

THE FATE OF SUBHALOS ACCRETED AT Z=1

fraction of
surving subhalos

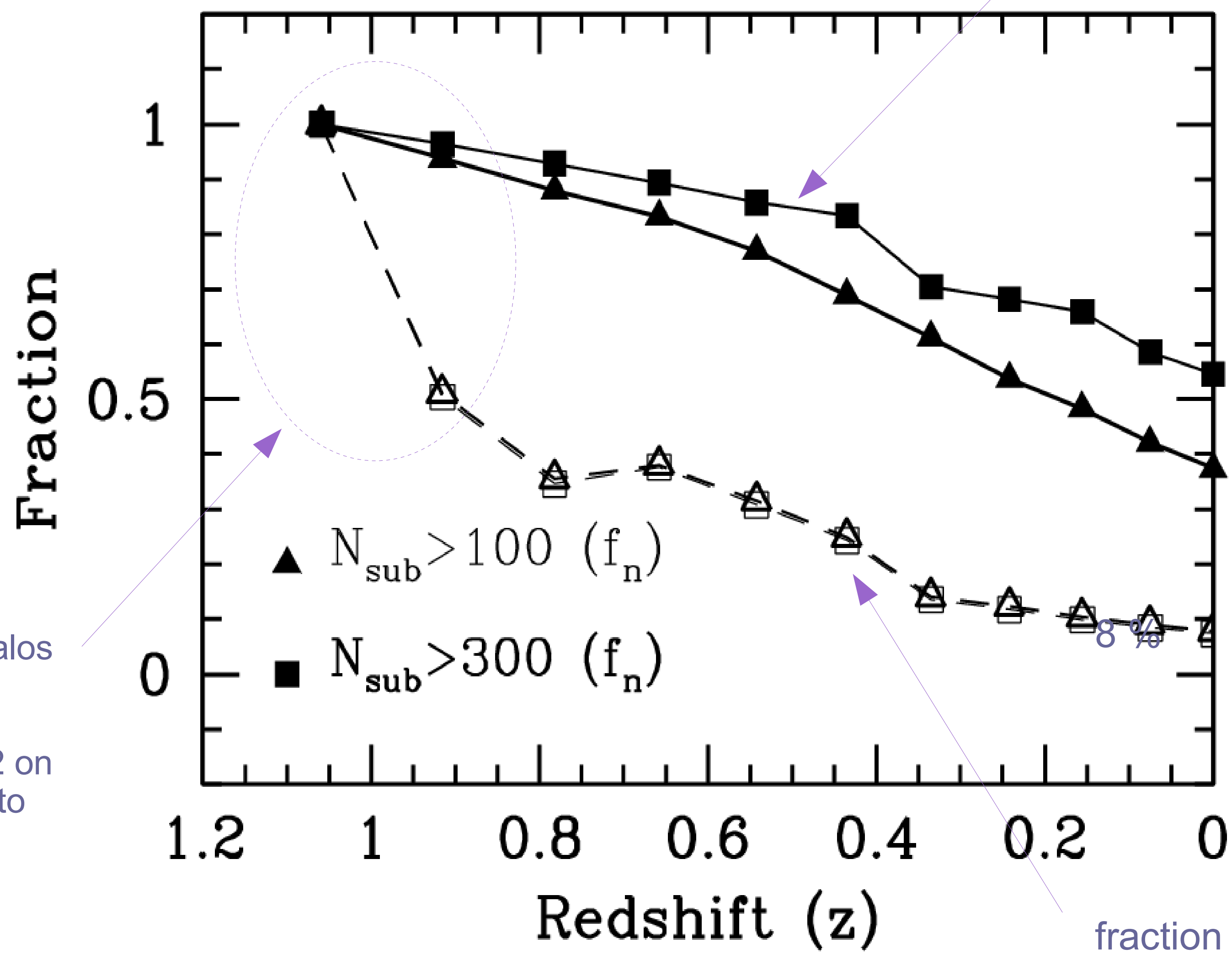

while > 90% of subhalos are still tracked after accretion, their mass drops by a factor of 2 on average, in part due to the substructure identification method

fraction of mass in
surving subhalos

The accretion time coincides with the peak in the mass accretion history of halos

MEAN MASS ACCRETION HISTORY OF CLUSTER SUBHALOS

De Lucia et al. (2004)

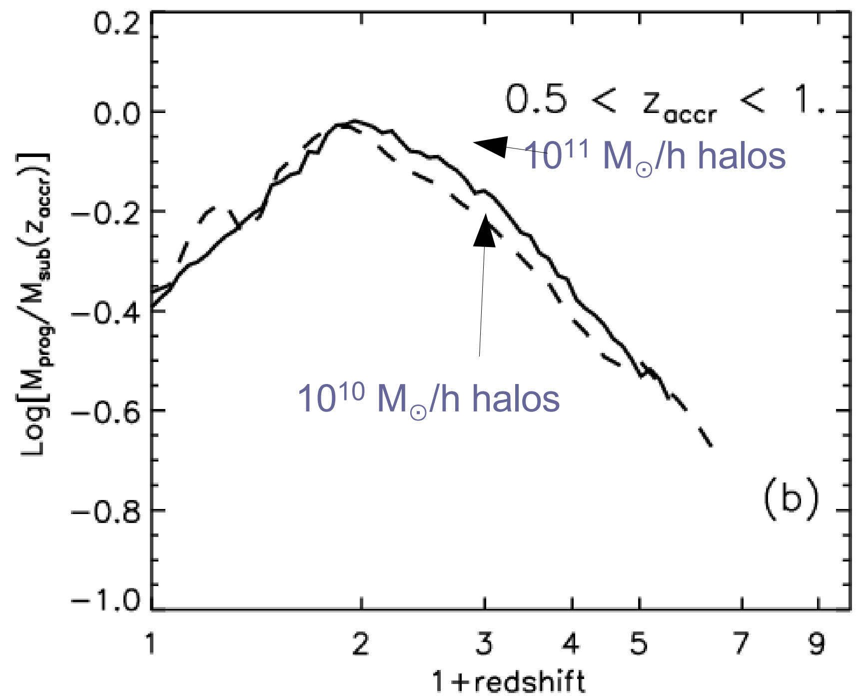

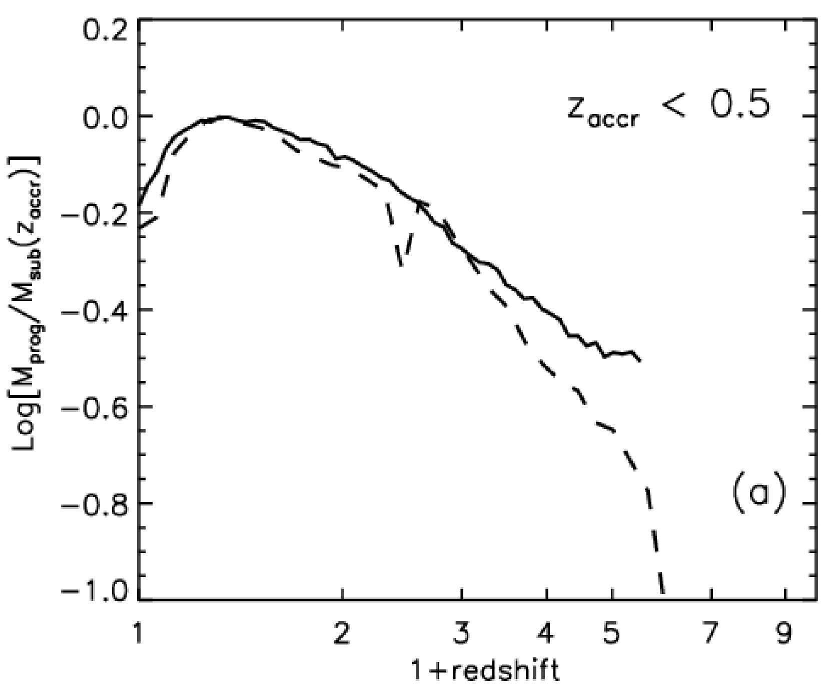

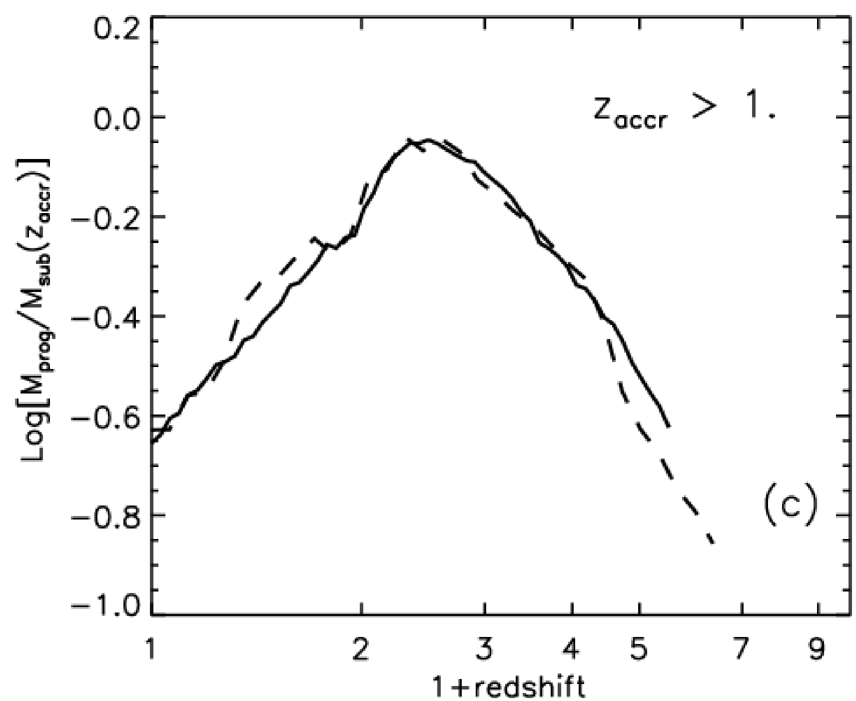

Streams and the phase-space structure of halos

Satellite debris remains visible for a while as a stream in the phase-space distribution of halos

EVOLUTION OF PHASE-SPACE DENSITY IN TIDAL DEBRIS

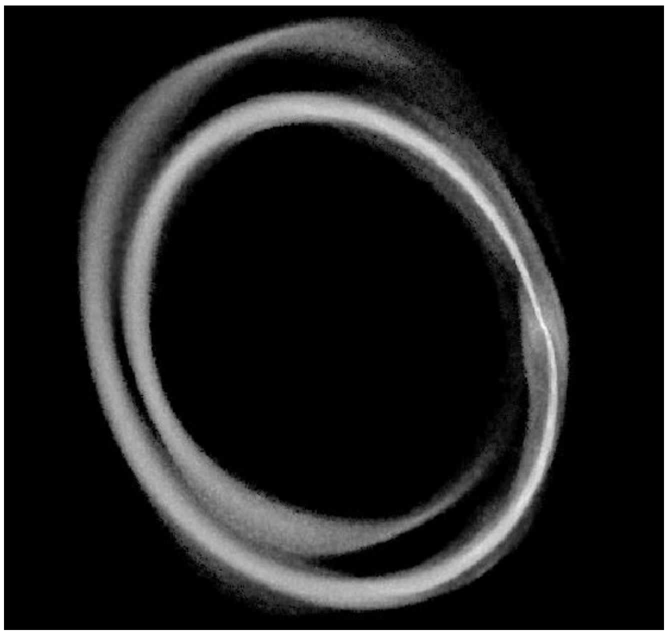

Moore et al. (2001)

Is our Solar neighbourhood dominated by a single stream, or rather by many thousands?

phase space evolution around a reference particle in tidal debris of an accreted satellite

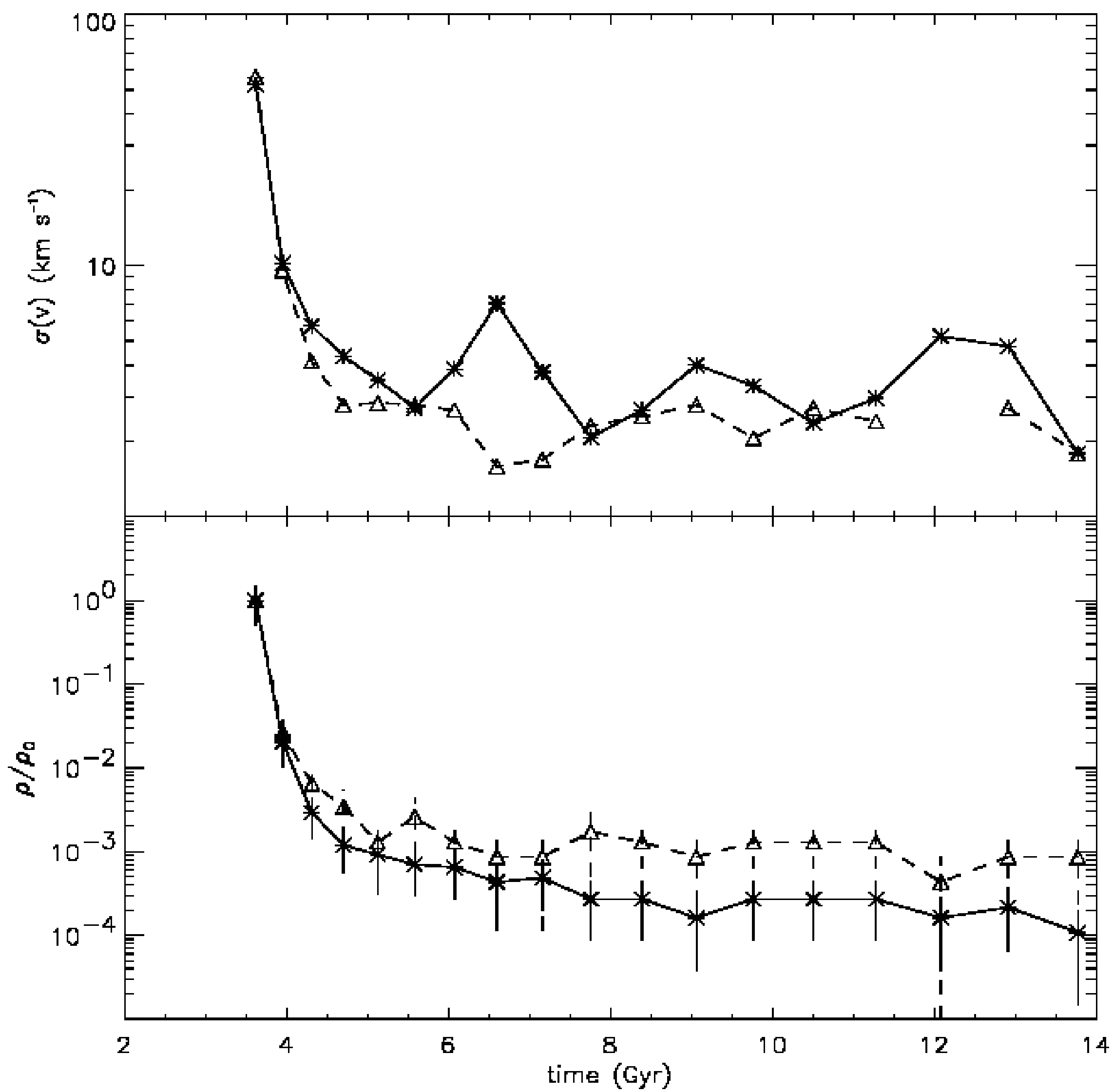

Helmi, White & Springel (2003)

Tracking subhalo accretion in a high-resolution simulation allows an estimate of the number of streams passing through a volume

NUMBER OF STREAMS PREDICTED FOR THE MILKY WAY AT THE SOLAR CIRCLE

Helmi, White & Springel (2003)

let N_k be the count of particles per stream in some volume

an estimate for the mass-weighted mean mass per stream, corrected for Poisson noise is

$$\hat{\mu} = \frac{\sum_{k=1,L} (N_k^2 - N_k)}{\sum_{k=1,L} N_k}$$

We define the mass-weighted number of streams as the total mass in the box divided by the mean mass per stream. This can the be estimated as:

$$\hat{F} = \frac{\sum_{k=1,L} N_k}{\hat{\mu}}$$

The Solar neighbourhood should be clumpy with a few 10^5 intersecting streams!

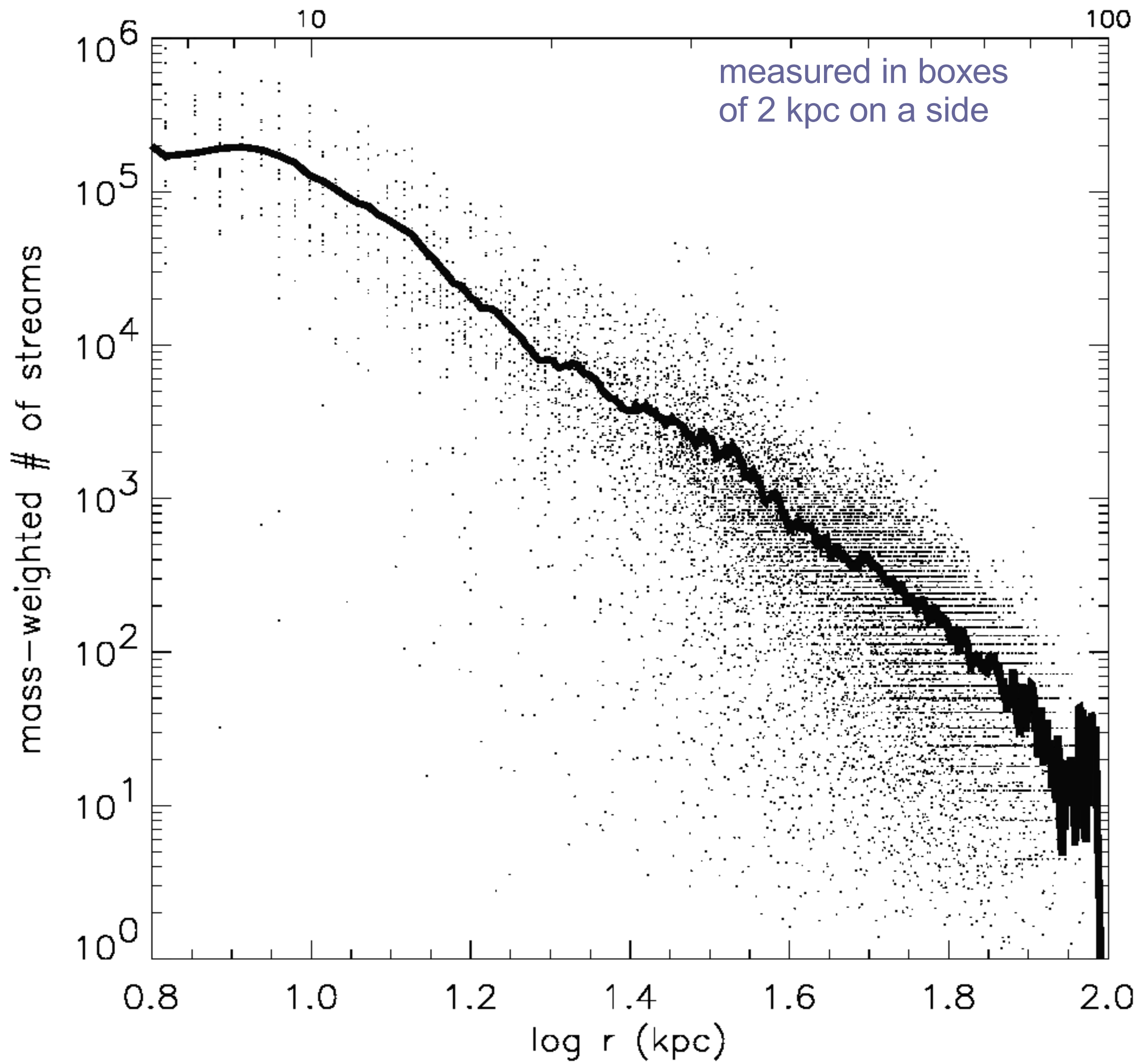

Radial structure of satellites

Subhalos are structurally different from their parent halo, with lower central densities and wider circular velocity curves

STRUCTURAL RESPONSE OF SUBHALOS TO MASS LOSS

Hayashi et al. (2003),
Stoehr et al. (2003):

- Stripping reduces the density of a subhalo at *all* radii
- peaks of circular velocity curves become narrower than parent halo
- inner structure of subhalos substantially *shallower* than NFW

This has implications for:

- direct dark matter detection
- correspondence between subhalos and observed dwarf galaxies in the MW

Stoehr et al. (2003)

Circular velocity curves for subhalos in the GA3 simulation

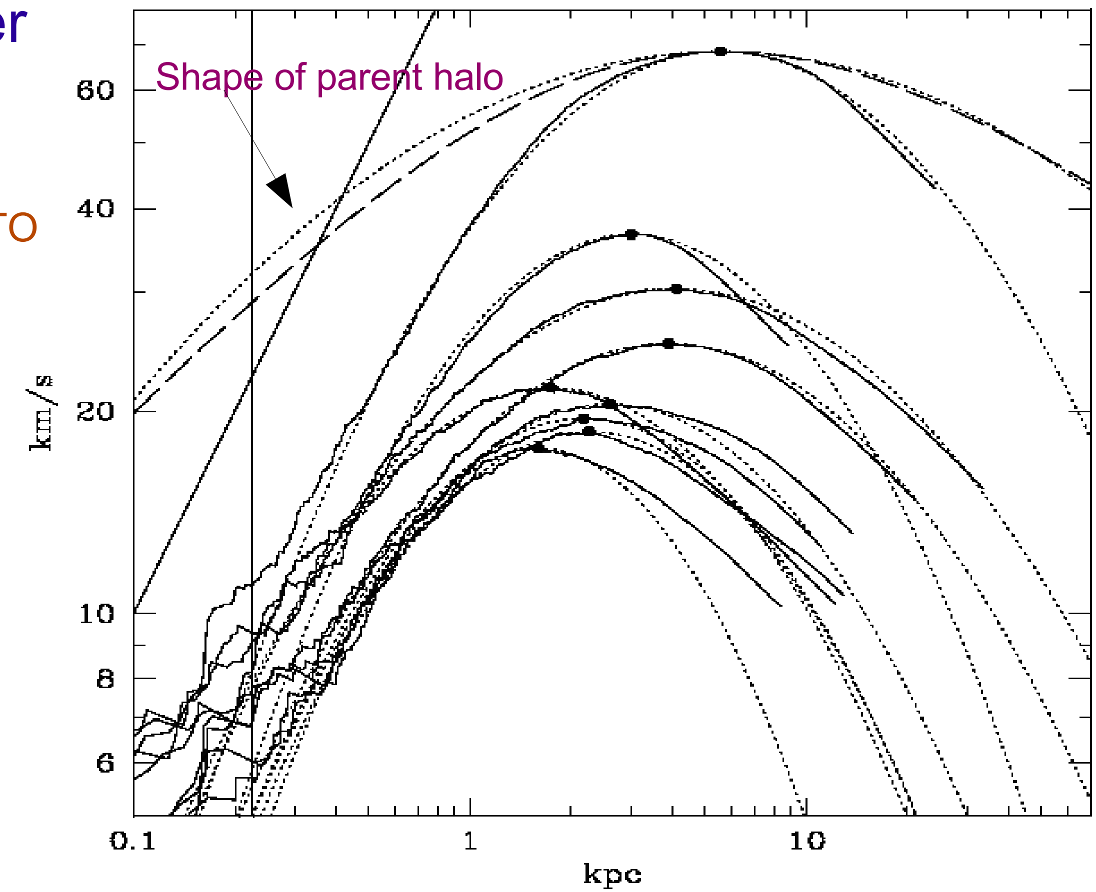

Moore et al. (2001)

Structural time evolution of an infalling subhalo

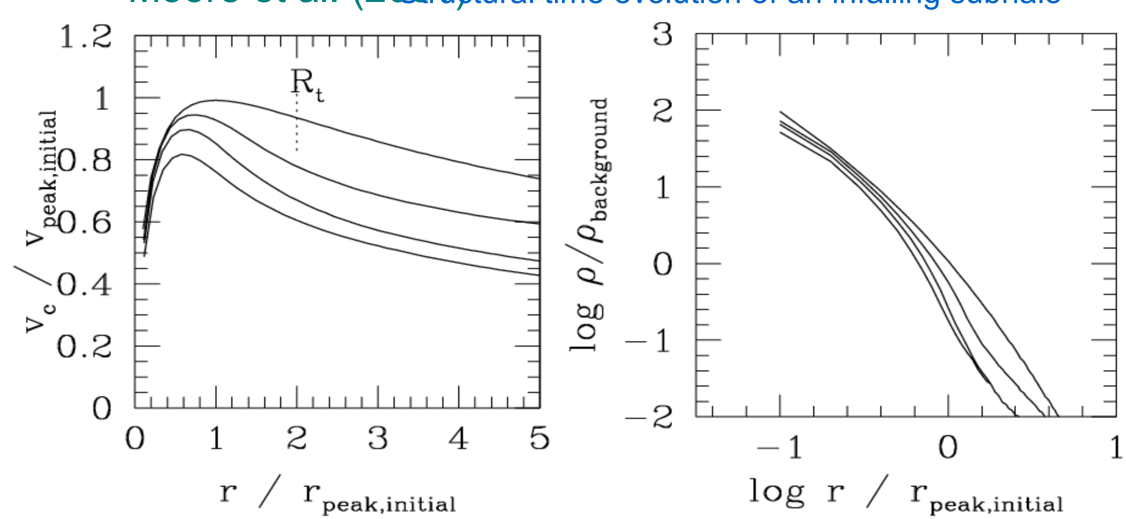

Implications of subhalos for annihilating dark matter

Dark matter could be self-annihilating, in which case the presence of subhalos should boost the expected flux

THE ANNIHILATION SIGNAL DUE TO SUBSTRUCTURES

Stoehr, White, Springel, Tormen, Yoshida (2003)

Annihilation flux:

$$F = \frac{N_\gamma \langle \sigma v \rangle}{2\, m_{\rm DM}^2} \int_V \frac{\rho_{\rm DM}^2(\mathbf{x})}{4\pi\, d^2(\mathbf{x})}\, {\rm d}^3x$$

Expect signal from:

- central halo cusp
- subhalos if their cuspy as well

Estimate relevant density integral from:

$$J = \int_V \rho_{\rm DM}^2\, {\rm d}V = \sum_{i=1}^{N_{200}} \rho_i\, m_i$$

(Particle densities are estimated with Voronoi tesselation. Corrections for Poisson noise are applied.)

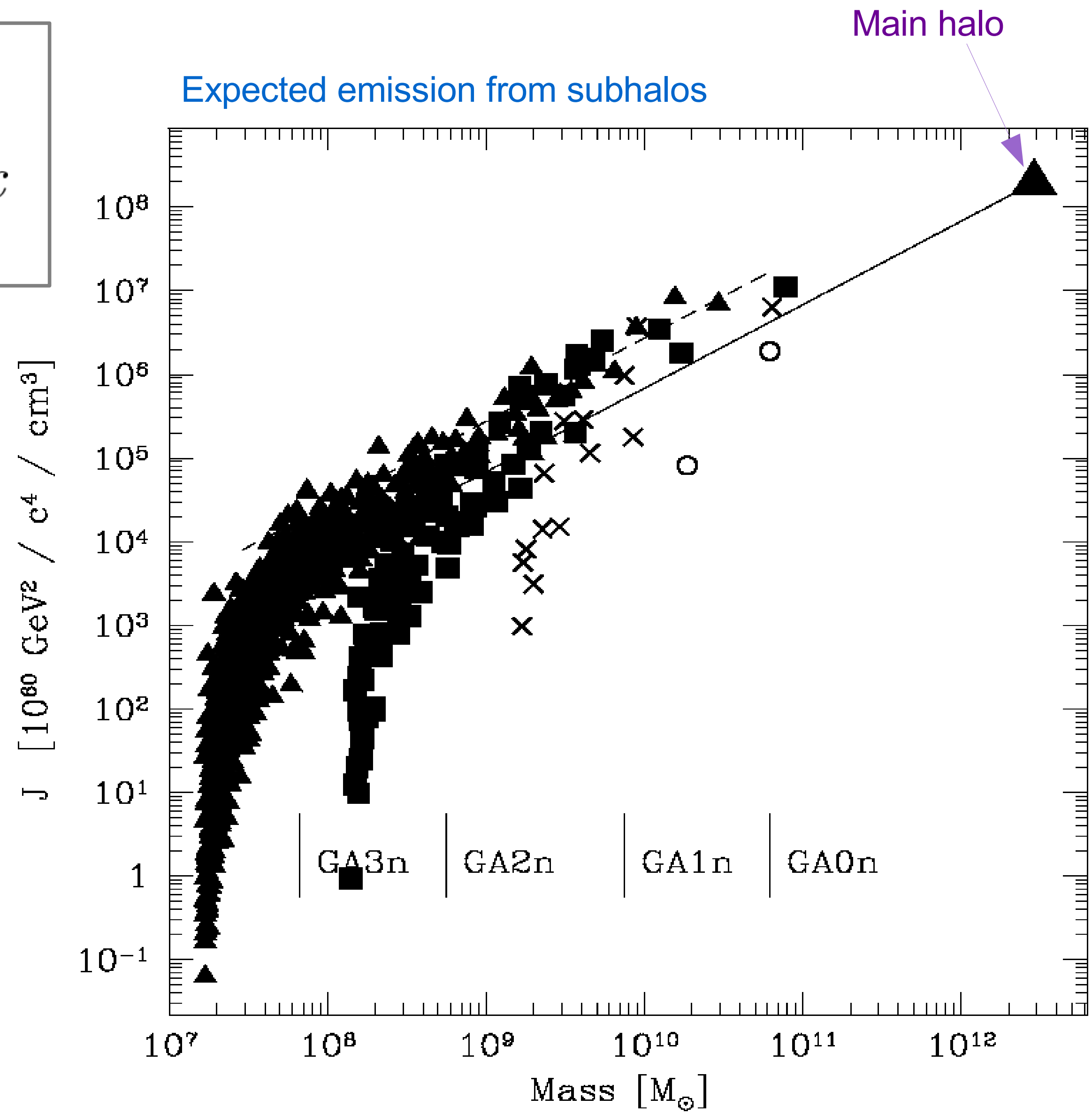

Substructures boost the annihiliation radiation by only a small amount, and none of them outshines the Galactic center

DISTRIBUTION OF THE ANNIHILATION SIGNAL BY SOURCE AND BY RADIUS

Convergence of emission from different sources

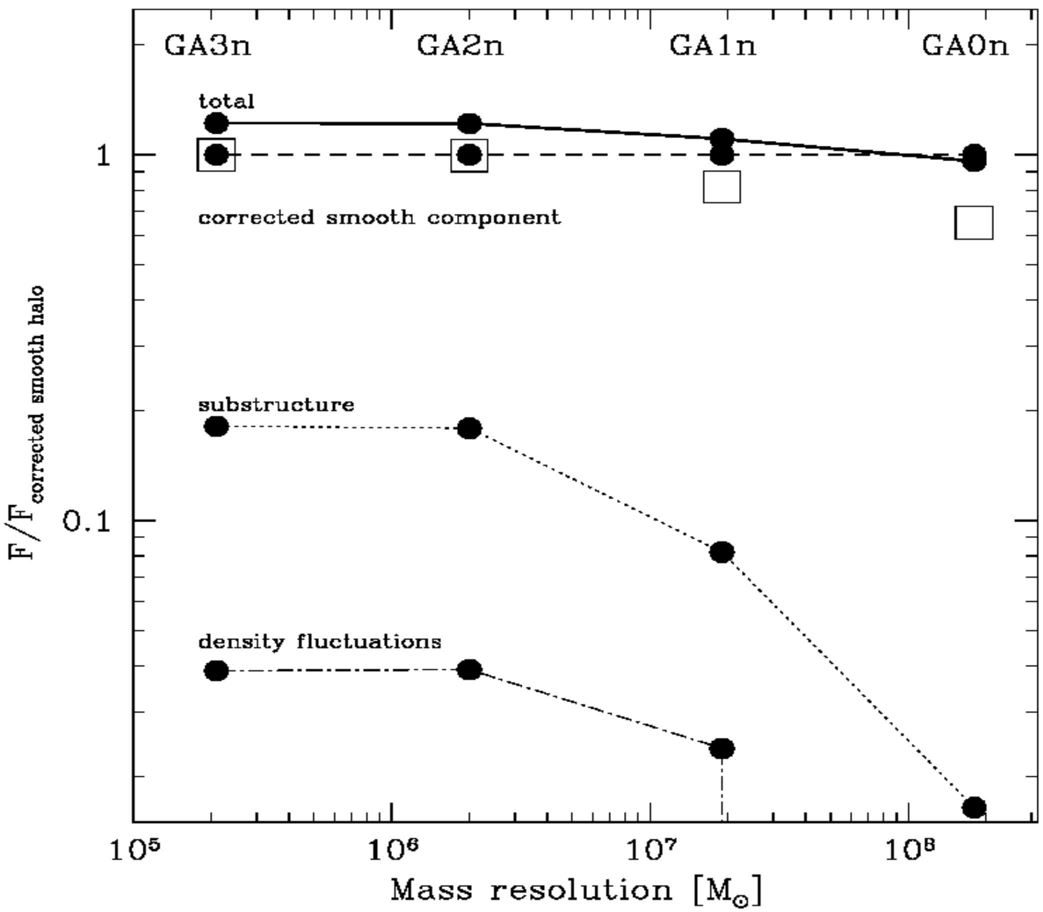

Cumulative radial distribution of emission

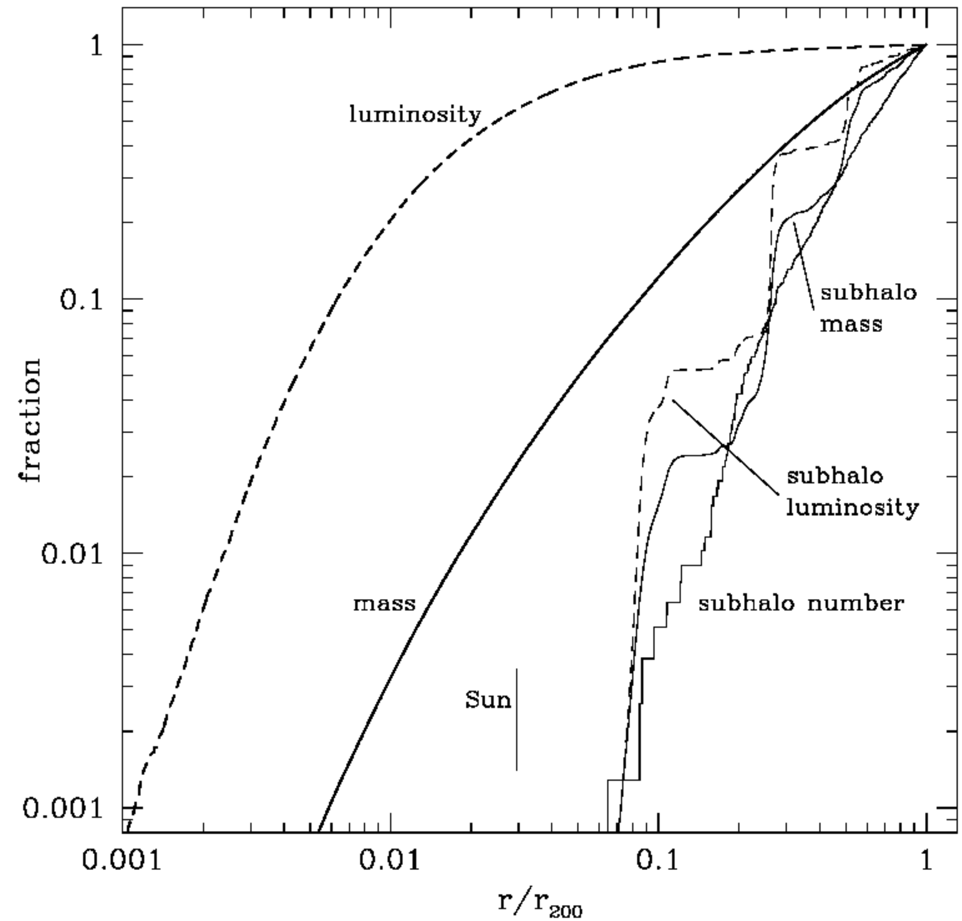

- annihilation signal from subhalos is **dominated by the most massive** ones, is preferentially in the **outer parts**, and is overall **less than** from the smooth inner halo (unlike Taylor & Silk 2003, Calcaneo-Roldan & Moore 2000)
- unlikely that any of the subhalos would outshine the center (Sagittarius is already 24 kpc away)
- central emission has an angular scale of several tens of degrees. It may be best observed off-centre, 25-35 degrees away from the Galactic center

Satellite population in the Milky Way

The "missing satellites" are viewed as a vexing problem for CDM

THE SATELLITE VELOCITY FUNCTION OF CDM COMPARED WITH MILKY WAY SATELLITES

Klypin et al. (1999)

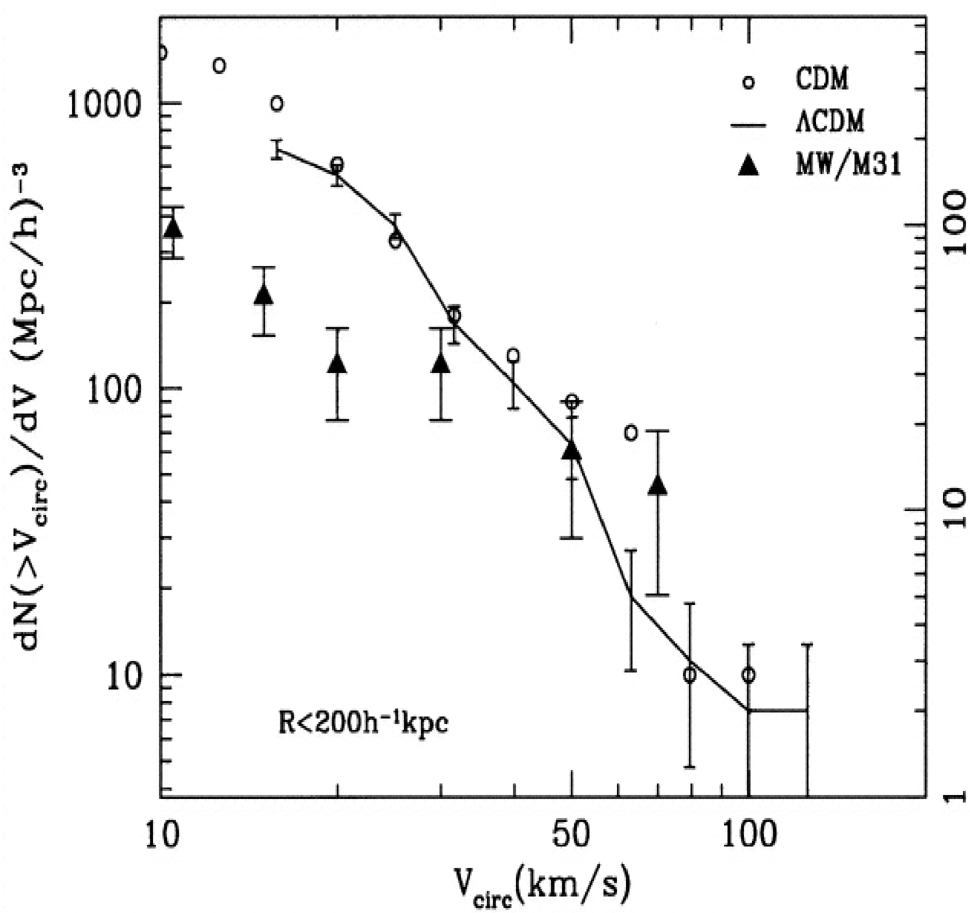

Moore et al. (1999)

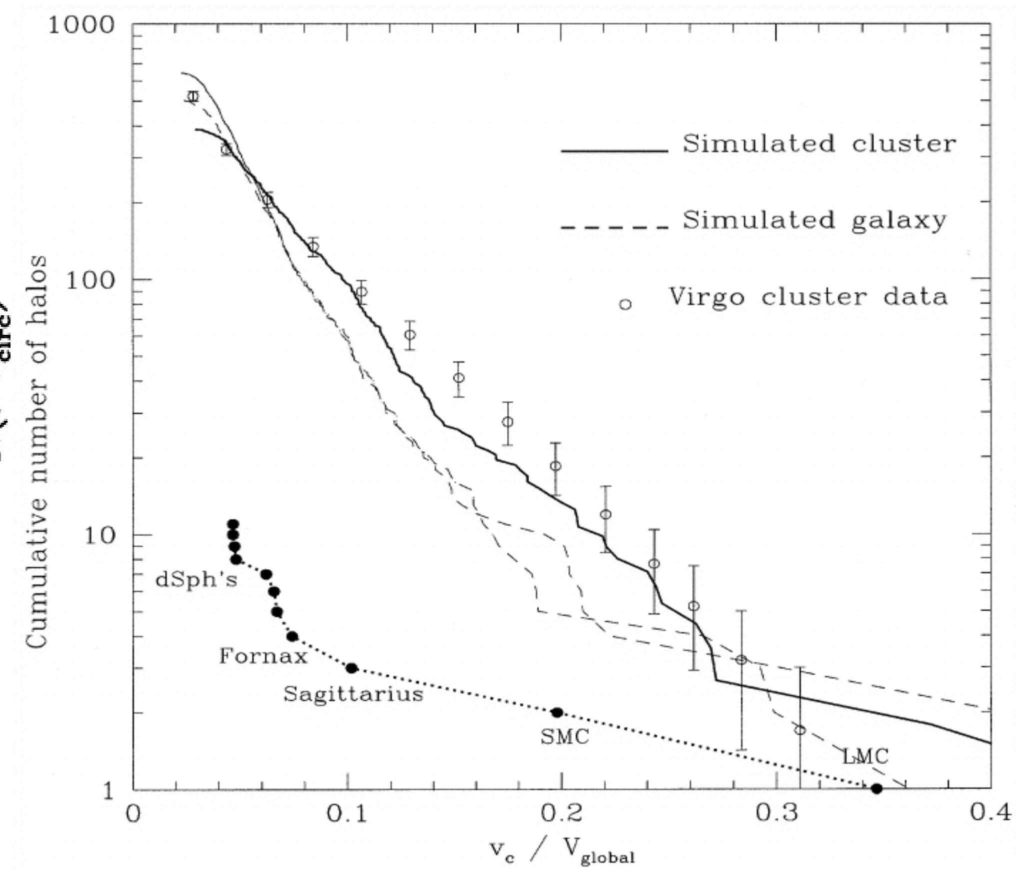

Are the most massive subhalos too big?
And what about the large abundance of small ones?

The most massive subhalos in the simulations can plausible host all the known satellites in the Milky Way

THE PREDICTED CENTRAL VELOCITY DISPERSION COMPARED WITH MW SATELLITES

Stoehr, White & Springel (2002)

The observed **line-of-sight velocity dispersions** of the MW's dwarf galaxies need to be compared to a **stellar model put inside the simulated dark matter subhalos**, not to the subhalo circular velocities.

Assumptions:

- spherical symmetry and isotropic velocity dispersion tensor
- stellar density drops to zero at finite truncation radius (as observed)
- stellar density of dwarfs modelled with a King model

$$\sigma_p^2(r_p) = \frac{\int_{r_p}^{r_t} \mathrm{d}r \ \rho V_c^2 (r^2 - r_p^2)^{1/2}/r}{\int_{r_p}^{r_t} \mathrm{d}r \ \rho\, r/(r^2 - r_p^2)^{1/2}}$$

Number of subhalos where the predicted central dispersion is larger than observed

	r_c [kpc]	r_t/r_c	σ_0 $\left[\frac{km}{s}\right]$	N_{GA2}
Sagittarius	0.44	6.8	11.4(19)	11(2)
Fornax	0.46	5.1	10.5	13
Leo I	0.215	3.8	8.8	4
Sculptor	0.11	13	6.6	4
Leo II	0.16	3	6.7	1
Sextans	0.335	9.6	6.6	18
Carina	0.21	3.3	6.8	6
Ursa Minor	0.20	3.2	9.3	0
Draco	0.18	5.2	9.5	0

all 11 satellites of the MW can be accomodated in the 20 most massive subhalos

There is surprisingly good agreement between the kinematics of the observed satellites and the predicted ones for ΛCDM subhalos

COMPARISON OF VELOCITY DISPERSION PROFILES

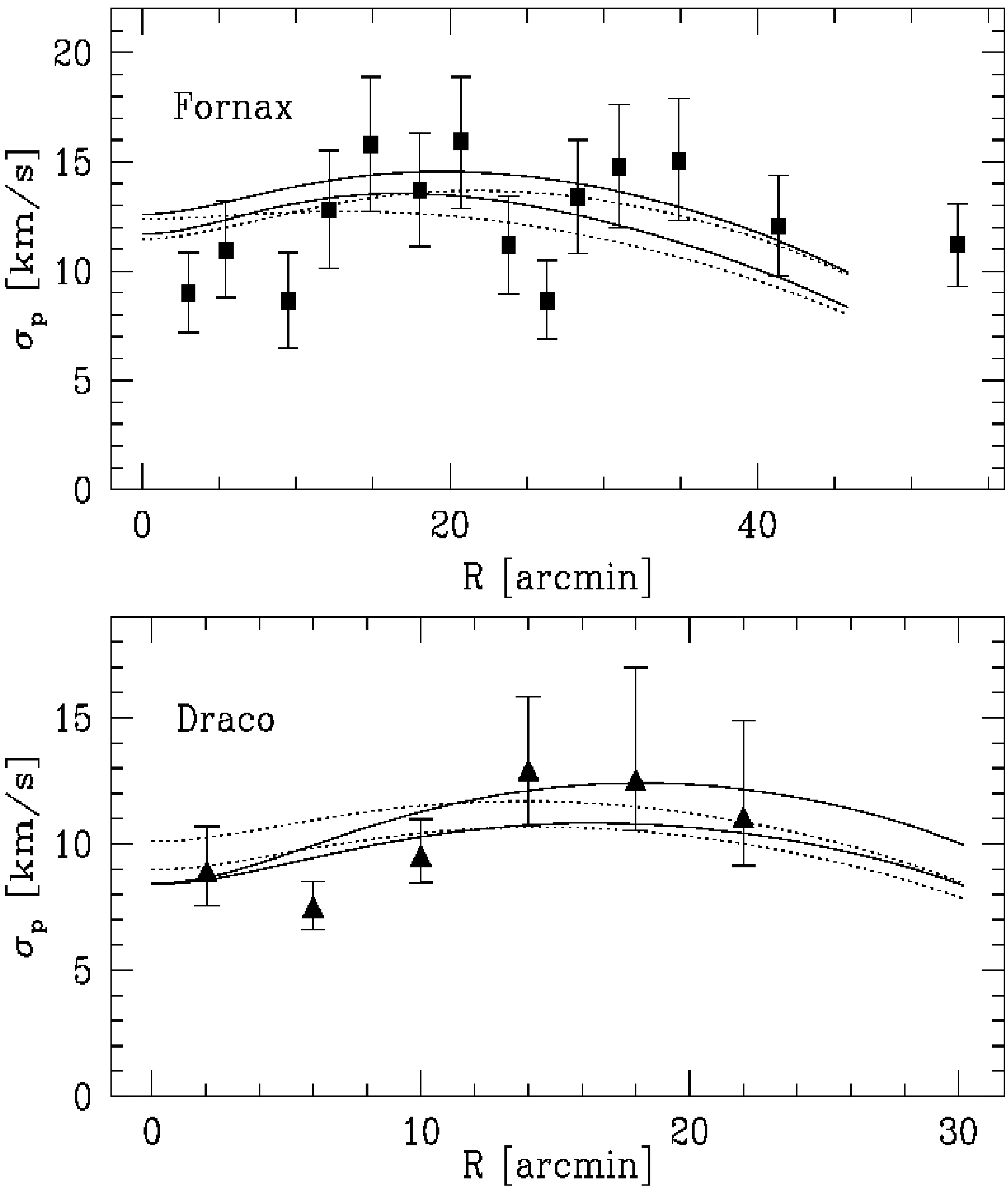

Note:

- dark matter subgalos are much more extended than the stellar edge at the "tidal" radius
- A further reduction of the central subhalo densities (e.g. by self-interacting dm) would make it difficult to explain the observed satellites

Stoehr, White & Springel (2002)

Provided reionization sterilizes small halos efficiently, the satellite population is well matched

THE VELOCITY DISTRIBUTION FUNCTION OF SUBHALOS THAT ORIGINATED IN RARE PEAKS

Moore et al. (2005)

Only those surviving subhalos which were already present at z=12 as 2.5σ peaks

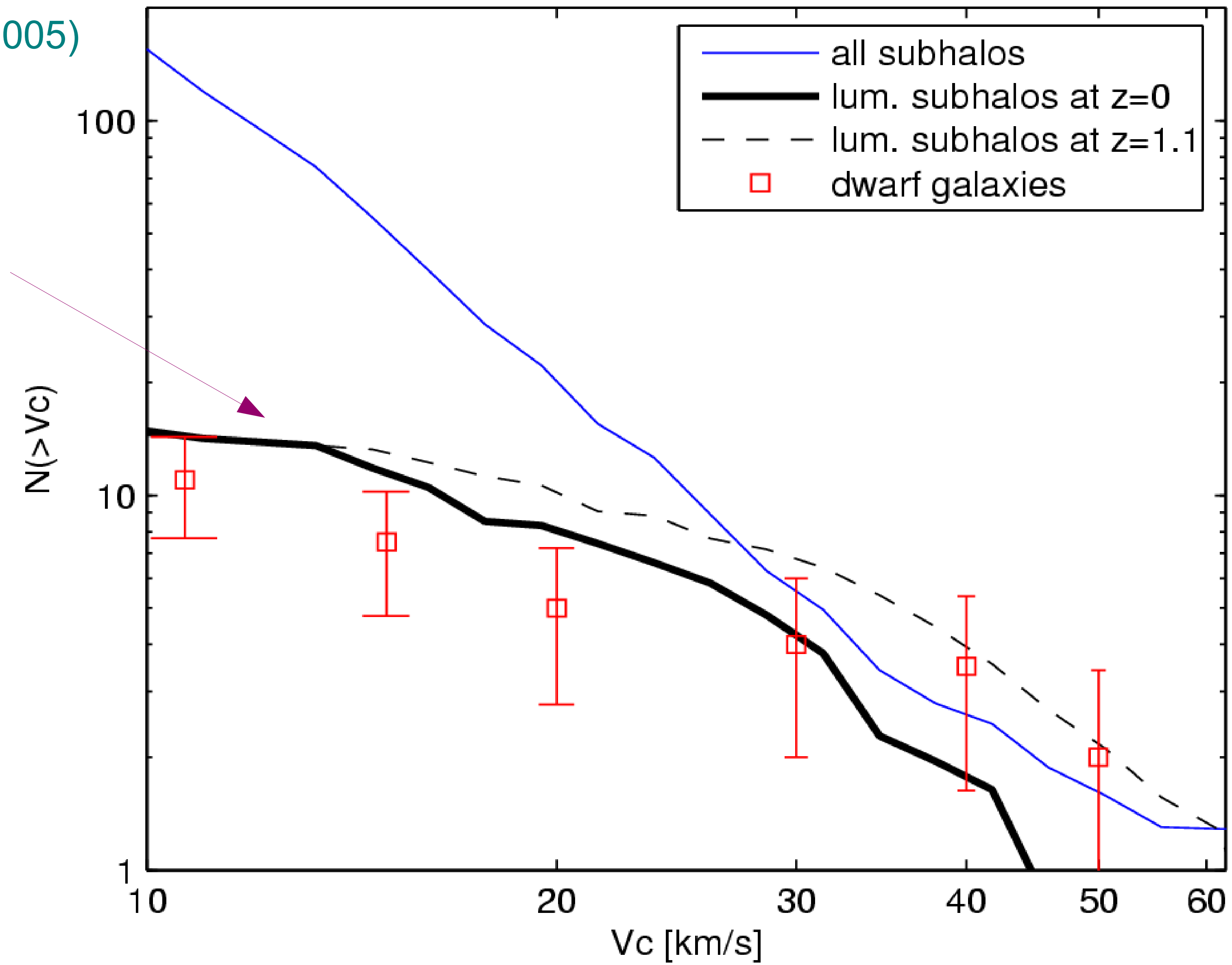

Some direct hydrodynamical simulations do not seem to provide a sufficiently strong suppression of small halos by the UV background

BARYON FRACTION AND FILTERING MASS

Hoeft, Yepes, Gottloeber & VS (2005)

Linear theory filtering mass, Gnedin (1998)

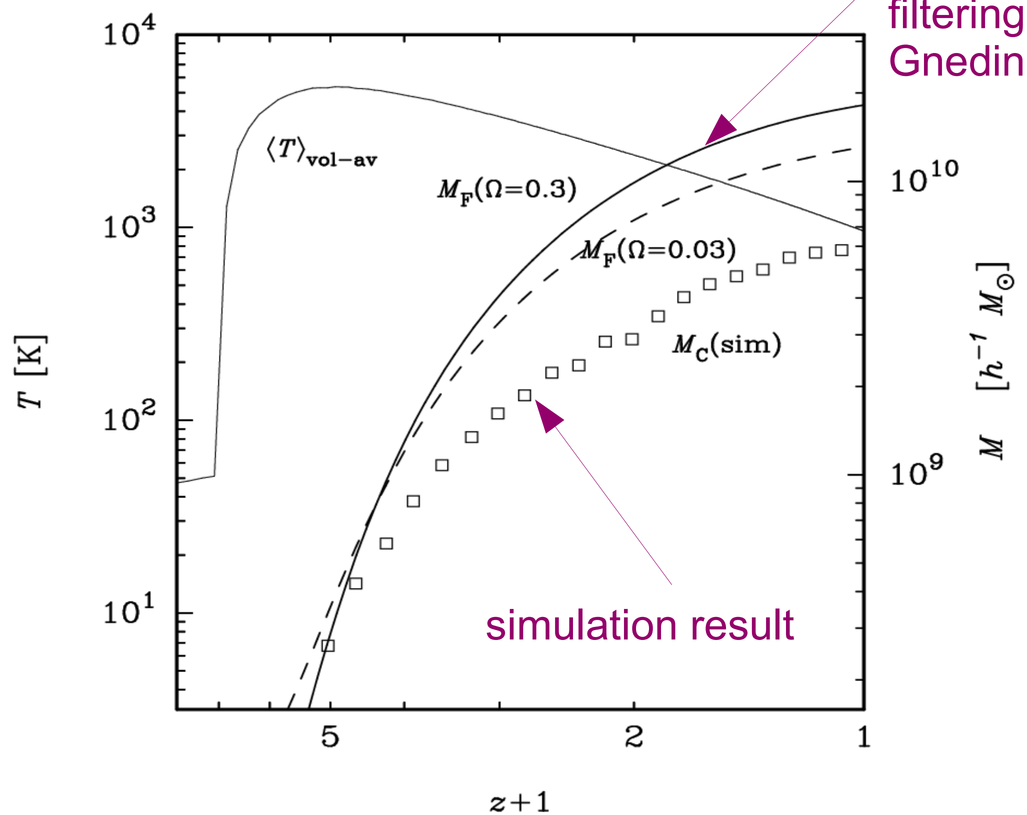

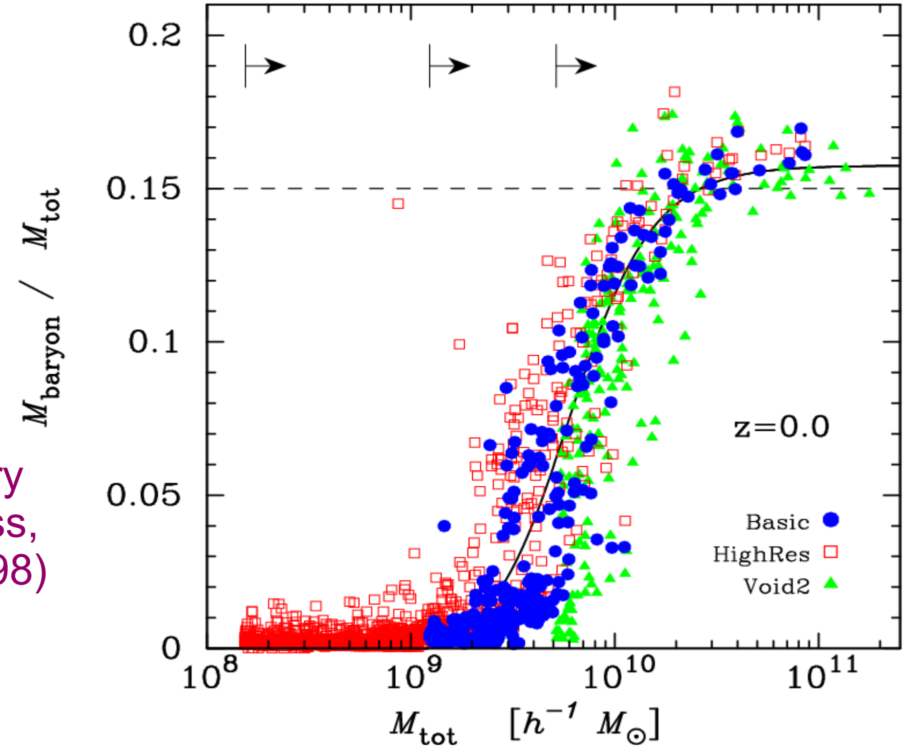

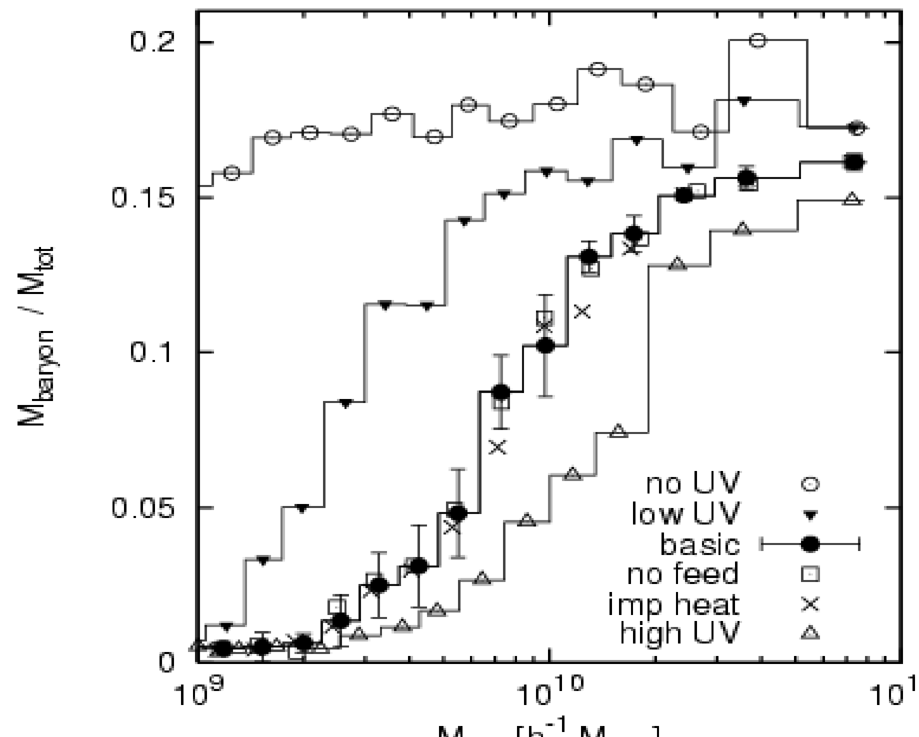

need to suppress cooling for V_c<35-40 km/sec (corresponds to 1.5×10^{10} $M_\odot$, or ~50000 K) to make small satellite population dark

Using subhalos for semi-analytic galaxy formation

Semi-analytic models are one of the most powerful techniques to study **galaxy formation**

MOST IMPORTANT INPUT PHYSICS

Hierarchical growth of dark matter halos

→ *understood with high accuracy*

Radiative cooling of gas within halos (dissipation)

→ *in principible well within reach of current simu-lations, yet plagued with numerical difficulties*

Star formation and associated feedback processes

→ *highly uncertain physics, numerically extremely difficult*

Spectrophotometric modeling of stellar populations

→ *some uncertainties, but no/small coupling to gas dynamics*

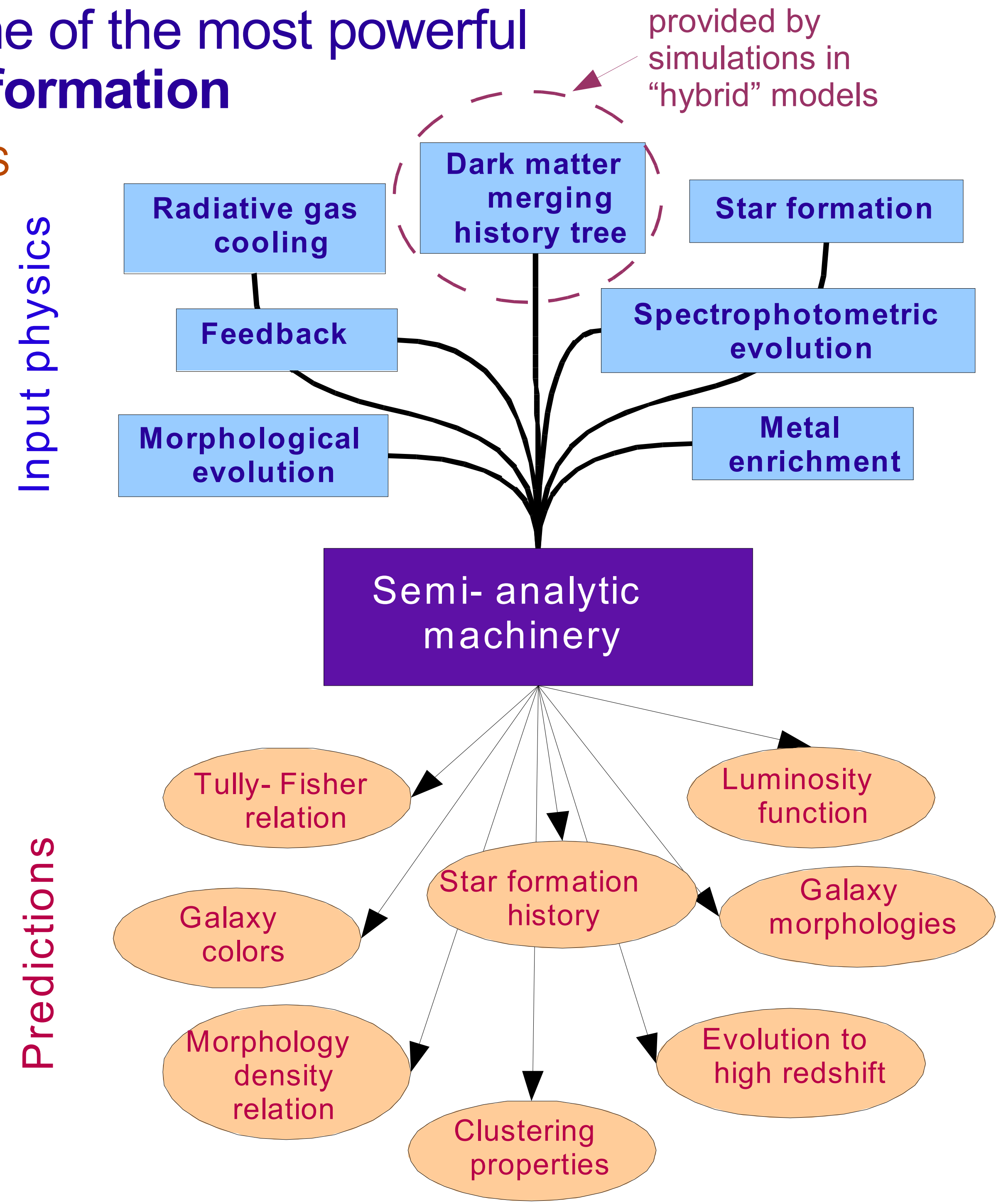

The N-body resolution can be pushed to a point where essentially all luminous galaxies have a corresponding dark matter structure

CLUSTER LUMINOSITY FUNCTION AT VARIOUS RESOLUTIONS

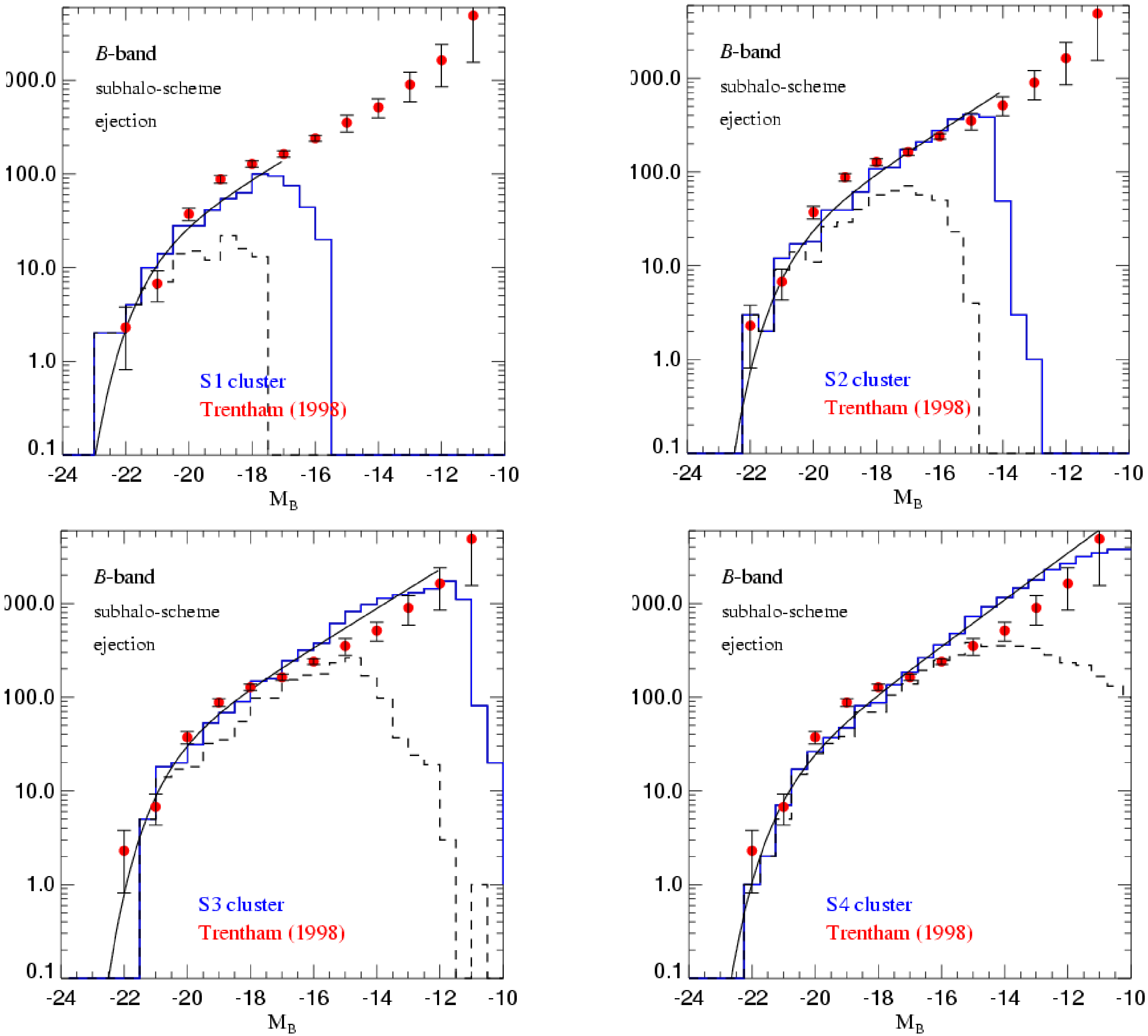

Explicit tracking of subhalos provides a more faithful description of the merging rates of satellites

CLUSTER LUMINOSITY FUNCTION

Direct tracing of subhalos in the N-Body simulation

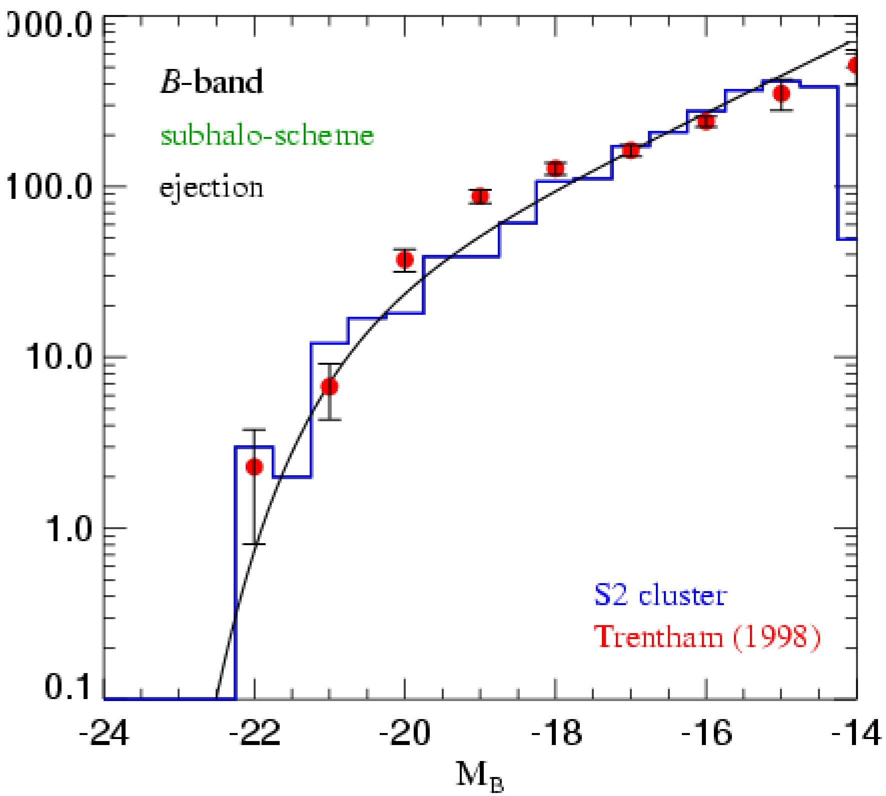

Standard semi-analytic estimates of satellite survival times

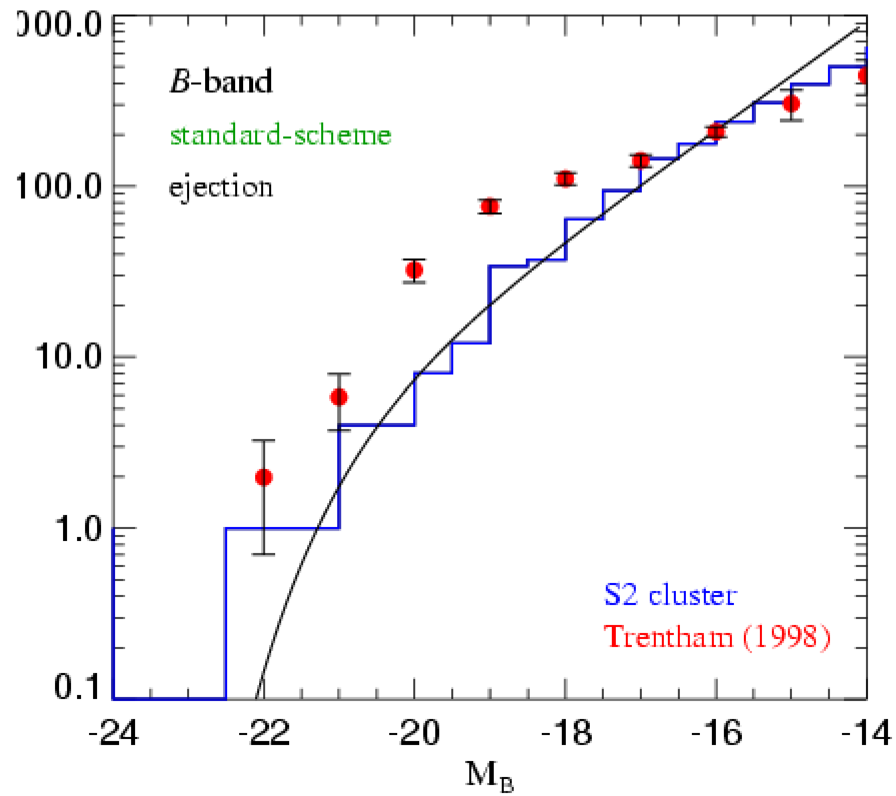

Springel, White, Tormen & Kauffmann (2000)

Rarely, subhalos may collide and merge within a larger halo

A MERGER OF SUBHALOS

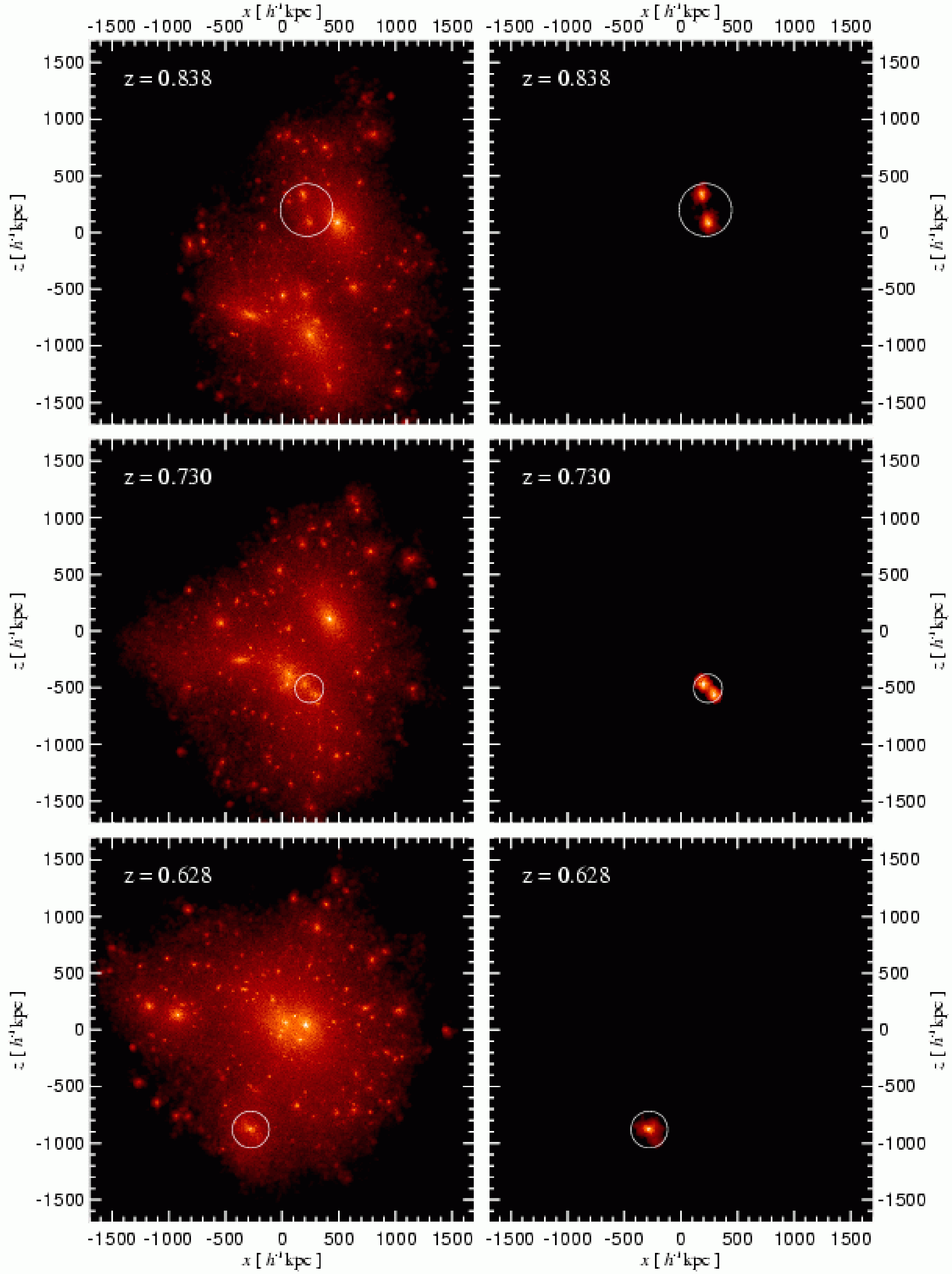

This happens rarely, but is kept track of in the semi-analytic model

(Only 1 out of 20 subhalos merge with another subhalo before they fall into the center.)

The morphology-density relation arises naturally in hierarchical models of galaxy formation

MORPHOLOGICAL MIX
AS A FUNCTION OF
CLUSTER-CENTRIC DISTANCE

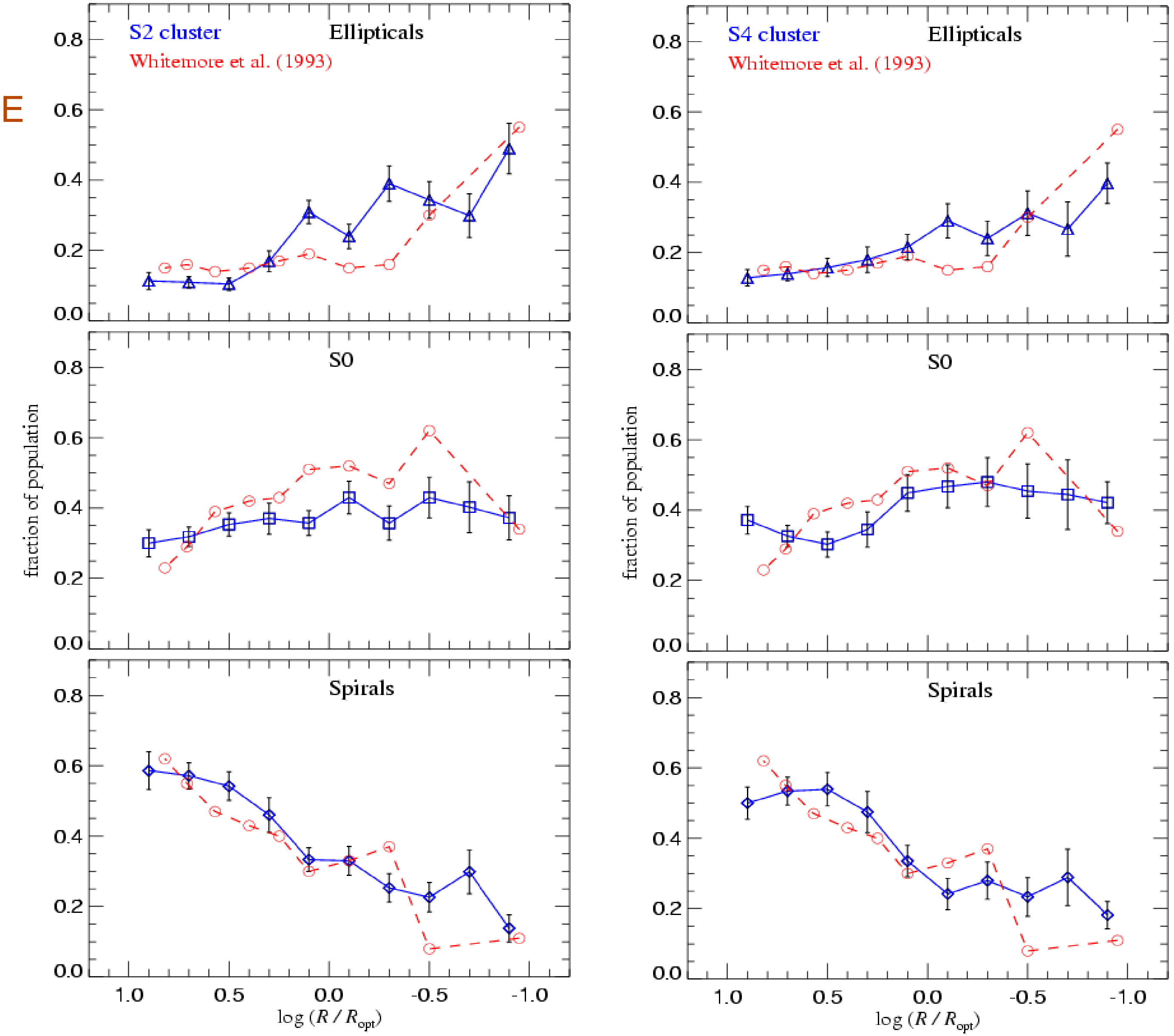

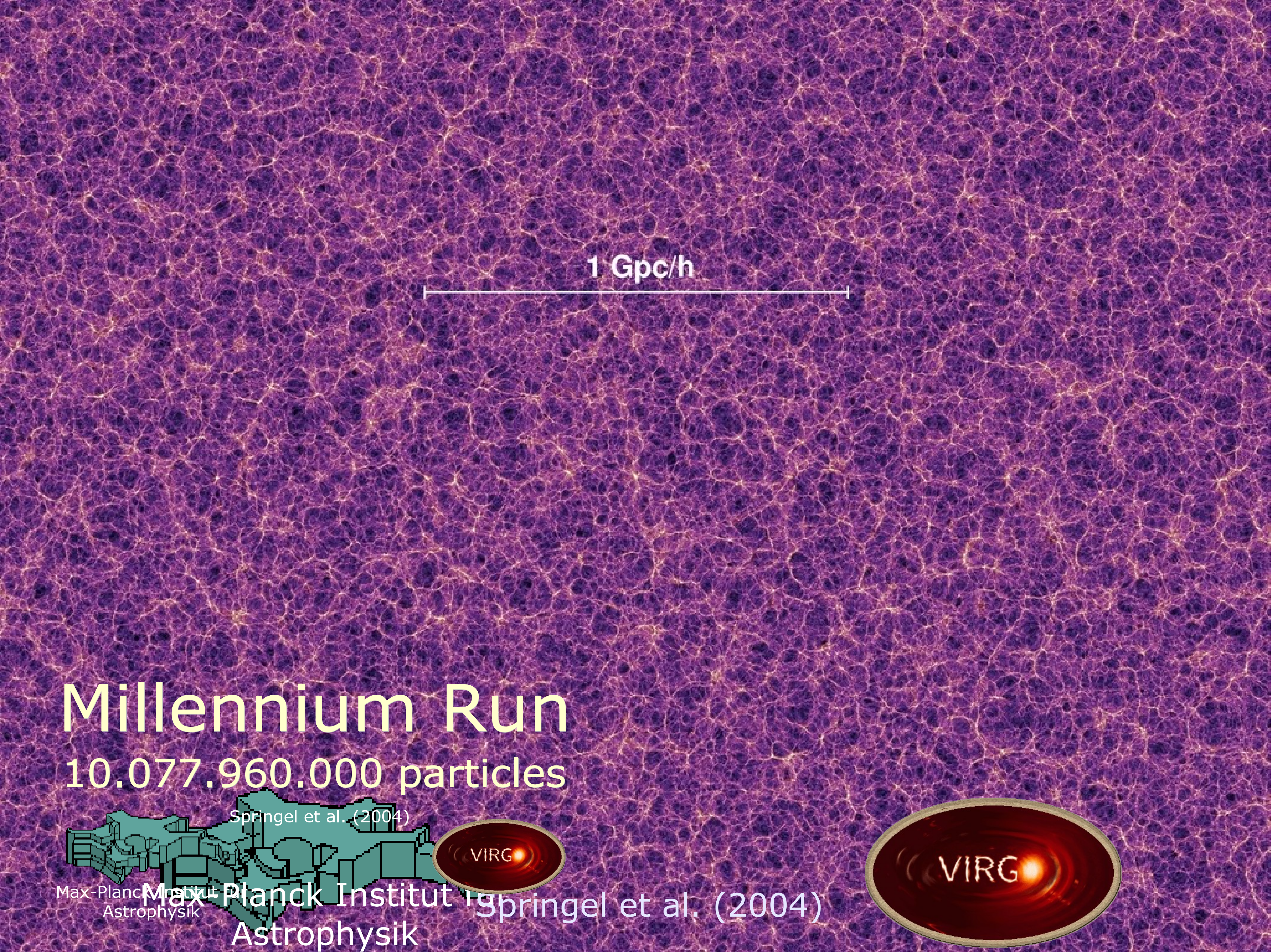

Millennium Run

10.077.960.000 particles

Springel et al. (2004)

Max-Planck-Institut für Astrophysik

Max-Planck Institut für Astrophysik

Springel et al. (2004)

The semi-analytic merger-tree in the Millennium Run connects about 800 million subhalos

SCHEMATIC MERGER TREE

- The trees are stored as self-contained objects, which are the input to the semi-analytic code
- Each tree corresponds to a FOF halo at z=0 (not always exactly)
- The collection of all trees (a whole forest of them) describes all the structures/galaxies in the simulated universe

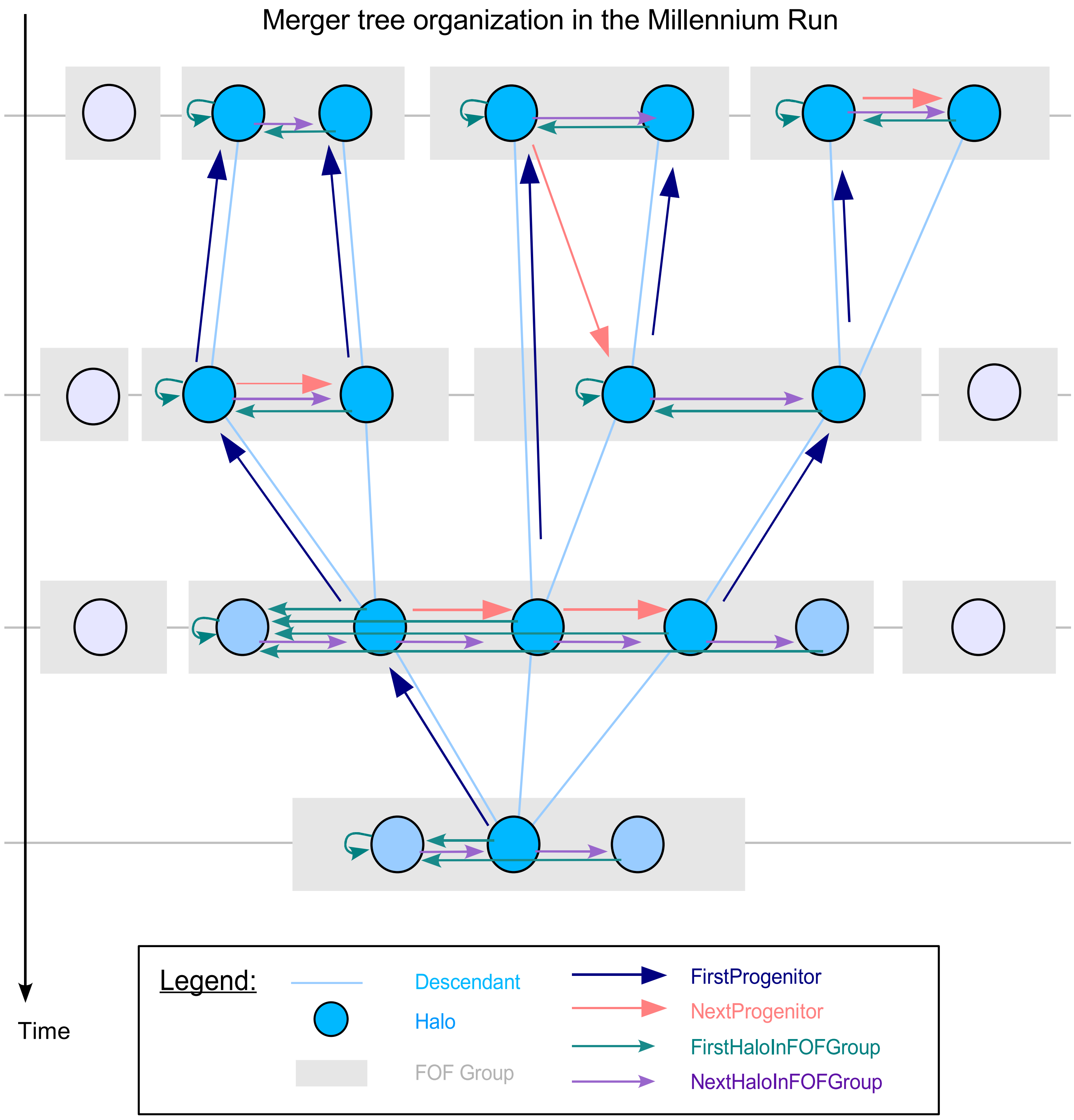

The merger tree in the Millennium simulation describes the orbits of all galaxies brighter than about 0.1 L_*

DARK MATTER AND GALAXY DISTRIBUTION IN A CLUSTER OF GALAXIES

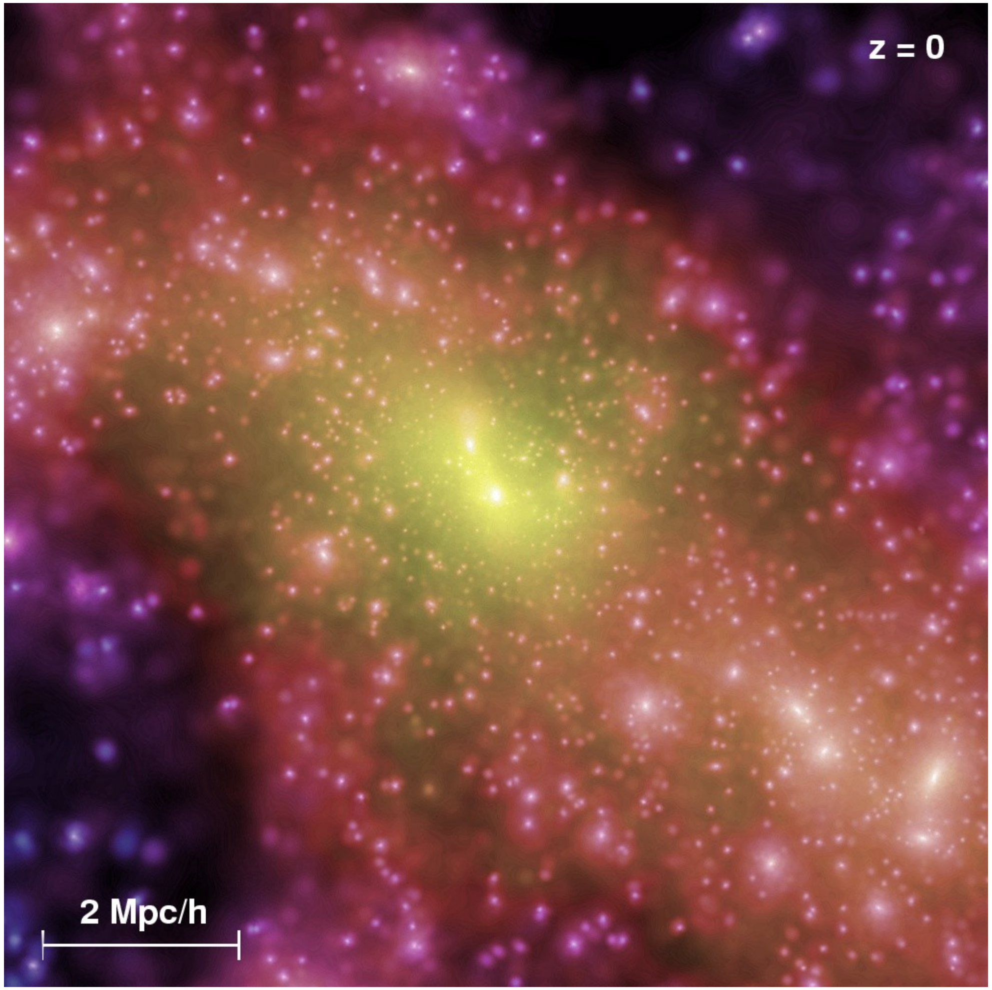

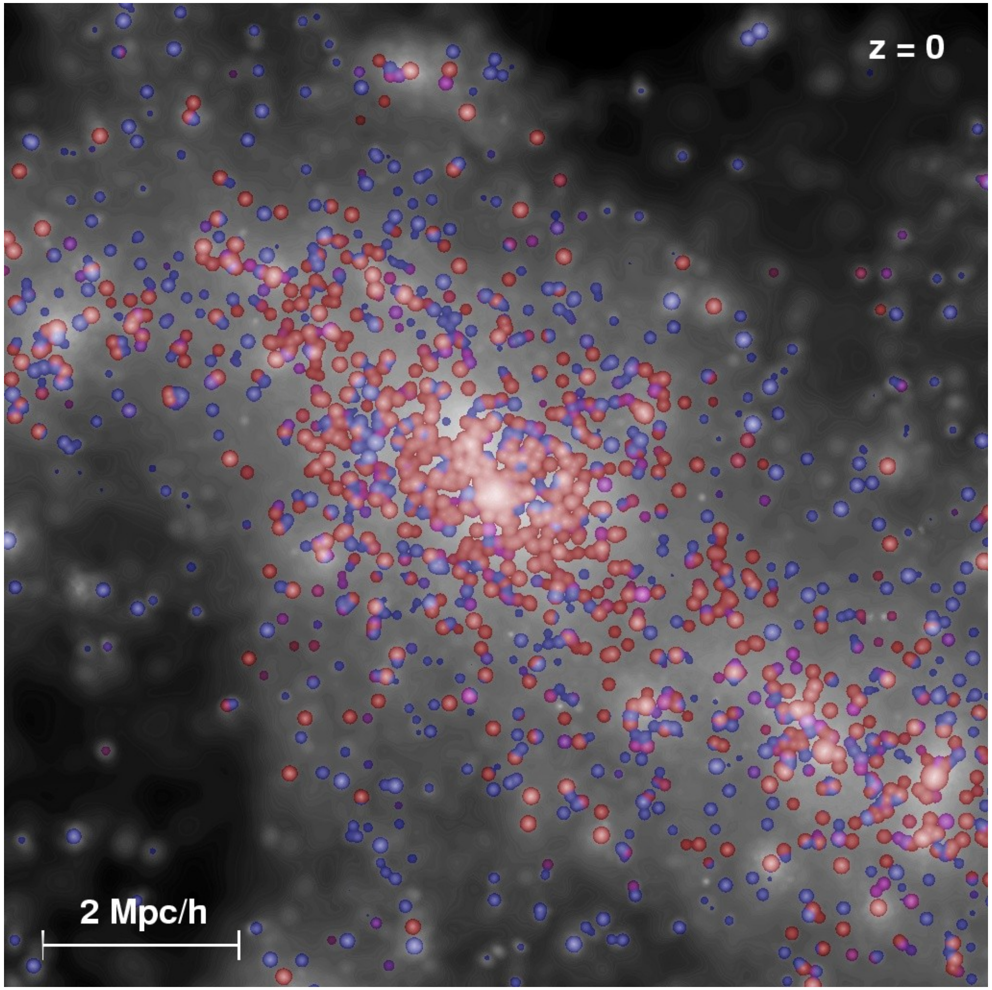

The light distribution of galaxies on large scales

DENSITY OF RED AND BLUE GALAXIES

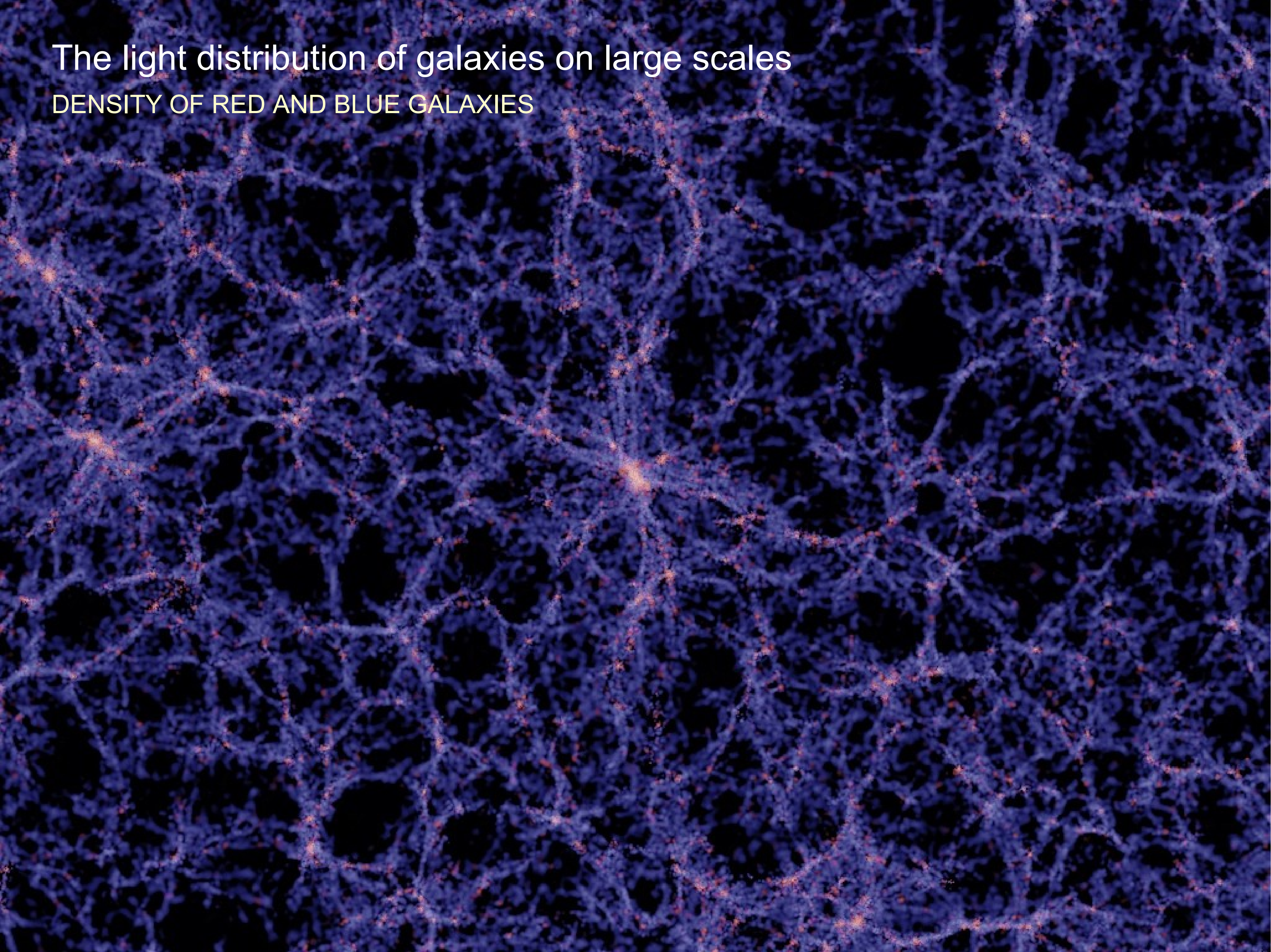

The distribution of dark matter on large scales

DARK MATTER DENSITY, COLOR-CODED BY DENSITY AND VELOCITY DISPERSION

The two-point correlation function of galaxies in the Millennium run is a very good power law

GALAXY TWO-POINT FUNCTION COMPARED WITH APM AND SDSS

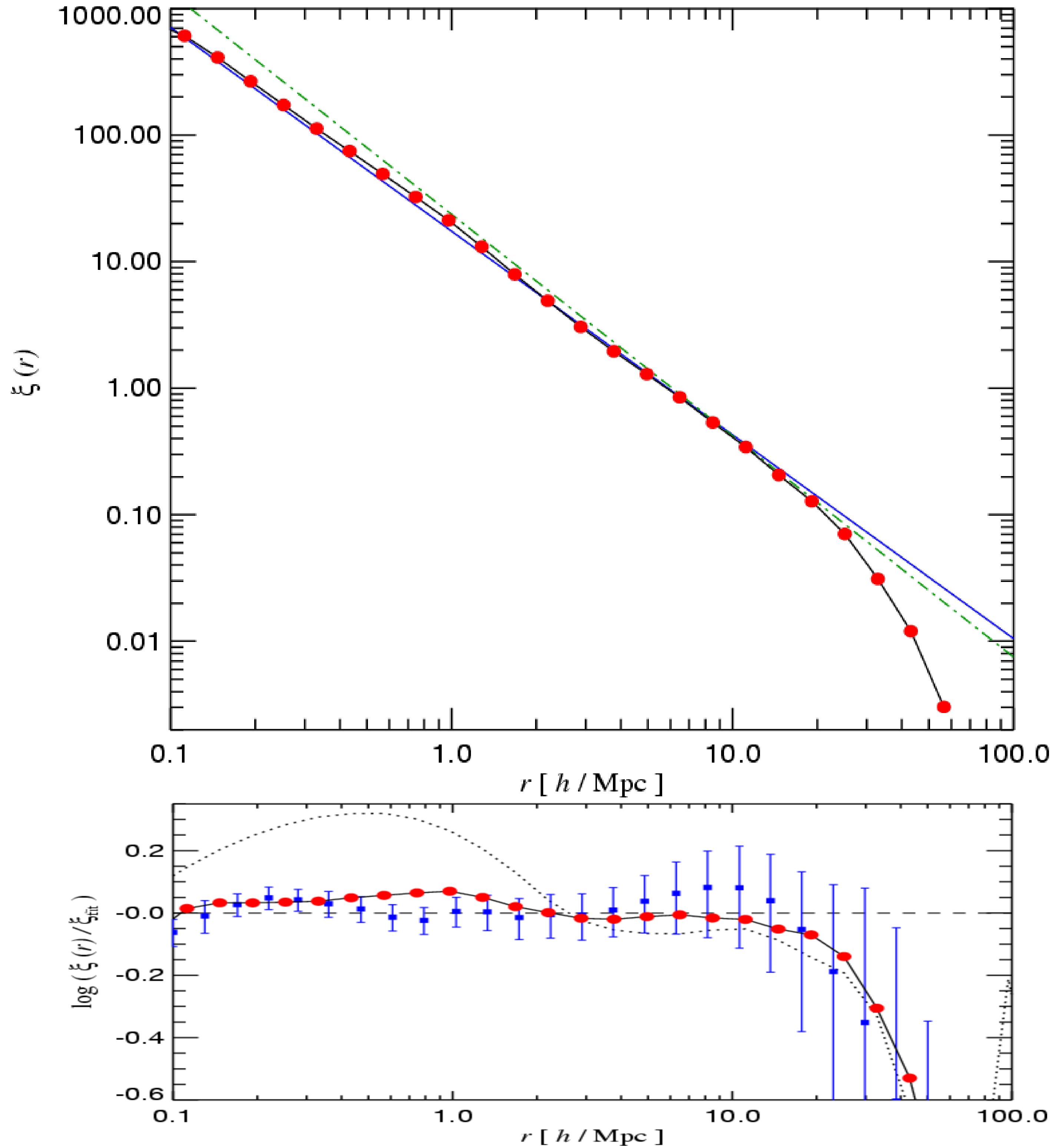

The semi-analytic model fits a multitude of observational data

CLUSTERING BY MAGNITUDE AND COLOR

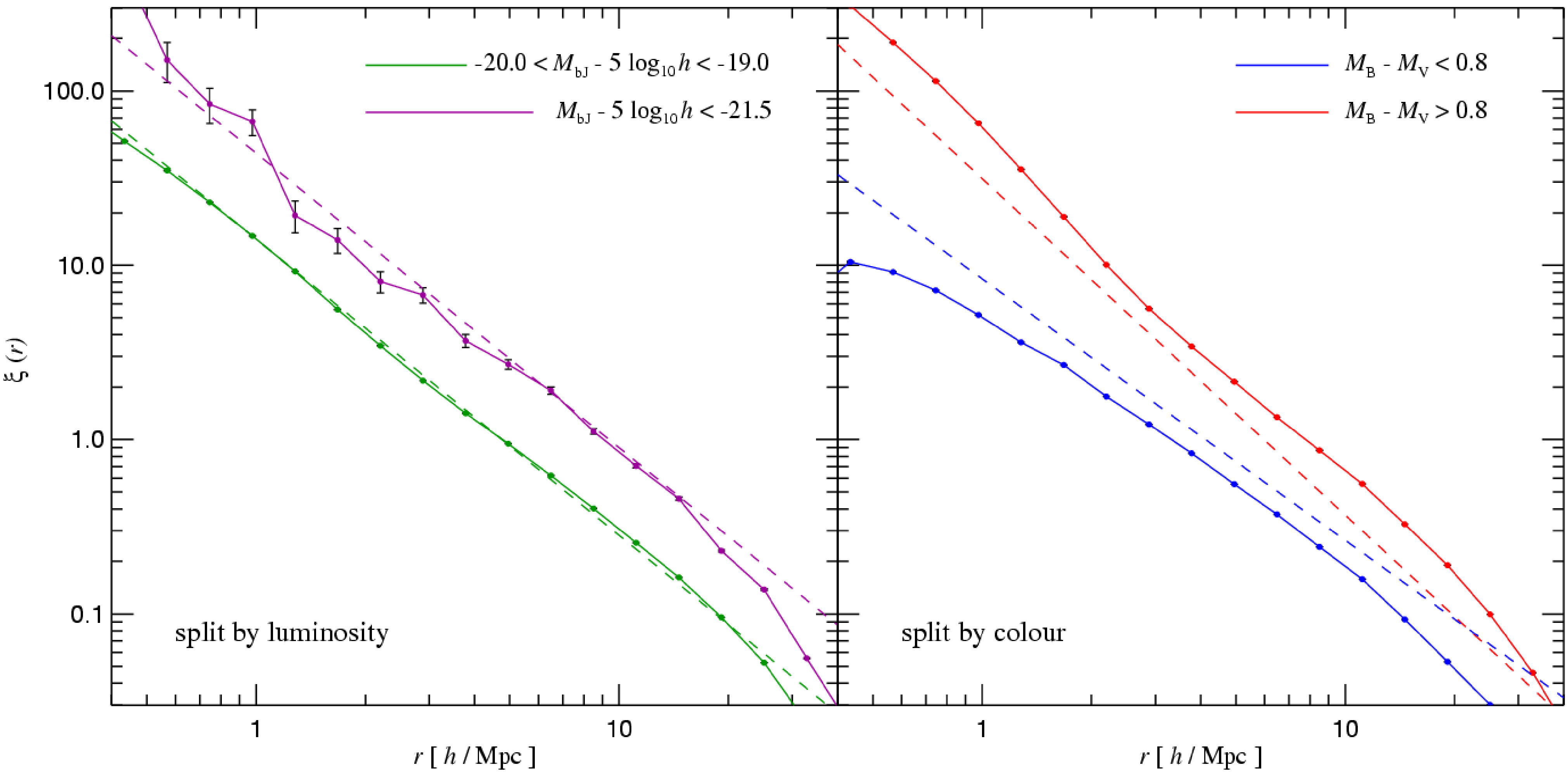

The semi-analytic model fits a multitude of observational data

B-V COLOUR DISTRIBUTION

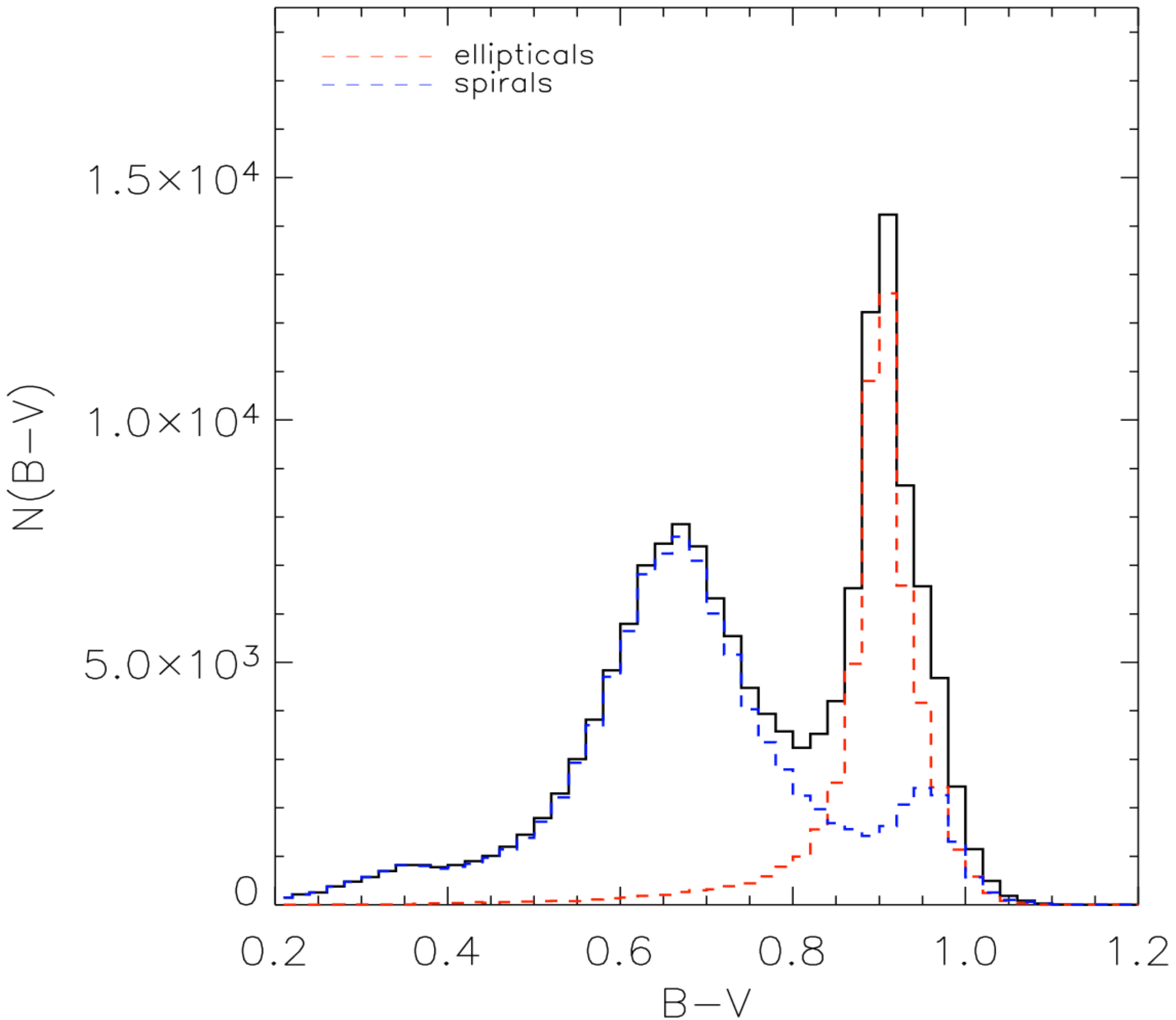

Croton et al. (2004)